INVESTIGATION OF NEW FORWARD OSMOSIS DRAW AGENTS AND PRIORITIZATION OF RECENT DEVELOPMENTS OF DRAW AGENTS USING MULTI-CRITERIA DECISION ANALYSIS

A Thesis

presented to

the Faculty of California Polytechnic State University,

San Luis Obispo

In Partial Fulfillment

of the Requirements for the Degree

Master of Science in Civil & Environmental Engineering

by

Jodie Wei Yu

June 2020

COMMITTEE MEMBERSHIP

TITLE:	Investigation of New Forward Osmosis Draw Agents and Prioritization of Recent Developments of Draw Agents Using Multi-Criteria Decision Analysis
AUTHOR:	Jodie Wei Yu
DATE SUBMITTED:	June 2020
COMMITTEE CHAIR:	Amr El Badawy, Ph.D. Assistant Professor of Environmental Engineering
COMMITTEE MEMBER:	Tryg Lundquist, Ph.D., P.E. Professor of Environmental Engineering
COMMITTEE MEMBER:	Rebekah Oulton, Ph.D., P.E. Associate Professor of Civil & Environmental Engineering

ABSTRACT

Investigation of New Forward Osmosis Draw Agents and Prioritization of Recent Developments of Draw Agents Using Multi-Criteria Decision Analysis

Jodie Wei Yu

Forward osmosis (FO) is an emerging technology for water treatment due to their ability to draw freshwater using an osmotic pressure gradient across a semi-permeable membrane. However, the lack of draw agents that could both produce reasonable flux and be separated from the draw solution at a low cost stand in the way of widespread implementation. This study had two objectives: evaluate the performance of three materials — peptone, carboxymethyl cellulose (CMC), and magnetite nanoparticles (Fe_3O_4 NPs) — as potential draw agents, and to use multi-criteria decision matrices to systematically prioritize known draw agents from literature for research investigation. Peptone showed water flux and reverse solute flux values comparable to other organic draw agents. CMC's high viscosity made it impractical to use and is not recommended as a draw agent. Fe_3O_4 NPs showed average low fluxes (e.g., 2.14 LMH) but discrete occurrences of high flux values (e.g., 14 LMH) were observed during FO tests. This result indicates that these nanoparticles have potential as draw agents but further work is needed to optimize the characteristics of the nanoparticle suspension. Separation of the nanoparticles from the product water using coagulation was shown to be theoretically possible if only electrostatic and van der Waals forces are taken into account, not steric repulsion. If coagulation is to be considered for separation, research efforts on development of nanoparticle suspensions as FO draw agents should focus on

development of electrostatically stabilized nanoparticles. A combination of Fe_3O_4 NP and peptone showed a higher flux than Fe_3O_4 NPs alone, but did not produce additive or synergistic flux. This warrants further research to investigate more combinations of draw agents to achieve higher flux than that obtained by individual draw agents.

Potential draw agents were prioritized by conducting a literature review of draw agents, extracting data on evaluation criteria for draw agents developed over the past five years, using these data to rank the draw agents using the Analytical Hierarchy Process (AHP) and Technique for Order of Preference by Similarity to Ideal Solutions (TOPSIS). The evaluation criteria used in the ranking matrices were water flux, reverse solute flux, replenishment cost, regeneration cost, and regeneration efficacy. The results showed that the top five ranked draw agents were P-2SO_3-2Na, TPHMP-Na, PEI-600P-Na, NaCl, and NH_4-CO_2. The impact of the assumption made during the multi-criteria decision analysis process was evaluated through sensitivity analyses altering criterion weighting and including more criteria. This ranking system provided recommendations for future research and development on draw agents by highlighting research gaps.

Keywords: forward osmosis (FO), draw agents, nanoparticles, peptone, carboxymethyl cellulose, desalination, the Analytical Hierarchy Process (AHP), Technique for Order of Preference by Similarity to Ideal Solution (TOPSIS)

ACKNOWLEDGMENTS

I would like to thank my thesis committee for their contributions towards this thesis.

Thank you, Dr. Amr El Badawy, for being my advisor and helping and supporting me throughout this research.

Dr. Tryg Lundquist and Dr. Rebekah Oulton for being on my committee and pushing me in my learning.

Thank you to Taylor Fagan for assisting me during the first phase of research and being there to guide one another through this project.

Thank you to my parents, sister, family, and friends for their unending support and love.

TABLE OF CONTENTS

Page

LIST OF TABLES

Table Page

LIST OF FIGURES

Figure Page

1. Performance Evaluation of Peptone, Carboxymethyl Cellulose, and Magnetite Nanoparticles as Forward Osmosis Draw Agents

1.1 INTRODUCTION

Water scarcity is a global issue and there is a pressing need for sustainable and resilient sources of freshwater. According to the World Health Organization (WHO), half of the world's population will be living in water-stressed areas by 2025 [1]. Due to the declining number of clean-water sources and an increasing demand for drinking water from a growing population, water supply efforts have often turned towards desalination. However, current commercial desalination techniques, reverse osmosis (RO) and thermal desalination, are energy intensive and have high operation and maintenance cost [2].

The development of an energy-efficient desalination method can be achieved through the process of forward osmosis (FO). FO uses osmotic potential to drive water through a semi-permeable membrane from a feed solution side (with low osmotic potential) to a draw solution side (higher osmotic potential) [3]. The FO process is advantageous due to the reduction of hydraulic pressure requirements which leads to less energy demand and potentially lower costs than RO [4]. Low hydraulic pressures also result in less membrane fouling which reduces the frequency of membrane cleaning [5], [6]. While the FO process has its advantages, it still lacks feasible draw solutes. An ideal draw agent should result in high water flux and be easily manufactured, separated from the produced water, and regenerated with relatively low energy and cost. Furthermore, the draw agent should have minimal reverse solute flux [7].

Many types of draw agents are being researched and developed [8]. These materials used as draw agents could be categorized as inorganic compounds, organic compounds, and functional nanoparticles [8]. Inorganic compounds were some of the first draw agents to be tested due to their high osmotic pressure. However, a drawback to using inorganic compounds would be separation from the product water after the FO process, which requires costly methods such as membrane distillation, reverse osmosis (RO), or nanofiltration [9]. Organic materials are promising draw agents because they produce relatively high water flux and small reverse solute flux [5]. Figure 1.1 presents the performance (i.e., water flux and reverse solute flux) of some organic draw agents for FO applications [10].The water flux ranged from 0.21 to 25.0 $Lm^{-2}h^{-1}$ (LMH) and reverse solute flux ranged from 0.78 to 16.1 $gm^{-2}h^{-1}$ (gMH). The draw agents studied had a positive correlation between the water flux and the reverse solute flux (i.e., as water flux increased, reverse solute flux increased as well) as illustrated in Figure 1.1.

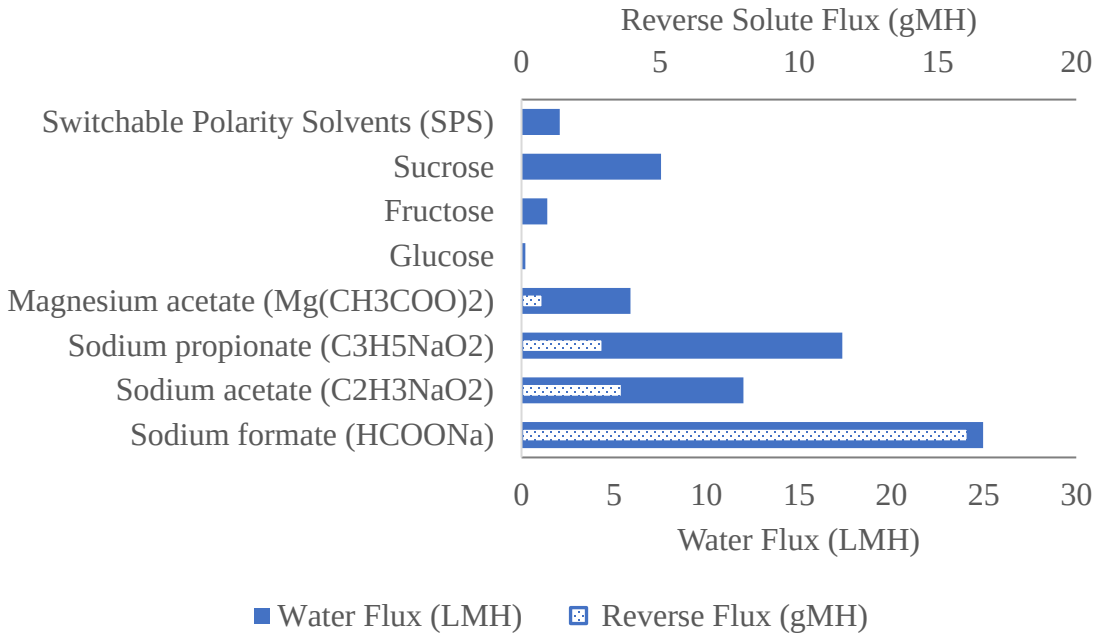

Fig. 1.1 Performance of various organic FO draw agents at a concentration of 200 g/L. Reverse flux of SPS, sucrose, fructose, and glucose were not reported [6].

Fig. 1.1 illustrates that not all organic draw agents produce high flux, and some of them produce high reverse solute flux. Another drawback of these organics includes high regeneration (i.e., separation) cost using reverse osmosis (RO), for example to separate sodium formate, sodium acetate, sodium propionate, and magnesium acetate [10]. So, when using organic draw agents for FO, these factors have to be taken into account.

Membrane orientation is also a key factor that affects the performance of FO processes. Asymmetric composite membranes are typically used in the FO process. These membranes are composed of two layers: a porous support layer and a dense active layer that performs the salt separation [11]. The active layer can be orientated to face the feed solution or the draw solution. In the pressure-retarded osmosis (PRO) mode, the active

layer faces the draw solution, while in FO mode the active layer faces the feed solution. PRO mode generally results in higher water flux and higher reverse solute flux than FO mode [12]. However, greater internal fouling occurs in the PRO mode; internal fouling is less reversible than external fouling that occurs when the membrane is operating in the FO mode [13]. This internal fouling results in the phenomena of concentrative internal concentration polarization (ICP). The ICP reduces water flux because of increased osmotic pressure that must be overcome with hydraulic pressure (Fig. 1.2) [11]. In the PRO mode, concentrative internal CP (CICP) occurs because the feed solution infiltrates the porous membrane and creates a layer against the inside of the active layer. In the FO mode, dilutive internal CP (DICP) occurs because the draw solution within the porous layer becomes diluted [11]. Since the draw solution is diluted in the porous layer during the FO mode, it causes less of a CP than when in the PRO mode. Internal fouling is harder to reverse because the solute molecules from the feed solution are compacted in the porous support layer, while external fouling only happens on the surface of the active layer. A cross-flow during the FO process can be used to prevent external fouling for the FO mode [13].

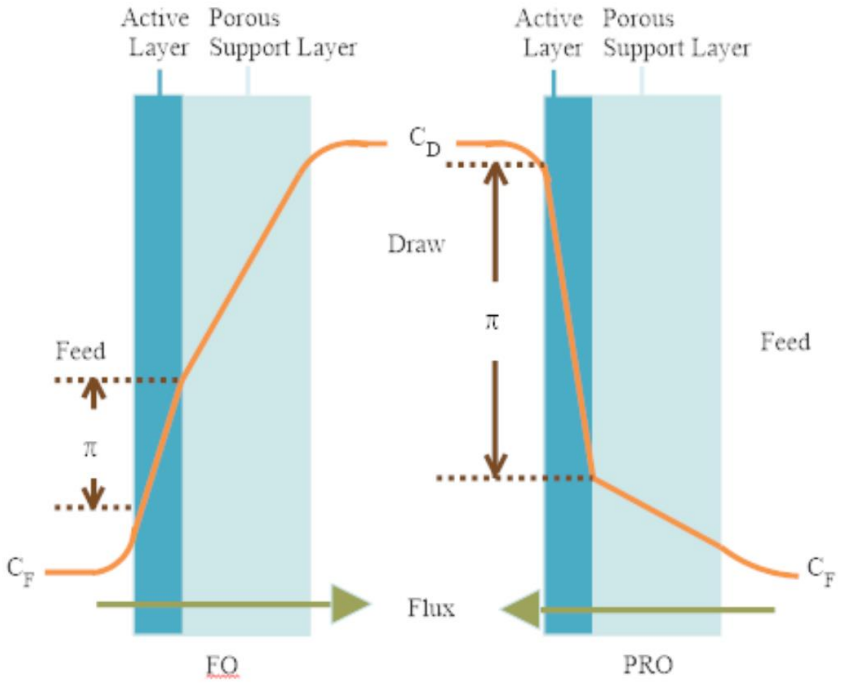

Fig.1.2 Internal concentration polarization of membranes in FO and PRO mode where CD is the concentration of the draw solution, CF is the concentration of the feed solution, and π is the osmotic pressure driving force (Jodie Yu).

More recently, magnetic nanoparticles (MNPs), have been used as draw agents in forward osmosis [4]. MNPs have benefits as a draw solution because of their small size. They can generate high osmotic pressures, reduce ICP due to their high diffusivities, and eliminate reverse draw solute flux [14]. MNPs have also become an area of study because they can be mechanically separated and regenerated by using a magnetic field rather than using membrane filtration processes or thermally [15]. However, implementing a magnetic field in large-scale applications would be difficult and costly.

The objective of the current study was to investigate the performance of three draw agents, peptone, carboxymethyl cellulose (CMC), and iron oxide nanoparticles (Fe_3O_4

NPs), for potential FO applications. Two hypotheses were tested in this research. The first hypothesis is that peptone and CMC have the potential to produce flux comparable to that of other organic draw agents but with lower reverse solute flux and lower cost of separation (for example, using ultrafiltration membranes) due to their relatively large molecular size. Additionally, peptone and cellulose have the advantages of being relatively inexpensive and environmentally safe chemicals [16], [17]. Furthermore, CMC is commonly used as a coating for iron nanoparticles [18]. The second hypothesis is that iron oxide nanoparticles a) will produce sufficient flux with no reverse flux because of their significantly larger size compared to the pore size of FO membranes and b) could be separated from the product water at a much lower cost using coagulation/filtration practices typically used for removing colloidal particles in drinking water treatment plants. Therefore, if the hypotheses proved to be true, the iron nanoparticles could potentially be coated with CMC and peptone to achieve a synergistic effect that leads to enhanced performance when these draw agents are combined.

The performance of peptone, cellulose, Fe_3O_4 NPs, and coated Fe_3O_4 NPs as potential FO draw agents was determined by measuring water flux, osmotic pressure, and reverse solute flux. The Derjaguin–Landau–Verwey–Overbeek (DLVO) theory was used for predicting the potential for using coagulation to separate the nanoparticles draw agent from the product water.

1.2 MATERIALS AND METHODS

This section details the experimental process and set up performed for the FO runs with the three draw agents – peptone, CMC, and Fe_3O_4 NP. Further characterization of peptone as a draw agent was also detailed through the osmotic pressure determination using a freezing-point depression. Particle interaction modelling was detailed to provide a separation method supplement since closure of labs prevented further separation research.

1.2.1 Materials

Granulated peptone (amino nitrogen (AN) ≥ 3.5%, total nitrogen (TN) ≥ 10.0%) was purchased from Fisher Bioreagents, USA. Sodium carboxymethyl cellulose ($C_{28}H_3ONa_8O_{27}$), average Mw~90,000 was obtained from Sigma Aldrich Chemical, USA. Iron oxide nanoparticle suspension (Fe_3O_4, 99.5+%, 15-20 nm, 20 wt% in water) was purchased from US Research Nanomaterials, Inc. (TX, USA). All chemicals were used as received without any further purification. Aqueous solutions were prepared with deionized (DI) water. The cellulose triacetate (CTA) forward osmosis membranes used were purchased from Fluid Technology Solutions (OR, USA).

1.2.2 Equipment

Clear Cast Acrylic FO membrane testing cell was purchased from Sterlitech (WA, USA). A 400S Series Portable Conductivity Meter was obtained from Apera Instruments (OH, USA). Traceable Excursion-Trac Data logging Thermometer was purchased from Fisherbrand (USA). Masterflex L/S Economy Variable-Speed Drive Pump and Masterflex

Console Gear Pump from Cole Parmer (USA) were used for pumping the draw and feed solution at the desired flow rates.

1.2.3 Preparation of the FO Draw Solutions/Suspensions

Peptone or CMC were dissolved in DI water to prepare draw solutions with concentrations from 30 to 200 g/L. Peptone readily dissolved compared to CMC. The sodium carboxymethyl cellulose (CMC) was dissolved very slowly in DI water at a temperature of 65 ^{o}C. The solution was intermittently vortexed to dissolve the CMC. Concentrations of 10 g/L, 50 g/L, and 60 g/L were prepared.

Draw suspensions of Fe_3O_4 NP were prepared at concentration ranging from 1 g/L to 5 g/L. Although the majority of the Fe_3O_4 NPs remained suspended, some nanoparticles were observed to fall out of suspension due to the high concentrations used. To minimize settling, the Fe_3O_4 NP draw agent suspensions were placed on a stir plate throughout the duration of the FO test runs.

A draw agent consisting of a combination of peptone and Fe_3O_4 NP was also tested. Peptone and Fe_3O_4 NP were mixed at concentrations of 200 g/L and 3 g/L, respectively for 24 hours to allow for physical sorption of the peptone to the Fe_3O_4 NP before conducting the FO test.

1.2.4 Forward Osmosis Testing Apparatus and Process

A schematic of the FO test apparatus is presented in Fig. 1.3. The cellulose triacetate (CTA) FO membrane, with an effective membrane area of 21cm^2, was inserted in the FO cell configured in the PRO mode where the active layer was facing the draw solution. The draw solutions (peptone, CMC, and iron oxide NPs) and a feed solution (DI water) of equal volume (300mL) were pumped through the FO test cell at a flow rate of 0.5 L/min. To avoid membrane fouling from previous runs affecting subsequent runs, the CTA membrane specimens were replaced with new ones after each test and flushed with DI for one hour before use.

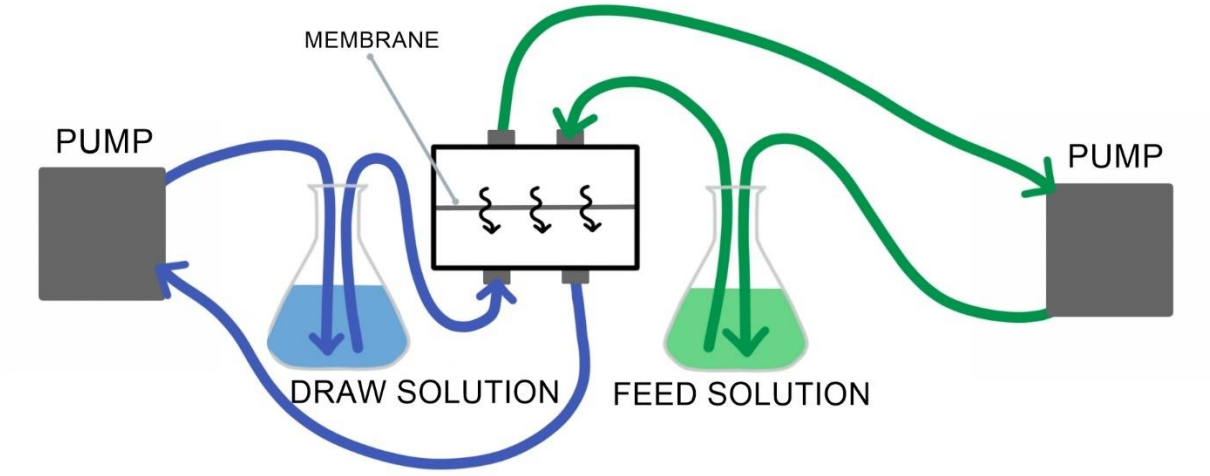

Fig. 1.3 FO process setup. The direction of the feed flow was in opposite direction to draw solution flow to improve contact (Ashley Fagan).

The weight of the draw solution and the total dissolved solids (TDS) concentrations of the draw and feed solutions were recorded in 15-minute intervals over the duration of the FO test run (120 minutes). The water flux was calculated using Equation 1:

$$J_w = \Delta V / A \Delta t \quad (1)$$

Where, J_w is the water flux in the units of $L/m^2 \cdot h$ (LMH), ΔV is the change in volume of the draw solution or the feed solution, A is the effective membrane surface area, and Δt is the change in time between intervals.

The reverse solute flux was calculated using Equation 2:

$$J_s = \frac{C_t * (V_{FO} - J_W * A_m * t) - C_O * V_{FO}}{A_m * t} \quad (2)$$

Where, J_s is the reverse solute flux across the FO membrane in the units of gMH. C_o and C_t are the solute concentrations in the feed solution at the start and end of the time interval, respectively in g/L. V_{FO} is the volume of the feed solution in L and J_w is the average water flux in LMH. A is the effective membrane area in m^2 and t is the time interval in hours.

1.2.5 Osmotic Pressure Prediction Using the Freezing-Point Depression Method

The osmotic pressure of the peptone and CMC solutions at varying concentrations was measured using the freezing point depression method [19], [20]. A 15 mL aliquot of draw solution was placed in a freezer (-22 ^oC) and the temperature of the solution was measured every minute until the solution solidified. The solute's temperature profile was approximated by three curves: the solvent cooling curve, the solvent freezing to a solid

curve, and the solid cooling curve. The freezing point was found at the intersection of the first two curves and compared to the freezing point of pure water to find the freezing point depression. The freezing point depression was then used to find the osmotic pressure of the solution using Equation 3:

$$\pi = \frac{\Delta T}{1.86} * 22.66(bar) \quad (3)$$

Where, π is the osmotic pressure in bar and ΔT is the temperature difference between the freezing point of water and the solution (i.e., the freezing point depression).

1.2.6 Calculation of the DLVO Interaction Forces

Separation of the nanoparticles draw agents from the product water could be achieved by gravity settling and granular media filters if the nanoparticles can be coagulated. Coagulants destabilize colloidal particles by altering the balance between the interaction forces (e.g., electrostatic, steric, and van der Waals forces) that keeps the particles stable [21], [22]. Jar tests are used to determine the coagulation feasibility as well as the optimal coagulant dose for colloidal particles including nanoparticles. An alternative approach based on the DLVO theory was used in this study to achieve this goal. The DLVO theory was used to calculate the interaction energy profiles of colloidal particles in the presence of different concentrations of alum, which is a commonly used coagulant in drinking water treatment. The interaction energy profiles were used in this study as indicators for the feasibility of using coagulation to separate the iron oxide nanoparticles (draw agents) from the water produced using forward osmosis processes.

The DLVO theory states that all objects exhibit both attractive and repulsive interactions resulting from van der Waals (vdW) forces and electrostatic forces, respectively [23]. The attractive vdW forces (V_H) are described by the Hamaker constant (A_{12}) in Equation 4 [24].

$$V_H = \frac{-A_{12}r}{12hk_BT} \quad (4)$$

Where, r is the radius of the particles, h was the separation distance between the particles, k_B is the Boltzmann constant, and T is the temperature of the solution.

The repulsive electrostatic force (V_D) was defined by the inverse of the Debye length (k^{-1}), or the distance which a charge is shielded. Electrostatic forces were calculated with Equation 5 [24].

$$V_D = \frac{2\pi e_0 \varepsilon \varphi^2 ln\left(1+e^{\frac{-h}{k^{-1}}}\right)}{k_BT} \quad (5)$$

Where, e_0 is the permittivity in the vacuum, ε is the permittivity relative to a vacuum, and φ is the surface potential (zeta potential was used in this study) of the particles.

To cause aggregation, the electrostatic forces (i.e., repulsive forces) must be overcome by neutralizing the charge and compressing the electric double layer which is described by k^{-1}, and calculated using Equation 6 [24].

$$k^{-1} = \sqrt{\frac{e_0 \varepsilon k_B T}{2N_A e^2 I}} \quad (6)$$

Where, N_A is Avogadro's number and I is the ionic strength of the solution.

The solution's ionic strength plays an important role in affecting the thickness of the diffuse double-layer. As ionic strength increases, or the coagulant concentration increases, the

double-layer thickness decreases [21]. The ionic strength was calculated using Equation 7 [24].

$$I = \frac{1}{2}\sum_{j=1}^{n} c_j z_j^2 \quad (7)$$

Where, c_j is the molar concentration of the coagulant and z_j is its charge.

The total interaction energy was then calculated using Equation 8.

$$V_T = V_H + V_D \quad (8)$$

The Fe_3O_4 NP used in this experiment had a proprietary surface coating that kept them very stable despite their high concentration (20% by weight in water). The manufacturer reported that the zeta potential of the Fe_3O_4 NP used in this study is -10.8 mV [25]. Electrostatically stabilized NPs that have a zeta potential between -10 and +10 mV are considered approximately neutral and will readily aggregate [26] [27]. However, the stock Fe_3O_4 NP suspension used in the study was very stable. This indicates that these nanoparticles are most likely coated with a polymeric material that provides a steric repulsion mechanism to prevent their aggregations. Nanoparticles coated with polymers have been reported to exhibit high stability regardless of the magnitude of surface charge [28].

If the nanoparticles are sterically stabilized, then the steric repulsion forces must be taken into account when calculating the total interaction energy profiles. Steric repulsion is made up of two interaction energies (osmotic and elastic) that are a result of the overlap of two polymer surfaces [6]. The osmotic interaction (V_o) was calculated using Equation 9 [6].

$$V_O = 2\frac{R4\pi}{v_1}\varphi_p^2\left(\frac{1}{2}-\chi\right)L^2\left(\frac{h}{2L}-\frac{1}{4}-ln\left(\frac{h}{L}\right)\right) \quad (9)$$

The elastic interaction (V_E) was calculated using Equation 10 [6].

$$V_E = 2\left(\frac{2\pi R}{M_W}\varphi_P L^2\rho_p\right)\left(\frac{h}{L}ln\left(\frac{h}{L}\left(\frac{3-h/L}{2}\right)^2\right)-6ln\left(\frac{3-h/L}{2}\right)+3\left(1+\frac{h}{L}\right)^2\right) \quad (10)$$

The total steric force (V_S) was calculated using Equation 11 [6].

$$V_S = V_O + V_E \quad (11)$$

Where, R is the diameter of the particles, v_1 is the molar volume of the solvent, φp is the volume of fraction of polymer within the brush layer which was assumed to be 0.01 [29], χ is the Flory-Huggins solvency parameter which was assumed to be 0.45 for a well-ordered monolayer [23], and L is the thickness of the polymer brush which was assumed to be 100 nm [6]. So, with the steric forces, the total interaction was calculated using Equation 12.

$$V_T = V_H + V_D + V_S \quad (12)$$

Two scenarios were assumed in this study to evaluate the interaction energy profiles: 1) the draw agent is electrostatically stabilized Fe_3O_4 NP having a zeta potential of - 40 mV, which is a reasonable for these nanoparticles in neutral pH conditions [30] and 2) the draw agent is sterically stabilized Fe_3O_4 NP having a zeta potential of -10 mV. The rationale for testing these scenarios is to evaluate the impact of the nanoparticle stabilization mechanism on the feasibility of destabilizing it using coagulation.

1.3 RESULTS

This section details the FO performance of peptone, CMC, Fe_3O_4, and peptone combined with Fe_3O_4. The water flux and reverse solute flux were compared between the three draw agents. Interparticle energies for Fe_3O_4 was modelled to find the theoretical dose of coagulant needed to separate them from the final draw solution.

1.3.1 Performance of Peptone Draw Solution

To determine the optimal membrane orientation mode, water flux and reverse solute flux were measured with the membrane oriented in the FO and PRO modes. This test was conducted using 30 g/L peptone draw solution. The PRO mode resulted in a considerably higher flux and reverse solute flux compared to those obtained from the FO mode (Figure 1.3). Based on these results, the PRO membrane orientation mode was used for the entirety of the experiments. This decision is justified based on the fact that high flux is key for FO processes and the high reverse solute flux values obtained herein are still in the low range of reverse solute flux values reported in the literature for other organic draw agents (Figure 1.4).

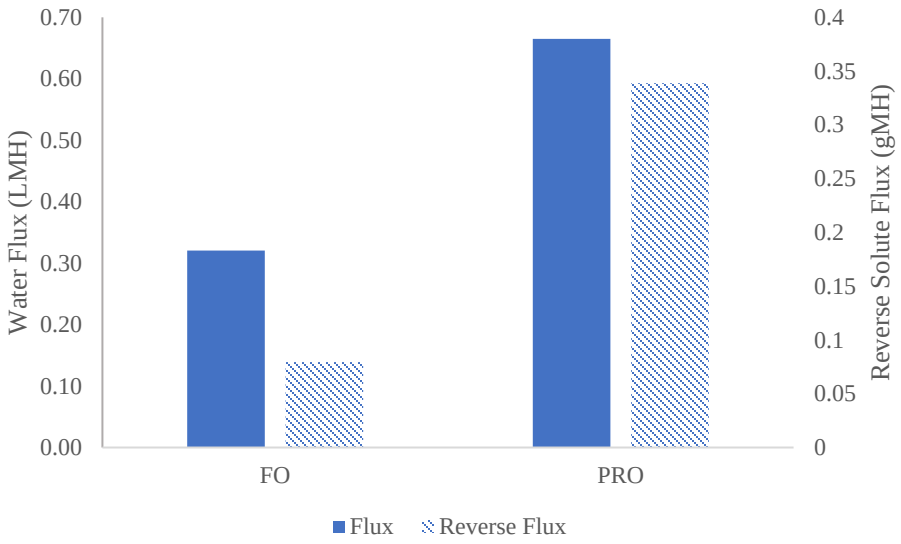

Fig. 1.4 Comparison of draw agent performance at different membrane modes. The test was conducted using 30 g/L peptone draw solution.

Both the water flux and reverse solute flux increased as peptone concentration increased (Fig. 1.5). However, over the concentration range of 30-200 g/L peptone, the water flux increased by 0.016 LMH per gram peptone added while the reverse solute flux only increased by 0.0005 gMH per g peptone. This indicates that the FO membrane was effective in rejecting the draw agent reverse flux, which may be a result of the relatively large size of peptone.

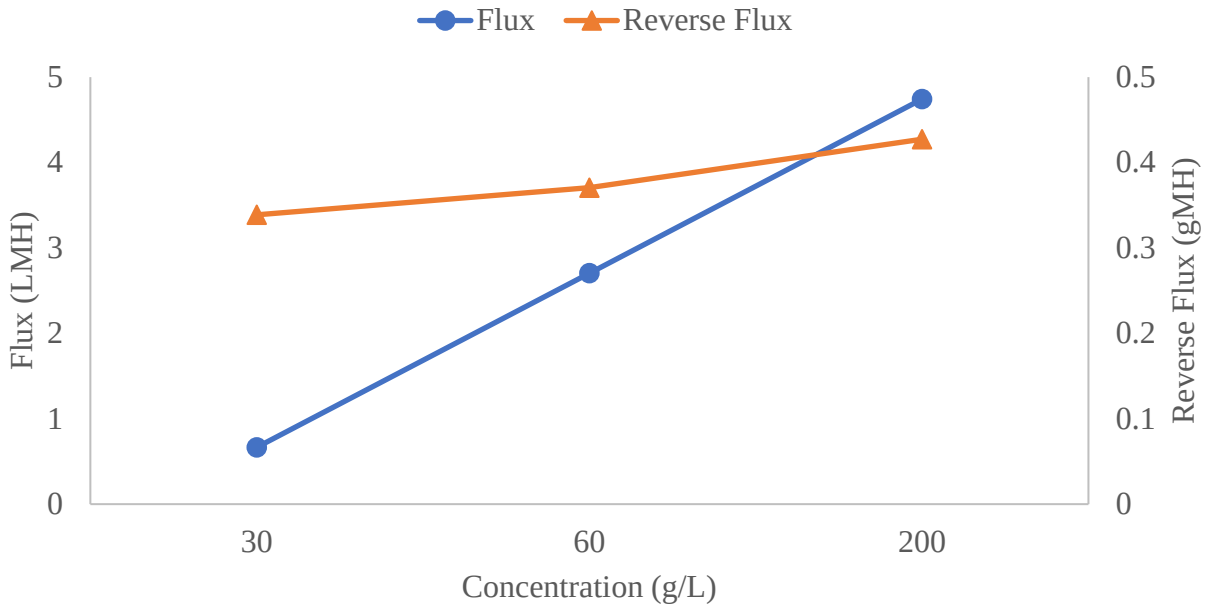

Fig. 1.5 Water flux and reverse solute flux of the peptone draw solution at different concentrations.

At the highest concentration tested (20%), the water flux and reverse solute flux were 4.74 LMH and 0.43 gMH, respectively based on the average values of the 15-minute measurements. It is noted that high fluctuations were observed for the flux and the reverse salt flux between measurements at the 15-minute intervals (Fig. 1.6). This is expected because the measurements were taken while the system was running (i.e., the pumps are quickly drawing and returning liquids to and from the feed and draw reservoirs).

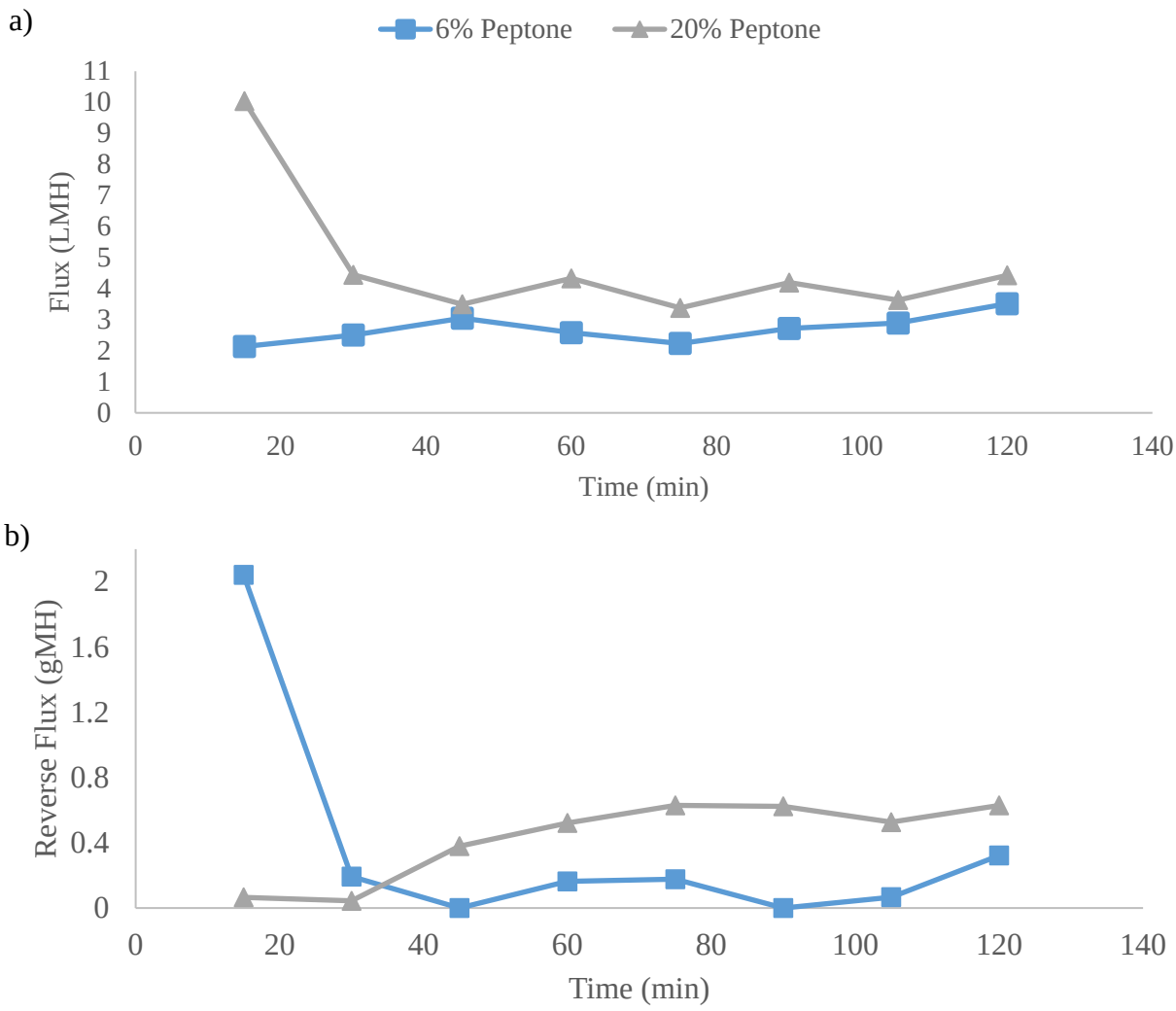

Fig. 1.6 Peptone concentration effect on (a) water flux and (b) reverse solute flux over time.

The osmotic pressure of peptone was measured based on the freezing point depression. Figure 1.7 shows an example of the method for determining the freezing point for 1 g/L peptone solution. The cooling curves were fitted with best fit lines, and the intersection of the solvent cooling and solvent to solid curve was found to be the freezing point of -0.17°C.

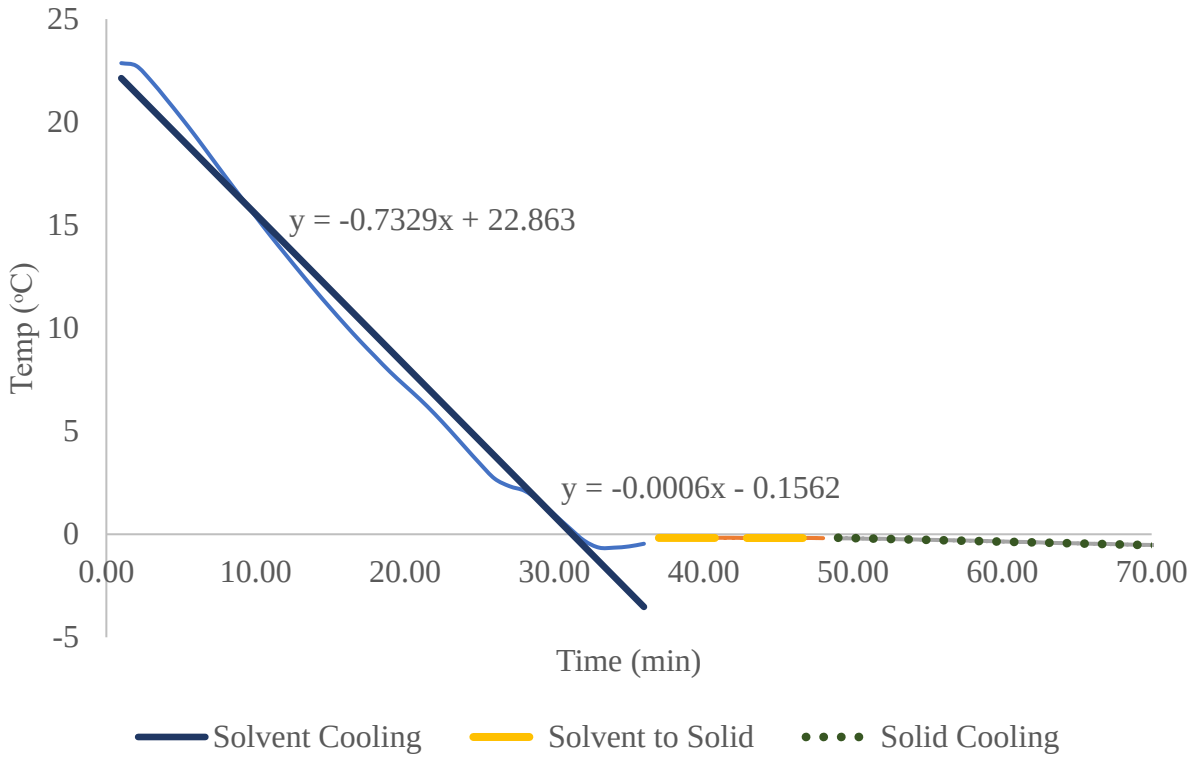

Fig.1.7 Freezing point depression of 1 g/L peptone solution.

The osmotic pressure results for peptone are presented in Fig. 1.8. The osmotic pressure increased linearly with the increase in peptone concentration. This can explain the reason for the increase in water flux as the concentration increases.

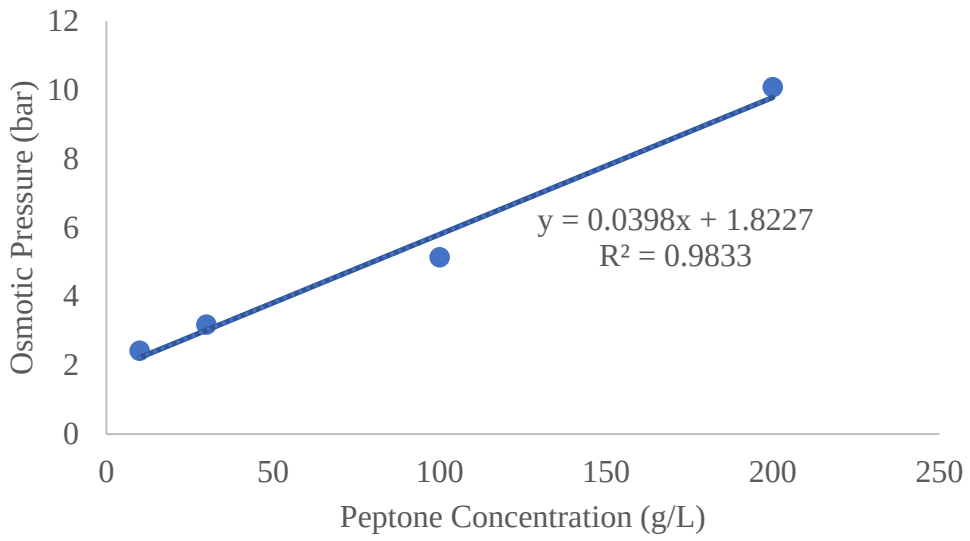

Fig. 1.8 Osmotic pressure of the peptone draw solution as a function of concentration.

1.3.2 Performance of CMC Draw Solution

CMC produced water flux values and minimal solute flux (Figure 1.9). For example, the average water flux and reverse solute flux of the 60 g/L CMC solution were 2.77 LMH and 0.015 gMH, respectively. However, the flux and the solute flux showed no marked change as the CMC concentration increased. A noticeable increase in the viscosity of the CMC solution as its concentration increased may be an explanation for the lack of flux response to CMC concentration increase. Interestingly, the water flux resulting from CMC was comparable to that of peptone at similar concentrations. Overall, it was somewhat challenging to accurately determine the flux and reverse flux because of the difficulty in recovering the solution from the tubes for solution weight measurements.

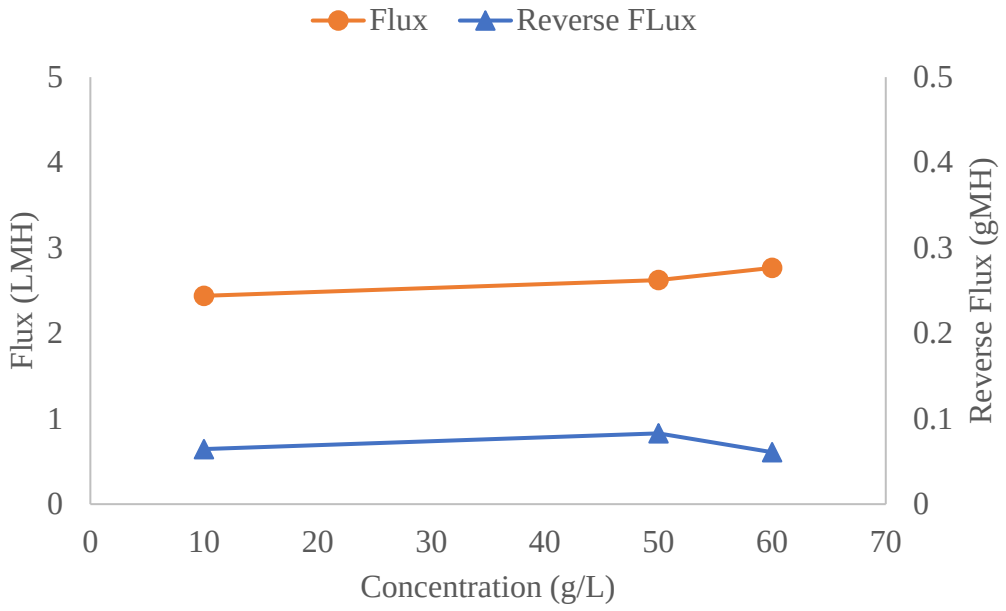

Fig. 1.9 The effect of CMC concentration on water flux and reverse solute flux.

1.3.3 Performance of Fe_3O_4 NP Draw Suspension

The performance of Fe_3O_4 NP draw suspension was tested at various concentrations (0.1, 0.5, 1, 3, and 5 g/L). It is noted that the nanoparticles were generally stable in suspension throughout the test run with minimal aggregation observed. Overall, the water flux was low and the reverse flux of ions was negligible regardless of the nanoparticle concentration tested (Figure 1.10). However, flux values as high as 14 LMH were observed at some time intervals as shown in Figure 1.11. This variability is likely a result of polydispersity of the nanomaterial suspension (the nanomaterials have a size distribution rather than being monodisperse). Since the properties of nanomaterials are size-dependent, there is heterogeneity of the osmotic pressure at the membrane surface as batches of nanomaterials of different sizes are being recirculated in the FO system.

Nonetheless, the occurrence of the random spikes of high water flux is promising and further research is needed to optimize and enhance the quality of the nanoparticle suspension in terms of size uniformity to sustain this high level of flux.

Using higher concentrations of nanoparticles may have the potential to produce higher flux. For example, 3 g/L nanoparticles tested in this produced a water flux of 2.45 LMH compared to < 1 LMH produced by 3 g/L peptone (Figures 1.5 and 1.10). Also, the lowest peptone concentration tested was 30 g/L (which is 6 times higher than the highest NP concentration tested of 5 g/L) produced flux < 1 LMH. Therefore, future testing with higher nanoparticle concentration is warranted and may produce higher water flux than peptone.

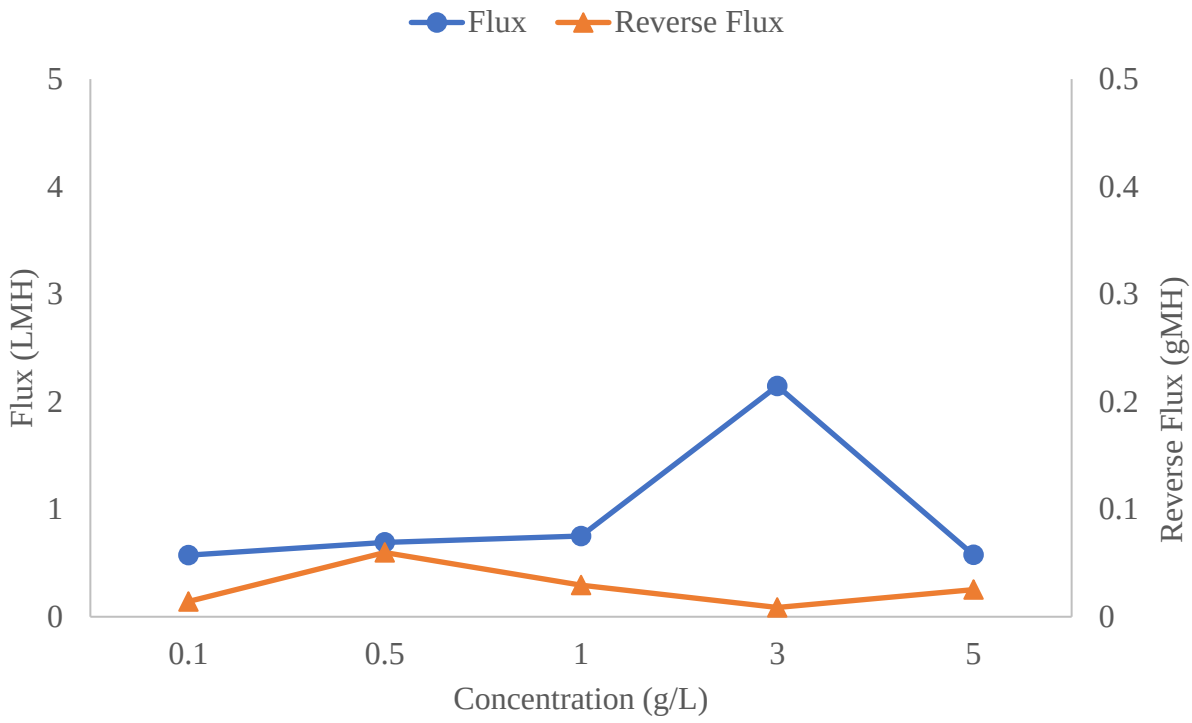

Fig. 1.10 Fe_3O_4 NP concentration effect on water flux and reverse solute flux.

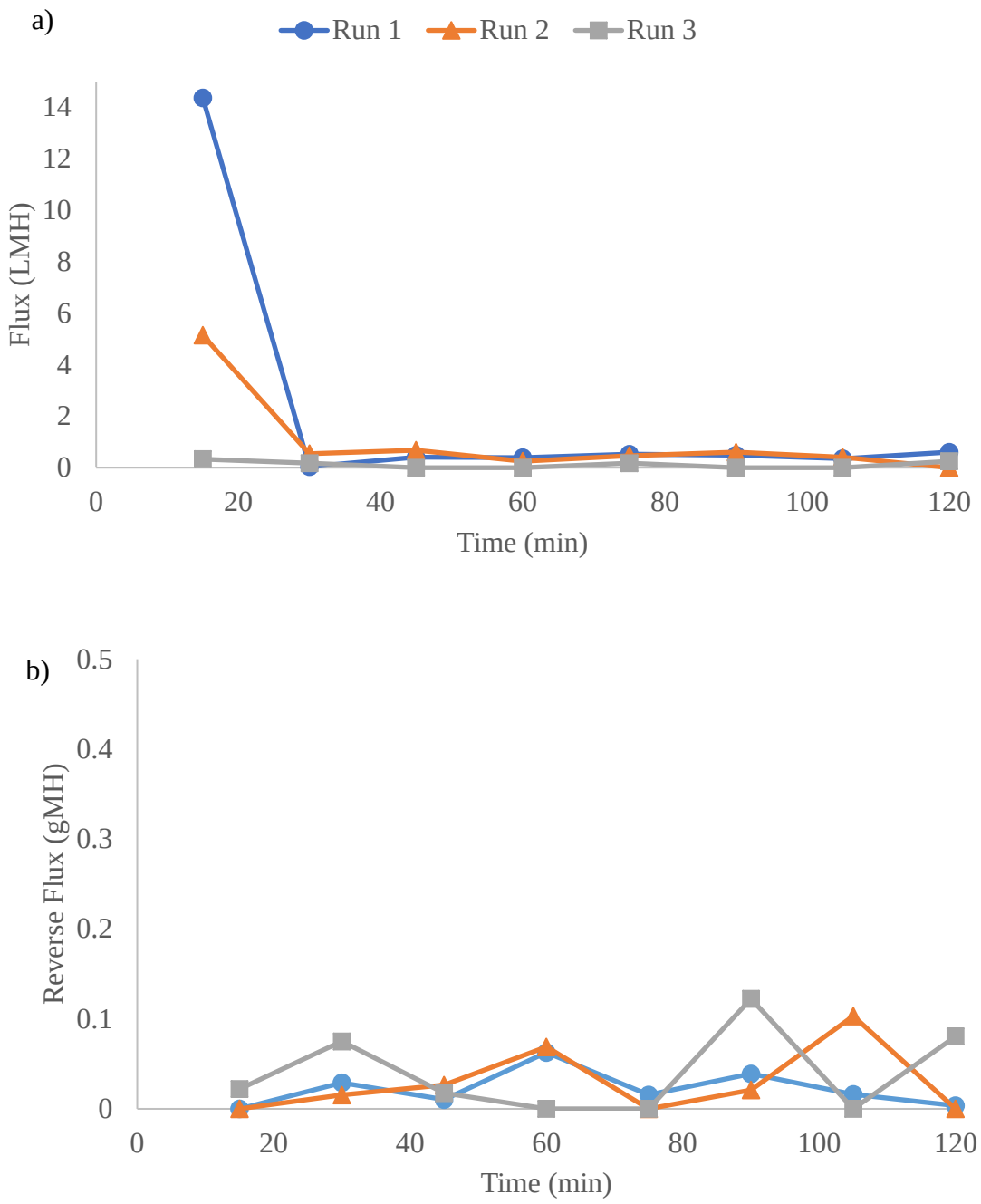

Fig. 1.11 Fe_3O_4 NP concentration effect on (a) water flux and (b) reverse solute flux over time.

1.3.4 Performance of Fe_3O_4 NP/Peptone Combination

The performance of a combination of 200 g/L of peptone and 3 g/L of Fe_3O_4 NPs was evaluated and the results are presented in Figure 1.12. The water flux increased significantly within the first 30 minutes but remained stable afterwards. The average water flux and reverse flux was around 1.58 LMH and 0.56 gMH, respectively. The water flux in this case was greater than the flux recorded for the NPs alone but the effect of combining peptone with nanoparticles was not additive or synergistic.

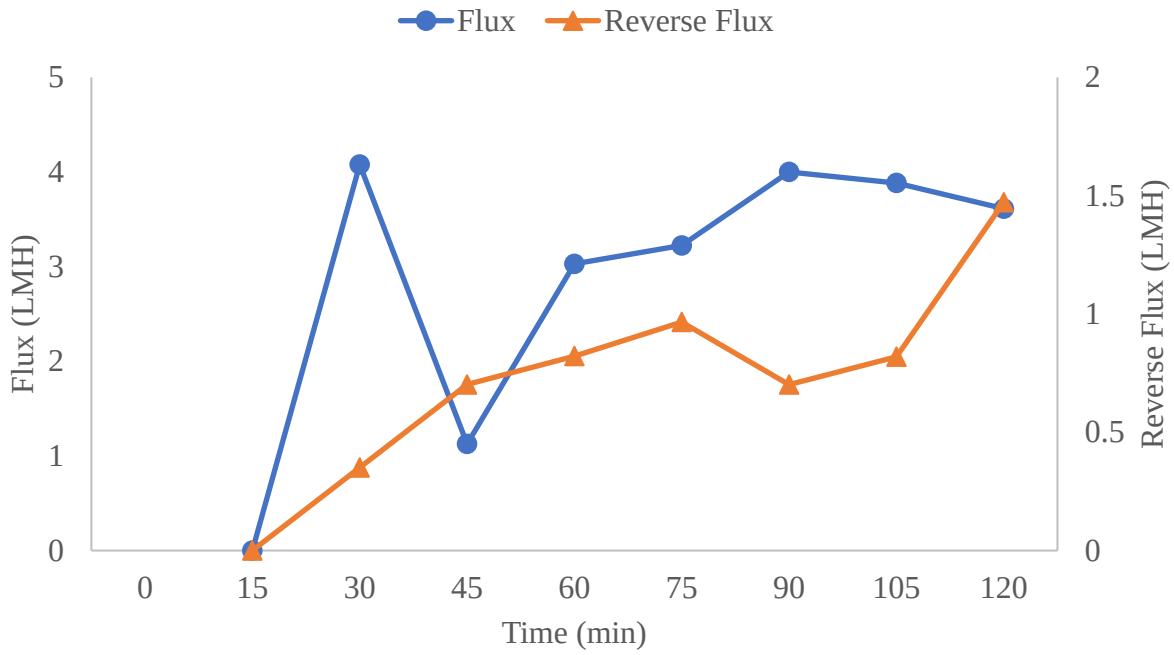

Fig. 1.12 Fe_3O_4 NP and peptone solution flux and reverse solute flux over a 120-minute run.

1.3.5 Interaction Energy Profiles

1.3.5.1 Scenario 1: Coagulation of electrostatically stabilized nanoparticles

The DLVO theory was used to predict the interaction energy profiles of electrostatically stabilized Fe_3O_4 NPs (with a zeta potential of - 40 mV) in response to the addition of different doses of alum. Figure 1.13 presents an example of the vdW attraction energy, the electrostatic repulsion energy, and the total energy of the NPs for an ionic strength of 0.1 mM resulting from the addition of alum sulfate to solution. At this ionic strength, there is a high energy barrier between the nanoparticles which indicate that aggregation of the nanoparticles is unlikely using this alum dose.

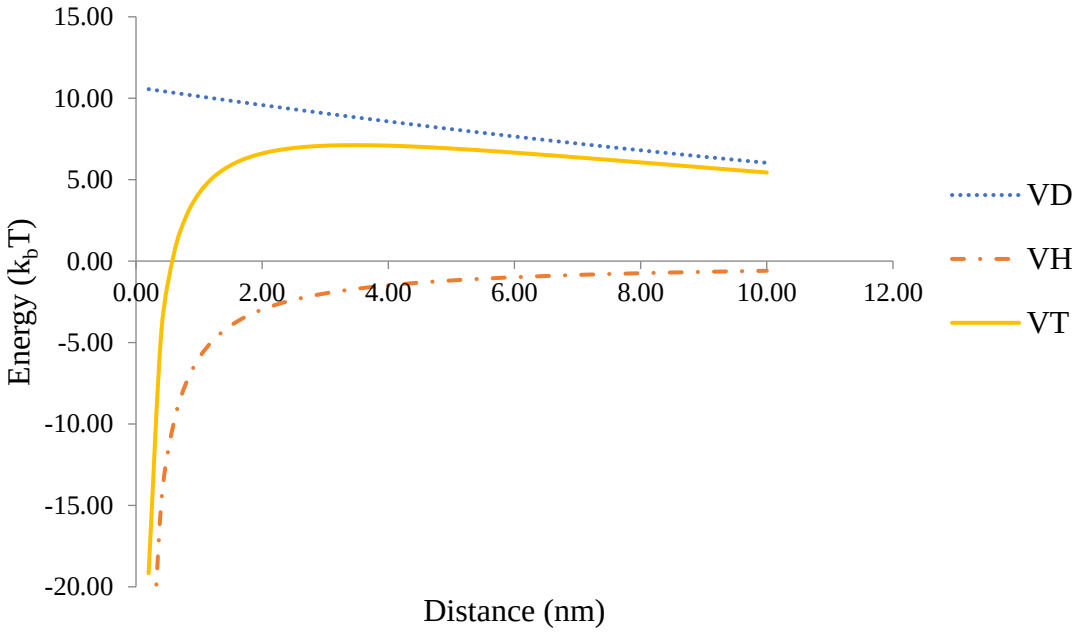

Fig. 1.13 Energy profile of Fe_3O_4 NPs in 0.1 mM ionic strength solution considering electrostatic and vdW forces.

A range of ionic strength values was tested and the resulting interaction energy profiles are presented in Figure 1.14. In general, the energy barrier decreased with the increase in ionic strength. At an ionic strength of 60 mM (396 mg/L alum), the total interaction is dominated by the vdW forces which indicates favorable conditions for aggregation of the NPs. This shows that an alum dose that results in a solution with 60 mM ionic strength may be needed to separate electrostatically stabilized Fe_3O_4 NPs draw agents from the product water. However, jar tests are needed for the determination of the actual dose required.

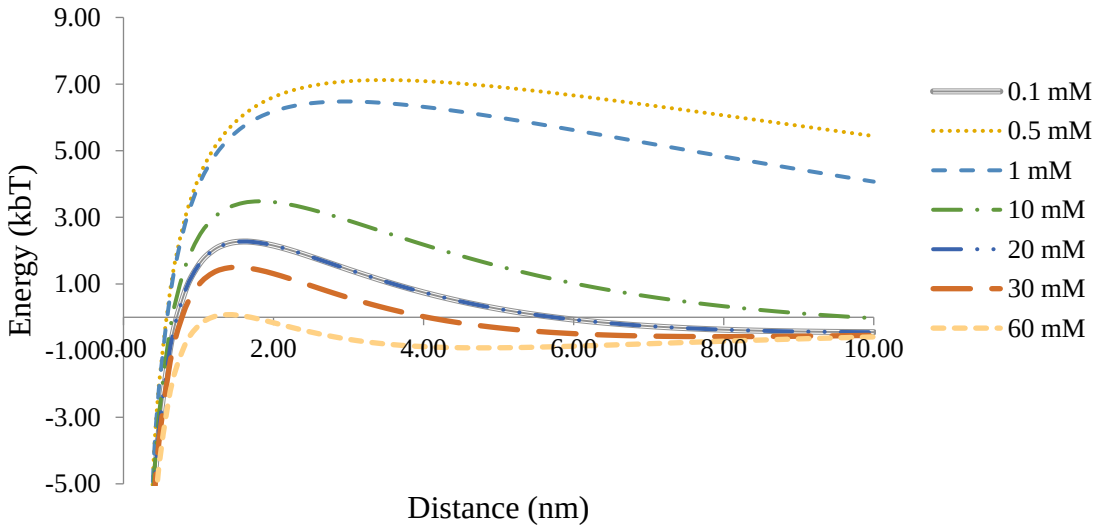

Fig. 1.14 Total interaction energy of the nanoparticles at various ionic strengths of aluminum sulfate (only electrostatic and vdW forces were considered).

1.3.5.2 Scenario 2: Coagulation of sterically stabilized nanoparticles

When a polymer coating was considered for the stabilization of the nanoparticles, the steric repulsion interaction had to be taken into account for determining the interaction energy profile. The total energy interaction was calculated by adding a steric repulsion

term to the DLVO interaction energy equations. Figure 1.15 presents the interaction energy at different values of ionic strength. The repulsion forces were higher compared to the scenario with no steric interactions. This resulted in a net substantial energy barrier even at the highest ionic strength values tested (i.e., 100000 mM). These results indicate that coagulation with alum may not be a feasible separation strategy for sterically stabilized nanoparticle draw agents.

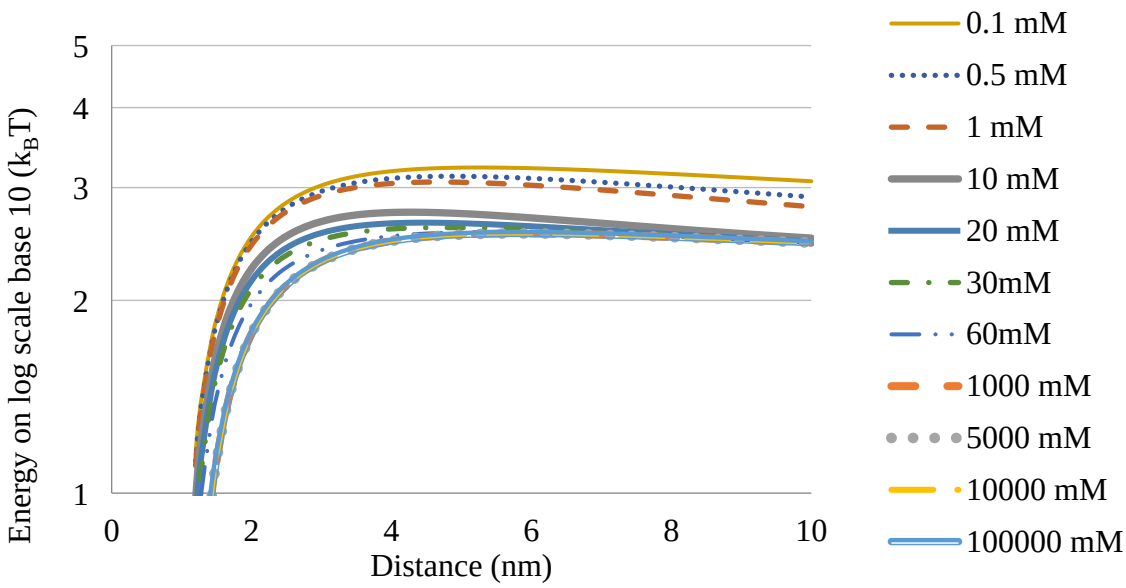

Fig. 1.15 Energy profile of sterically stabilized Fe_3O_4 NPs in liquid with different ionic strength (electrostatic, vdW, and steric forces were considered).

1.4 DISCUSSION

The results from the previous section were discussed here detailing the draw agents FO performance against each other and other organic draw agent. The large amount of coagulant needed deduced from the interaction energy profile results for Fe_3O_4 NPs were further discussed. Future work was also discussed to improve upon further FO runs, optimization of the draw agents, and lab-scale separation studies.

1.4.1 Performance of Draw Agents Tested

Peptone was demonstrated as a draw agent in an FO process. The water flux produced by peptone was comparable to the flux of some types of organic agents reported in the literature (Figure 1.15). One advantage of peptone compared to other organic draw agents is that the reverse flux was extremely low (Figure 1.16).

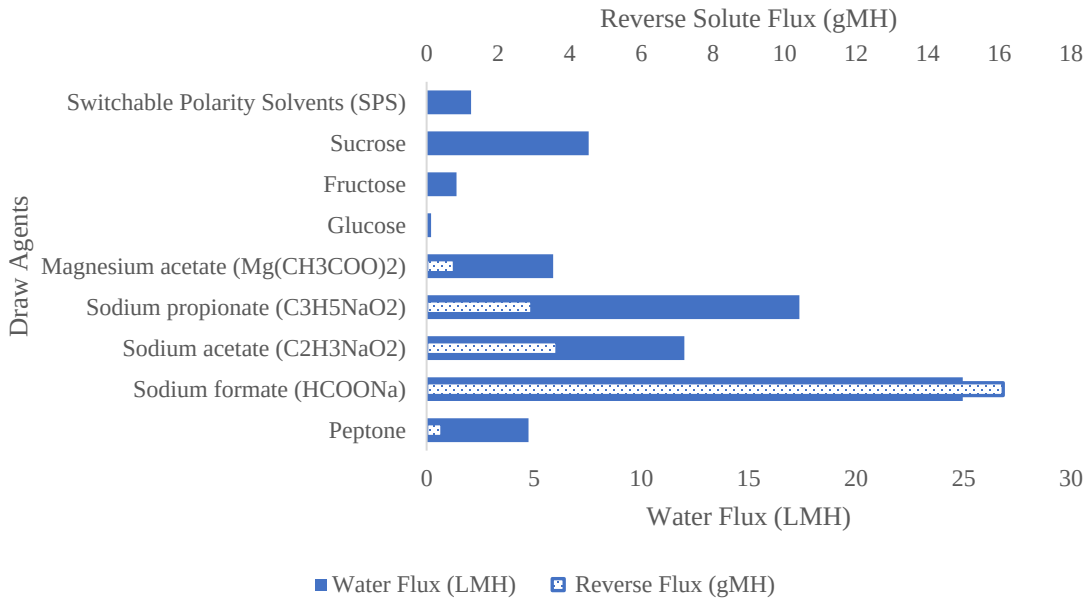

Fig. 1.16 Peptone solution water flux and reverse solute flux in comparison to other organic draw agents at 200 g/L draw agent concentration [6].

CMC resulted in water flux comparable to that of peptone at similar draw agent concentrations. However, it was not feasible to test concentrations of CMC greater than 60 g/L because of solubility limits and the high viscosity of the liquid at the concentration range tested. This high viscosity indicates the testing higher CMC concentrations may have not resulted in higher flux because of the potential formation of a thick layer of viscous liquid on the FO membrane surface [31]. Furthermore, recovering the high

viscosity draw solution from the system would be a challenge for large-scale application. However, future research could test CMC as a coating on the surface of nanoparticles as draw agents. This might drastically reduce the need for high CMC concentrations, which reduces the viscosity of the draw solution, while improving the stability and the flux obtained from nanoparticle draw solute.

The Fe_3O_4 NPs resulted in overall low water flux values and as expected minimal reverse flux. However, the occurrence of random spikes in water flux that far exceeded the other organic draw agents tested is promising. It is speculated that the inconsistency of the nanoparticle draw agent results is related to high particle size polydisperisty. Future research is required to optimize the nanoparticle suspension characteristics and understand the true reasons behind the inconsistent behavior. Grafting the nanoparticles' surfaces with organic molecules that show high osmotic pressures is another area for future research to develop effective nanoparticle draw agents.

1.4.2 DLVO and Steric Interactions

The interaction energy profiles showed that electrostatically stabilized nanoparticles follow the classical colloidal DLVO behavior and demonstrates that it may be feasible to use alum for coagulation of such nanoparticles. However, jar tests need to be conducted to determine the actual coagulant dose and whether coagulant aids will be required to effectively separate these particles from the product water. On the other hand, sterically stabilized nanoparticles have high energy barriers that coagulation does not overcome with reasonable doses. This suggests that future research efforts on development of nanoparticle draw agents should focus on optimizing electrostatically stabilized

nanoparticle suspension because this will keep the opportunity of separation using coagulation practices that are typically used in drinking water plants.

1.5 CONCLUSIONS

This research investigated the performance of peptone, CMC, and Fe_3O_4 NPs as FO draw agents. The FO performance was defined by the water flux, reverse solute flux, and potential for separation from the product water. The flux and reverse solute flux were experimentally determined while the separation was studied theoretically using DLVO and steric repulsion calculations. Peptone produced reasonable water flux and low reverse solute flux in comparison with other organic draw agents reported in the literature. The high viscosity of CMC solutions made it difficult to test higher concentrations. Despite production of water flux and low reverse flux, CMC is not recommended because the high viscosity makes it challenging to use in practice as a draw agent. The Fe_3O_4 NPs produced low water flux. Occasional observation of drastically higher flux values is a promising sign. With some optimization of the nanoparticle suspension characteristics, and potentially using higher concentrations, it may be possible to produce high water flux without having reverse flux. The other potential advantage of using nanoparticles as draw agents is the possibility of using coagulation to separate the nanoparticle draw agents from the water produced.

Modelling of the nanoparticle interaction energies showed that if only electrostatic forces and vdW forces were considered aggregation was theoretically possible, but the actual doses need to be determined using a jar test. On the other hand, the DLVO predictions

showed that coagulation is not a feasible option for separation of sterically stabilized nanoparticles. Therefore, future research efforts on development of nanoparticle suspensions as FO draw agents should focus on electrostatically stabilized nanoparticles if coagulation is to be considered as an option for separation. Developing nanoparticles with low polydispersity may be the key for achieving high water flux when nanoparticles are used as FO draw agents. Simultaneous use of combination of FO draw agents has not been tested in the literature. Combining draw agents may produce synergetic effects on flux production and warrants further research.

2. Prioritization of Draw Agents for FO Applications Using Multi-Criteria Decision Analysis

2.1 INTRODUCTION

Forward osmosis (FO) is an emerging water treatment technique that has gained increasing popularity since 2000 and has been viewed as one of the most promising technologies for water treatment [32]. It has the advantage of using osmotic pressure of a draw solution as the driving force for water purification. This results in lower energy costs and membrane fouling compared to pressure-driven membrane processes like reverse osmosis (RO), ultrafiltration (UF), nanofiltration (NF), and microfiltration (MF) [32], [33]. The FO process is dependent on the presence of an osmotic pressure difference between the feed and draw solution, so selection of the proper draw agent governs the effectiveness of the FO process. An ideal draw agent would produce high water flux and low reverse draw solute flux at a relatively low cost and can be recovered using simple and cost-effective methods [34]. In recent years, a multitude of innovative draw agents with various physicochemical properties has been developed. However, there is no systematic guide to date that can be used to inform decisions on best FO draw agent(s) for further research and development and/or commercialization. Therefore, the current study aims to conduct a multi-criteria decision analysis to determine the best available FO draw agents. The outcomes of this investigation will help prioritize research and development on FO draw agents and will highlight promising draw agents for large-scale applications.

To achieve the study objective, a comprehensive literature review was conducted to gather the recent developments on FO draw agents. The draw agents identified from the review were ranked based on important FO operation and performance criteria using multi-criteria decision-making (MCDM) techniques. The literature review informed the criteria used for the ranking process. To systematically rank the draw agents, two decision support techniques were employed, the Analytic Hierarchy Process (AHP) and the Technique for Order of Preference by Similarity to Ideal Solution (TOPSIS). AHP was the method of determining the weights of each criteria and TOPSIS was the tool for ranking the alternatives (i.e, the FO draw agents) using the MCDM process.

AHP is the most widely used MCDM method that ranks alternatives in a hierarchical structure and relies on the judgement of the decision makers to make numerical comparisons of criteria using the Saaty scale [35]. The Saaty scale (Table 2.1) compares the relative importance of two criteria against one another in a pairwise matrix by assigning each criterion with a number on the scale [36].

Table 2.1 Scale of Relative Importance for Pairwise Comparison Adapted from Saaty [37]

Relative Importance Scale	Definition	Explanation
1	Equal Importance	The two alternatives contribute equally to the objective
3	Moderately	Experience and judgement slightly favor one over another
5	Strongly	Experience and judgement strongly favor one over another
7	Very strongly	Experience and judgment very strongly favor one over the other. Its importance is demonstrated in practice
9	Extremely	The evidence favoring one over the other is of the highest possible validity
2,4,6,8	Intermediate Values	Compromise between the preference in weights
Reciprocals	Opposites	Inverse comparison

A consistency ratio is calculated to check the decision-maker's judgement and should be ≤ 0.1 [37] for the weights obtained from the AHP analysis to be satisfactory. TOPSIS is hinged on the idea that the highest ranked alternative should have the shortest development distance to reach the ideal solution and the farthest from the negative ideal solution, or the Euclidean distance [38]. The AHP outcomes are used in the TOPSIS process to determine a performance index which is an indicator for the relative closeness to the ideal solution. The collective outcomes of the AHP and TOPSIS processes is a ranking of the draw agent alternatives in a preference order.

2.2 METHODOLOGY

This section details the process of the systematic ranking and prioritization of draw agents. The process began with a literature collection, analysis of draw agent

characteristics, the AHP method and calculations, and the TOPSIS ranking and calculations. This process was then evaluated for bias using a sensitivity analysis.

2.2.1 Literature Collection and Analysis

The literature review process involved the following stages: 1) defining the scope of the review, 2) searching the literature to gather the relevant studies, 3) screening the reference list of other literature reviews on FO draw agents to retrieve any relevant studies that may have been overlooked in our review, 4) extracting relevant data from the gathered studies, and 5) analyzing the data. The scope of the review was to collect all research published since 2015 on innovative FO draw agents. Figure 2.1 illustrates the process followed to accrue the studies relevant to the scope of the review. Three main databases used in this review were ScienceDirect, American Chemical Society, and Compendex. The keywords used in the search were "draw agent" and "forward osmosis." The review focused on draw agents that are dissolved or suspended in aqueous solutions and excluded polymeric hydrogels. Hydrogels are crosslinked hydrophilic polymer chains with water trapped within the network that do not dissolve in water unlike traditional draw agents that dissolve and disperse in a draw solution [39]. Hydrogels water-absorbing properties are not a result of osmotic pressure, but a phenomenon called swelling pressure [40]. Therefore, hydrogels were not considered in this study due to their different properties and measures of FO performance. Some traditional draw agents (e.g., NaCl, $MgSO_4$, $MgCl_2$, $CaCl_2$) were included in the review, despite being studied prior to 2015, for comparing the performance of the innovative draw agents to the traditional ones. Furthermore, review articles on FO draw agents within the past five

years were searched for any literature studies that were missed during this review process.

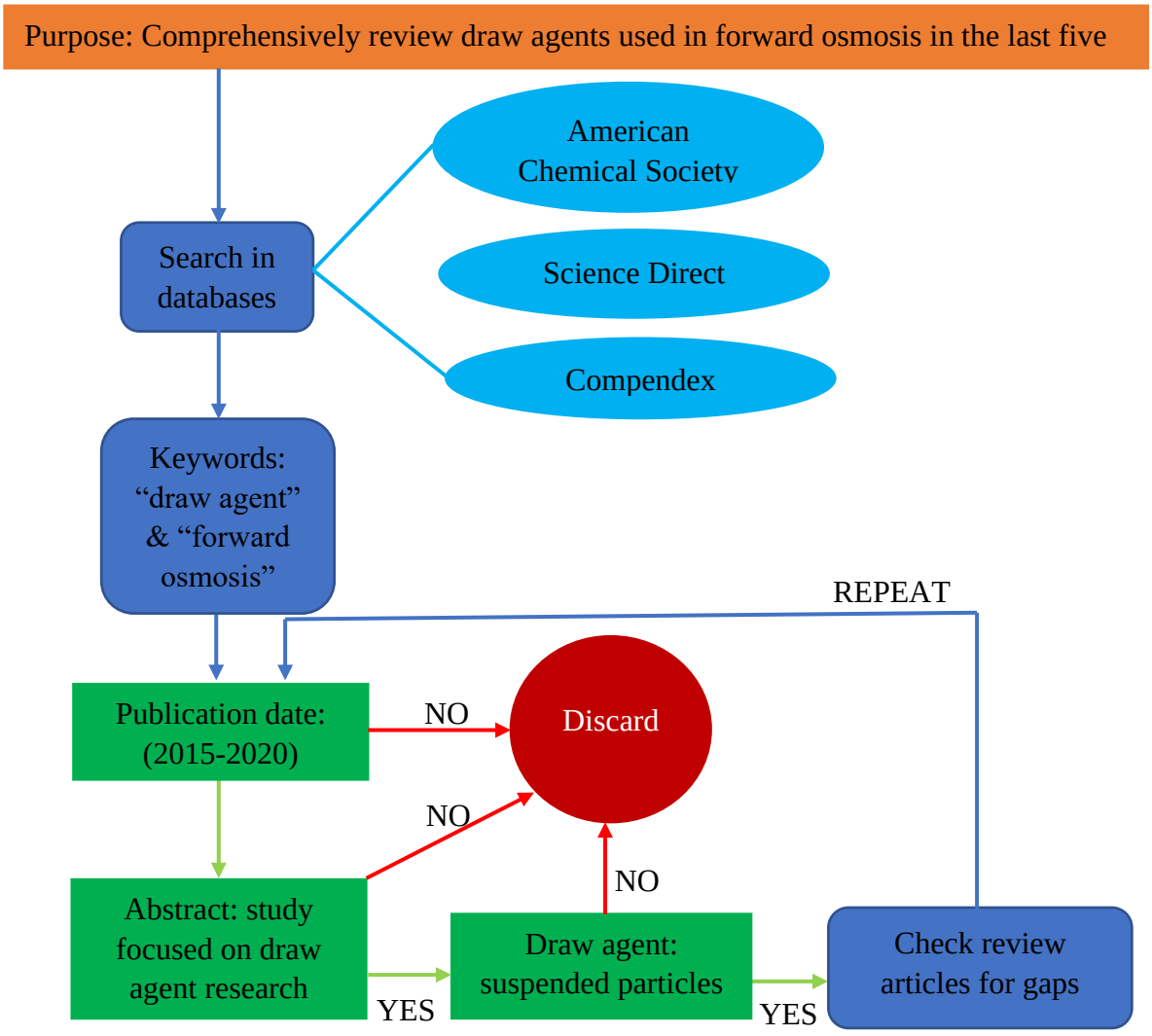

Fig. 2.1 The literature review and article selection processes.

Once the collection process was concluded, data from the studies were then extracted to create a detailed profile of each draw agent studied. Data extracted included water flux, reverse solute flux, osmotic pressure, viscosity, cost, regeneration methods and their cost, toxicity, flowrate, and membrane used. Some of the data were rarely reported in the

research articles such as replenishment cost of the draw agent. So, material cost estimates were performed to fill in gaps in some of the unreported information. The extracted data was quantitatively and qualitatively analyzed to draw some statistics about draw agents and to search for potential correlations between the characteristics of the draw agents and the performance of the FO process.

2.2.2 AHP Method

AHP was used to develop criterion weightings for the multi-criteria decision matrix process. Criteria such as flux, reverse solute flux, replenishment cost, regeneration cost, and regeneration efficacy were taken into account to achieve the goal of ranking the draw agents. The criteria were then compared against one another in a pairwise comparison matrix where variables in the rows were compared in the column (Table 2.2).

Table 2.2 Pairwise Comparison Matrix Method

Criteria	Column Variable	Column Variable	Column Variable
Row Variable	= Row/Column		
Row Variable			
Row Variable			

The comparison is based on the scale of relative importance and the judgement of the decision maker. The weighting scale used is based on the fundamental Saaty's Scale of comparative judgements (Table 2.1). The row element is compared to the column element in relative importance. Each element is then divided by the sum of each column. The weightings of each criterion are then computed by averaging the values of the row.

To minimize bias, consistency control must be conducted. The pairwise comparison was normalized by multiplying the matrix elements with the criteria weights. The weighted sum value was taken of each row by summing the elements and dividing by the criteria weight. λ_{max}, or the eigenvalue was computed by averaging each row's weighted sum value and criteria weights ratio. The consistency index (CI) (Eq. 2.1) was then computed and used along with the random index (Table 2.3), to calculate the consistency ratio (CR) (Eq. 2.2). The CR must be less than 0.1 to meet the limit of consistency.

$$CI = \frac{\lambda_{max} - n}{n-1} \tag{2.1}$$

Table 2.3 Random Index (RI) [41]

Matrix Size	Random Index (RI)
1	0.00
2	0.00
3	0.58
4	0.90
5	1.12
6	1.24
7	1.32

$$CR = \frac{CI}{RI} \tag{2.2}$$

2.2.3 TOPSIS Method

The TOPSIS method followed the sequential steps below:

(1) Values for each criterion consisted of the actual data retrieved from the studies for that criterion. If the criterion was not numeric (e.g., regeneration efficacy), linguistics values were converted to a rank based on a 5-point scale.

(2) The normalized pairwise matrix was calculated using Equation 2.3.

$$\bar{x}_{ij} = \frac{x_{ij}}{\sqrt{\sum_{i=1}^{n} {x_{ij}}^2}} \tag{2.3}$$

Where, x_{ij} is the row element and n is the number of elements in the row.

(3) The weighted normalized matrix is then calculated by multiplying the weights of the criteria obtained from the AHP using Equation 2.4.

$$v_{ij} = \bar{x}_{ij} \times w_j \tag{2.4}$$

Where, w_j is the weight of the criteria, and v_{ij} is the value of the normalized element.

(4) Then the positive and negative ideal solutions were determined with the beneficial and non-beneficial criteria respectively (Equations 2.5 and 2.6). The positive ideal solution maximizes the beneficial criteria and minimizes the non-beneficial criterial, while the negative ideal solution minimizes the beneficial criteria and maximizes the non-beneficial criteria [42]. A criteria is defined as beneficial when the criteria is desirable at higher values (e.g. flux) while a criteria is defined as non-beneficial when the criteria is non-desirable at higher values (e.g. reverse flux). Flux and regeneration efficacy were considered beneficial criteria, while reverse flux, replenishment cost, and regeneration cost are non-beneficial criteria.

$$v_j^+ = (v_1^+, v_2^+, \ldots, v_n^+) = (max v_{ij}) \tag{2.5}$$

$$v_j^- = (v_1^+, v_2^+, \ldots, v_n^+) = (min v_{ij}) \tag{2.6}$$

Where, v_j^+ and v_j^- are the positive ideal and negative ideal solution, respectively.

(5) The Euclidean distance from the positive and negative ideal solution were then calculated using Equations 2.7 and 2.8.

$$S_i^+ = \left[\sum_{j=1}^{m}(v_{ij} - v_j^+)^2\right]^{0.5} \quad (2.7)$$

$$S_i^- = \left[\sum_{j=1}^{m}(v_{ij} - v_j^-)^2\right]^{0.5} \quad (2.8)$$

Where, S_i^+ is the Euclidean distance from the ideal best solution and S_i^- is the Euclidean distance from the ideal worst solution.

(6) The performance index, or relative closeness to the ideal solution, was calculated using Equation 12.

$$P_i = \frac{S_i^-}{S_i^+ + S_i^-} \quad (2.9)$$

(7) The draw agents were ranked by decreasing order. The best alternative has the shortest distance from the positive ideal solution and the farthest distance from the negative ideal solution [43].

2.2.4 Sensitivity Analysis Method

Assumptions have been made throughout the MCDM process. Those assumptions were made to fill in gaps when the data required for completing the MCDM process were not reported in the studies. Additionally, assumptions were made to generate the pairwise comparison matrix that is needed for determining criteria weights using the AHP method.

2.2.4.1 Viscosity Assumptions

Missing viscosity values were replaced with 5 cP, which is based on the distribution of viscosity values reported in the collected studies. To ensure that these assumed values did not have an effect on the overall ranking of the draw agents, a sensitivity analysis was performed. The assumed viscosity values were evaluated by the change in the top 10

ranking of draw agents when the viscosity values were included as a criteria and not included in the matrix itself.

2.2.4.2 Reverse Flux Assumptions

Missing reverse solute flux values were replaced with 5 $g/m^2 \cdot h$ (gMH). This is the average value based on the distribution of reverse flux values from the data set. A sensitivity analysis on the reverse flux values was performed by comparing the change in ranking of the top 10 draw agents (based on 5 gMH reverse solute flux) when the reverse flux values were assumed to be the minimum value, the maximum value, and the average value.

2.2.4.3 Weightings Assumptions

Weightings were based on the judgement of the author. To evaluate any judgement bias, a sensitivity analysis was performed on the weightings used from the AHP and its effect on changing the ranking of the draw agents obtained using the original weights. The weightings of each criteria from the AHP were tested within a range and the effects of the rankings were evaluated (Table 2.4).

Table 2.4 Criteria weighting ranges tested in sensitivity analysis

Criteria	**Flux**	**Reverse Flux**	**Replenishment Cost**	**Regeneration Cost**	**Regeneration Efficacy**
Original Weighting	45%	19%	12%	14%	10%
Weighting Sensitivity Range	30-70%	10-50%	10-50%	10-50%	10-50%

2.3 RESULTS

The draw agent characteristics resulting from the literature review were presented in this section using statistical relationships to characteristics to compare against one another in the MCDM. These results further informed the AHP weighting results and final TOPSIS ranking. The sensitivity analysis altering different draw agent characteristics compared and characteristic weightings were also presented in this section.

2.3.1 Literature Review Results

From the forty-six articles collected, thirty-five of the articles were further analyzed to determine the criteria the draw agents would be ranked against. The published review articles showed three distinct categories of draw agents that researchers studied, inorganic compounds, organic compounds, and functional nanoparticles [32], [44]. The studies from the year 2015 to 2020 showed that the majority of research investigated organic draw agents, followed by inorganic compounds, and functional nanoparticles (Figure 2.2). Organic compounds investigated include switchable polarity solvents, polymers, polyelectrolytes, and general organic compounds (e.g. ethanol and wheat straw).

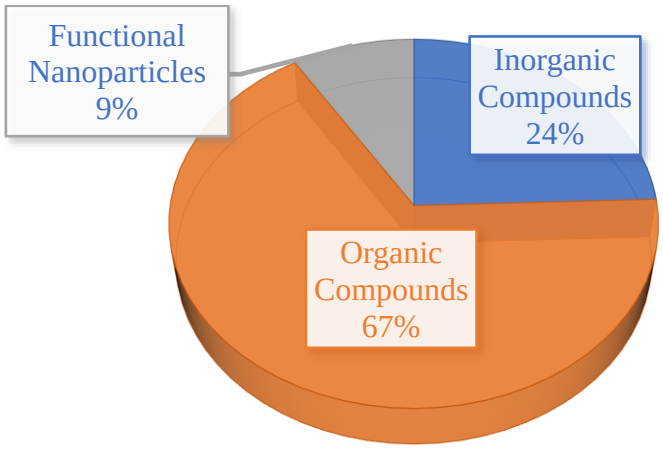

Fig. 2.2 Percentages of draw agents reviewed in each category.

The draw agents were further classified by their separation and regeneration methods. Organic compounds were regenerated mainly by membrane distillation, nanofiltration, and phase separation (Figure 2.5). Inorganic compounds were mainly separated through nanofiltration and chemical precipitation. Functional nanoparticles were usually magnetic and separated using a magnetic field to regenerate the draw agent (Figure 2.3).

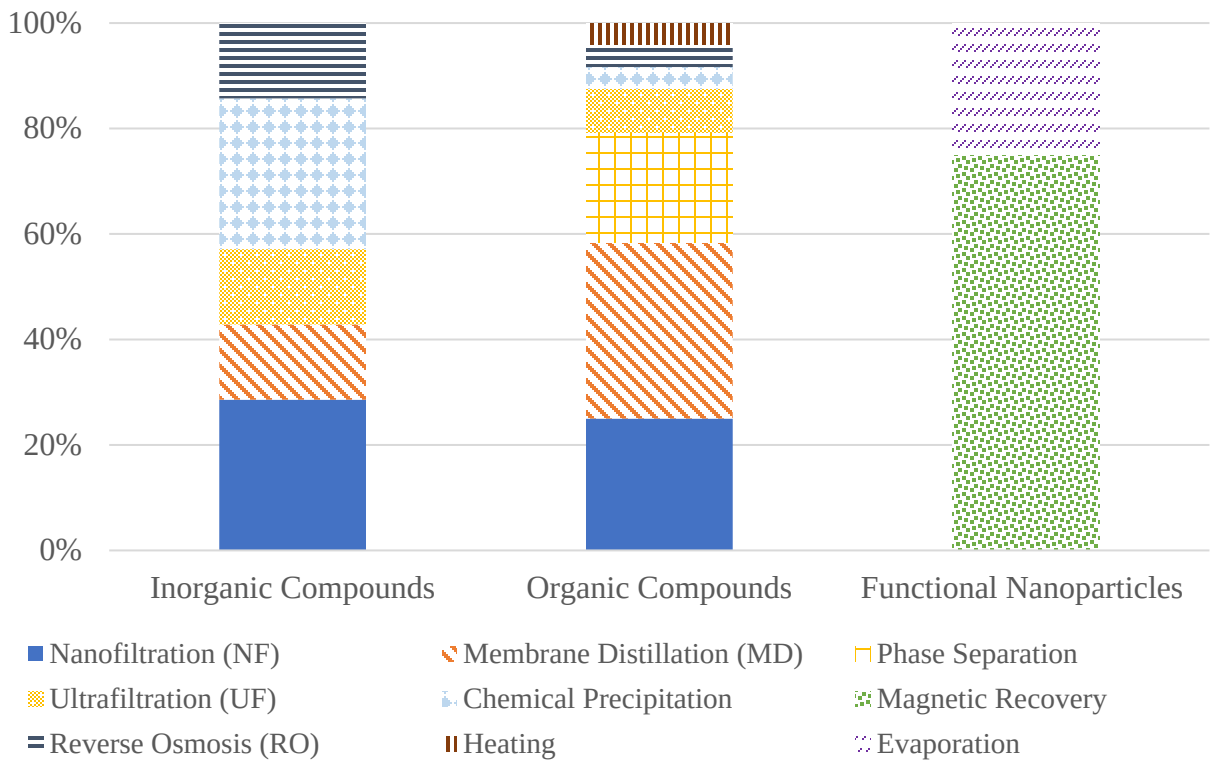

Fig. 2.3 Separation and regeneration methods of each reviewed draw agent in their category.

From these studies, experiments that used DI as their feed solution were further analyzed for fair comparison between draw agent effectiveness. Table 2.5 shows the flux, reverse draw solute flux, osmotic pressure, viscosity of the draw agent solution, replenishment cost (i.e., cost of draw agent), and regeneration method cost and efficacy for these studies in this review.

Table 2.5 Characteristics of draw agents tested against DI as the feed solution

	Draw Agent	Flux (LMH)	Reverse Flux (gMH)	Osmotic Pressure (bar)	Viscosity (cP)	Cost ($/kg)[a]	Regeneration	Source
Innovative Draw Agents	sodium carboxymethyl dextrans (CM-dextran-1000)	24.9	0.97	65	NR	1,990	NA	[45]
	Cationic Starch	4.10	1.62	12	70	721	UF	[46]
	Poly(propylene glycol) and non-ionic surfactant (PPG-725/TX-114)	10.0	0.18	50	8	3,752	MD	[47]
	Chlorhexidine gluconate based mouthwash (CMW)	14.0	0.98	67	2.2	148	MD	[48]
	diethylenetriamine pentakis(methylphosphonic) sodium salt (DTPMP-Na)	27.5	1.00	110	11.6	1,401	NF	[49]
	tetraethylenepentamine heptakis-(methylphosphonic) sodium salt (TPHMP-Na)	54.0	0.64	120	19.6	1,200		
	polyethylenimine (methylenephosphonic) sodium salt (PEI-600P-Na)	48.0	0.60	121	40	1,827		
	PEI-1800P-Na	17.5	0.4	170	73.8	1,617		
	thermo-sensitive polyelectrolyte of poly(N-isopropylacrylamide-co-acrylic acid) (PNA)	2.09 2.95	NR[b] NR	12 72	7.4 53.2	2,813	Heating	[50]
	Hydrolyzed poly(isobutylene-alt-maleicacid) (PIAM-Na)	34.0	0.20	42	7.4	203	MD	[51]
	Tetraethylammonium bromide ([N2222]Br)	10.6	23.7	21	NR	217	MD	[52]
	choline chloride-ethylene glycol (CC-EG)	3.60	0.098	370	33	18,362	Phase Separation	[53]
	potassium functionalised carbon nanofibers suspended in triethylene glycol (TEG-K/CNF)	13.3	0.25	70	NR	5,800	Evaporation	[54]
	4-Butylmorpholine (BuMP)	2.09	14.0	3	7.06	52,250	Phase separation	[55]
	4-cyclo-pentylmorpholine (CPMP)	1.98	2.53	11	1.64	4,440		
	Polypropylene glycol (PPG400)	3.64	19.0	11	6.64	108		
	1,4-piperazinediethanesulfonic acid disodium salt (P-2SO3-2Na)	76.4	8.3	122	3.20	4,402	MD	[56]
	Ethanol	17.0	240	47	NR	66	MD	[57]
	Pretreated and enzymatically Hydrolysed Wheat Straw (PHWS)	6.21	NA	43	NR	11	Direct Recovery	[58]
	SSP[c]	16.3	0.53	44	14	1,380	Precipitation	[59]
	PSSP5[c]	14.5	0.14	44	25	2,909		
	PSSP6[c]	13.7	0.08	41	30	2,909		
	PSSP11[c]	13.1	0.05	35	75	2,909		
	Polydiallyldimethylammonium Chloride (PolyDADMAC)	10.5	NA	16	7.2	1,021	NF	[60]

DADMAC	20.0	NA	51	1.2	99		
Glauber salt (sodium sulfate decahydrate, Na2SO4·10H2O)	7.03	0.42	96	1.3	152	NF	[61]
SiPEG-MN	2.13	NA	8	NR	31,354	Magnetic Recovery	[62]
NaCl and Oleic Acid (OA)	1.10	0.30	NR	NR	598	NR	[63]
NaCl and Sodium dodecyl benzene sulfonate (SDBS)	10.2	2.10	NR	0.88	386		
NaCl and Potassium Oleate (PO)	10.7	2.00	NR	0.91	935		
NaCl and Sodium Dodecyl Sulfate (SDS)	9.30	2.20	NR	0.93	1,023		
NaCl and Polyoxyethylene lauryl ether (Brij35)	6.90	1.60	NR	0.87	611		
NaCl and Polyethylene glycol tert-octylphenyl ether (Triton X-100)	8.00	2.20	NR	0.88	149		
1-cyclohexylpiperidine (CHP)	22.0	4.00	507	NR	3,526	Phase Separation	[64]
PSS (70,000)[d]	18.2	5.50	NR	1014	2,768	UF	[65]
PSS (200,000)[d]	13.0	9.20	NR	15000	112		
PSS (1,000,000)[d]	11.8	5.90	NR	537.9	3,453		
Poly (aspartic acid sodium salt) (PAspNa)	31.8	4.00	52	4.5	965,500	NF MD	[66]
hydrolyzed polyacrylamide (HPAM)	3.20	NA	8	180.4	13,900	Cleaning[e]	[67]
poly(sodium acrylate) polymer poly(N-isopropylacrylamide) (PSA–PNIPAM)-coated MNPs	11.7	NA	25	NA	30,185	Magnetic Separation	[68]
trimethylamine–carbon dioxide (TMA–CO2)	33.4	11.8	49	1.04	77	Phase Separation	[69]
ethylenediamine tetrapropionic (EDTP) acid (salt)	22.7	0.32	118	4.95	3,404	NF	[70]
protonated betaine bis(trifluoromethylsulfonyl)imide ([Hbet][Tf2N])	2.27	NR	NR	NR	5,330	Phase Separation	[71]
Branched PEI (Mw =25,000 Da)	11.0	1.01	19	25.98	543	NF	[72]
Triton X100 coupled to Na3PO4	5.68	0.13	38	1.63	1,230	UF-NF	[73]
High charge Na3PO4	12.5	0.84	13	1.2	46	MD	[74]
triethylenetetramine hexapropionic acid sodium (TTHP-Na)	23.1	0.75	133	12.37	13,649	NF	[75]
ethylenediaminetetraacetic acid (EDTA-2Na) coupled with nonylphenol ethoxylates (NP7)	8.80	0.07	59	1.2	378	NF	[76]
polyelectrolyte salt-poly (4-styrenesulfonic acid-co-maleic acid) sodium - P(SSA-co-MA)-Na-1	15.0	0.04	33	6.75	184	NF	[77]

Traditional Draw Agents	Ammonia Carbon Dioxide (NH_4-CO_2)	36.0	10.8	48	1	495	Thermal separation	[69]
	Sodium Chloride (NaCl)	40.0	22.2	4.01	1	99	RO	[69]
	Magnesium Sulfate ($MgSO_4$)	5.54	1.20	28	NR	284	RO	[78]
	Potassium Bicarbonate ($KHCO_3$)	10.1	2.00	42	NR	256	RO	[78]
	Sodium Bicarbonate ($NaHCO_3$)	8.89	1.70	28	NR	104	RO	[78]
	Sodium Sulfate (Na_2SO_4)	9.22	3.10	42	NR	141	RO	[78]
	Ammonium Sulfate ($(NH_4)_2(SO)_4$)	9.86	3.60	42	NR	159	RO	[78]
	Potassium Sulfate (K_2SO_4)	9.07	3.70	28	NR	496	RO	[78]
	Magnesium Chloride ($MgCl_2$)	9.72	5.60	42	NR	129	RO	[78]
	Calcium Nitrate ($Ca(NO_3)2$)	10.7	6.60	42	NR	289	RO	[78]
	Ammonium Chloride (NH_4Cl)	13.0	10.2	42	NR	226	RO	[78]
	Calcium Chloride ($CaCl_2$)	11.6	9.50	42	NR	265	RO	[78]
	Potassium Chloride (KCl)	13.5	15.3	42	NR	199	RO	[78]
	Ammonium Bicarbonate (NH_4HCO_3)	10.3	20.6	42	NR	216	RO	[78]
	Potassium Bromide (KBr)	12.9	29.2	42	NR	357	RO	[78]

Notes: [a]Replenishment costs calculated from vendors in Appendix(). [b]NR = not reported. [c]SSP = tetrabutylphosphonium styrenesulfonate, PSSP# = oligomeric poly(tetrabutylphophonium strenesulfonate (# = number of monomer units in the oligomer), [d]PSS# = poly (sodium4-styrenesulfonate) (# = molecular wgts), [e]Physical cleaning of the membrane

Characteristics that were observed from literature for optimal draw agent selection include high water flux and low reverse solute flux, which ultimately depend on draw agent properties such as high osmotic pressure and low viscosity. In general, high osmotic pressure was desired because it indicated higher water flux. Lower viscosity would indicate less internal concentration polarization (ICP) which would have less membrane fouling and thus, higher flux [63]. Other factors that would play a role in draw agent selection would be economic factors such as low replenishment cost, low regeneration cost, and higher regeneration efficacy. Regeneration efficacy was also desired since the initial osmotic pressure could be restored more efficiently reducing replenishment costs [79].

To further guide draw agent selection, other factors were gathered from the studies such as toxicity, feed solution, applications in research or industry, and operating conditions.

Toxicity was measured differently across each study with some using lethal dose, 50% (LD_{50}), biodegradability, or an MTT assay [46], [51]. Depending on the application in research or industry, FO performance was assessed with feed solutions such as dye wastewater, radioactive waste, tannery wastewater, or wastewater treatment [53], [80], [81]. As mentioned previously, comparison with FO performances of other draw agents tested with DI as their feed solution would not be a fair one. The osmotic pressure difference between a draw and a feed solution other than DI would result in less water flux and greater membrane fouling. However, these draw agents' properties were still reviewed but were not included in the MCDM process.

Operating conditions such as membrane type, membrane orientation mode, and flowrate can also affect the FO process performance. Membrane variability and utilization were tested in several studies for water flux and reverse solute flux. Variations in studies compared mainly CTA membranes or thin-film composite (TFC) membranes in either FO or PRO mode. However, carbon nanotube membranes or in house-made membranes, such as TFC membranes coated on a poly(ether sulfone) (PES) support layer [56], were tested as well. Flowrate was also tested in studies to achieve optimal FO performance. These additional characteristics other than draw agent properties, costs, or regeneration were analyzed for correlations to test if they were criteria that would affect the ranking process.

Water flux was plotted as a function of operating conditions (e.g., osmotic pressure and flow rate) or reverse solute flux to check for possible correlations between these

parameters and water flux (Figures 2.4 – 2.7). It is noted that these plots were only created for studies that used DI as the feed solution.

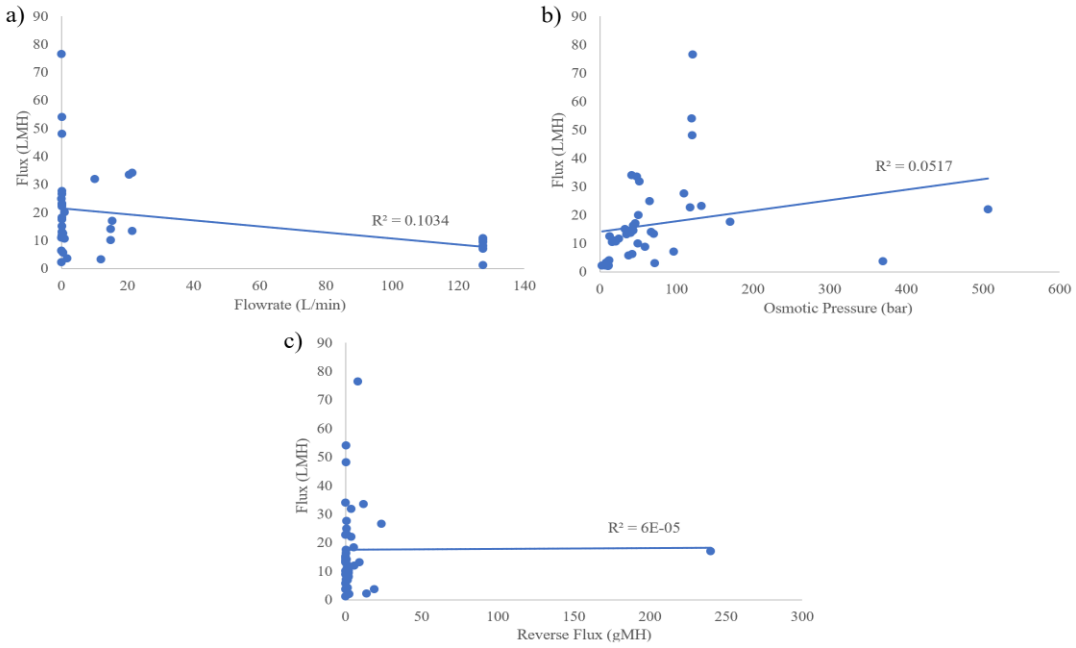

Fig. 2.4 Relationships of a) flowrate, b) osmotic pressure, and c) reverse flux against flux.

Figure 2.4 a shows a slight negative relationship between water flux and flowrate, favoring a lower flowrate for higher more desirable flux. Flux is reduced in the FO process due to a reduction of the osmotic pressure across the FO membrane due to internal fouling which is a phenomenon called concentration polarization (CP) which previous studies have shown can be decreased or increased depending on the flow rate [82], [83], [84]. There are four general categories of CP: concentrative internal concentration polarization (CICP), dilutive concentration polarization (DICP), concentrative external concentration polarization (CECP), and dilutive external concentration polarization (DECP). ICP is when fouling takes place in the porous support layer, while external concentration polarization (ECP) occurs on the surface of the active

layer. DECP and CICP occur when the membrane is in the PRO mode, while CECP and DICP occur while the membrane is in the FO mode. It was also reported that CICP could be mitigated by increasing the feed solution flow rate, and DICP was increased by increasing the draw solution flow rate [82]. Since the relationship between flux and flowrate may have been influenced by other methodology variability between studies such as membrane type and membrane orientation mode, these relationships were further analyzed by fixing the FO membranes used in the studies and the membrane orientation mode (Fig 2.5).

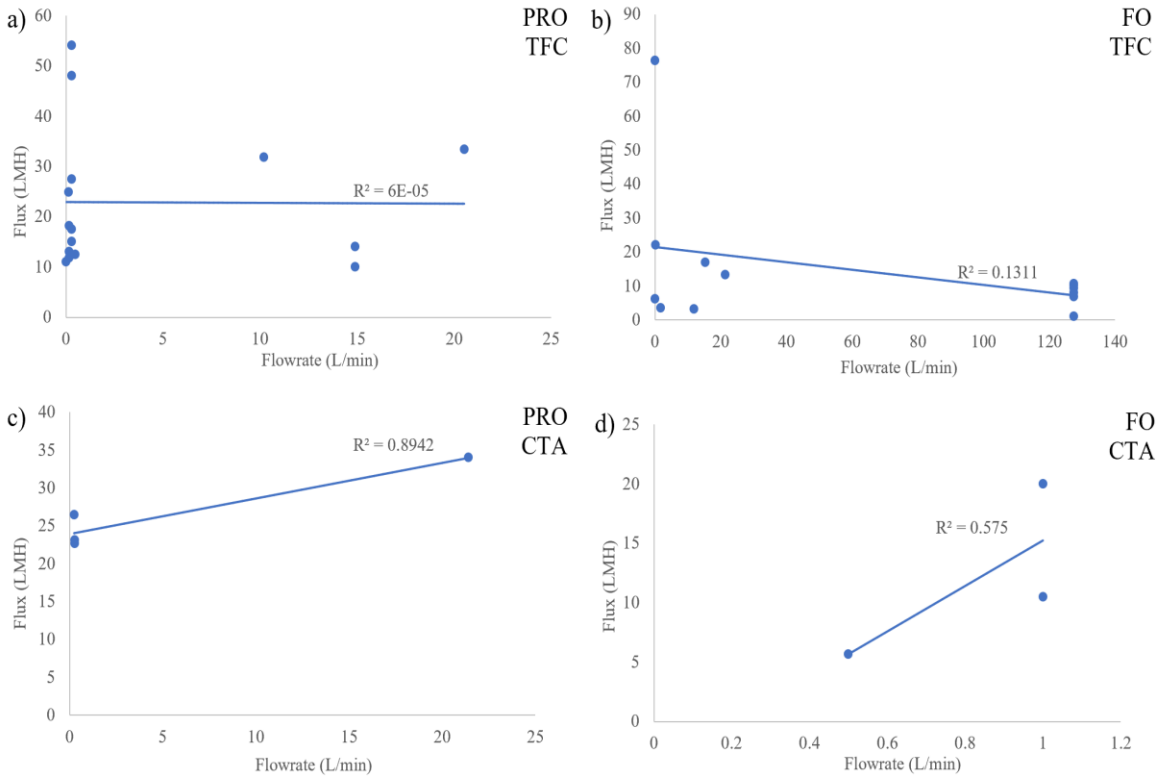

Fig. 2.5 Flowrate versus flux differentiated by membrane type and modes.

Figure 2.5 illustrated that the modes influenced water flux but depended on the type of membrane used. Studies on FO membrane showed that generally TFC membranes in PRO mode resulted in higher salt rejection and higher water flux than CTA membranes

[85], [86], but other factors such as the manufacturing method of the membrane mattered in the membrane characteristics such as size exclusion or surface charge. From Figure 3.4, both TFC membranes in PRO and FO modes showed a slight negative relationship between flux and flowrate while for CTA membranes in PRO and FO modes there was a positive relationship. TFC membranes showed that higher flowrates resulted in lower flux, while for CTA membranes, higher flowrates resulted in higher flux. So, for the CTA membranes in PRO mode, CICP was possibly reduced with a higher flow rate and increased flux. The TFC membranes in FO mode had a higher flux at a lower flow rate indicating that DICP could have been reduced. However, separate feed and draw solution flow rates were not reported for the studies, so other factors may have played a role in these results.

Osmotic pressure and flux showed a weak positive correlation. Figure 2.6, categorized the osmotic pressure relationship with flux based on membrane type, CTA or TFC. However, this differentiation still showed a weak correlation between the two variables. In a study by Yasuka, neutral polymers' increase in osmotic pressures did not have much effect on the flux [87]. Since a majority of the draw agents reviewed were organics, this might have been a reason that osmotic pressure did not result in a trend with flux.

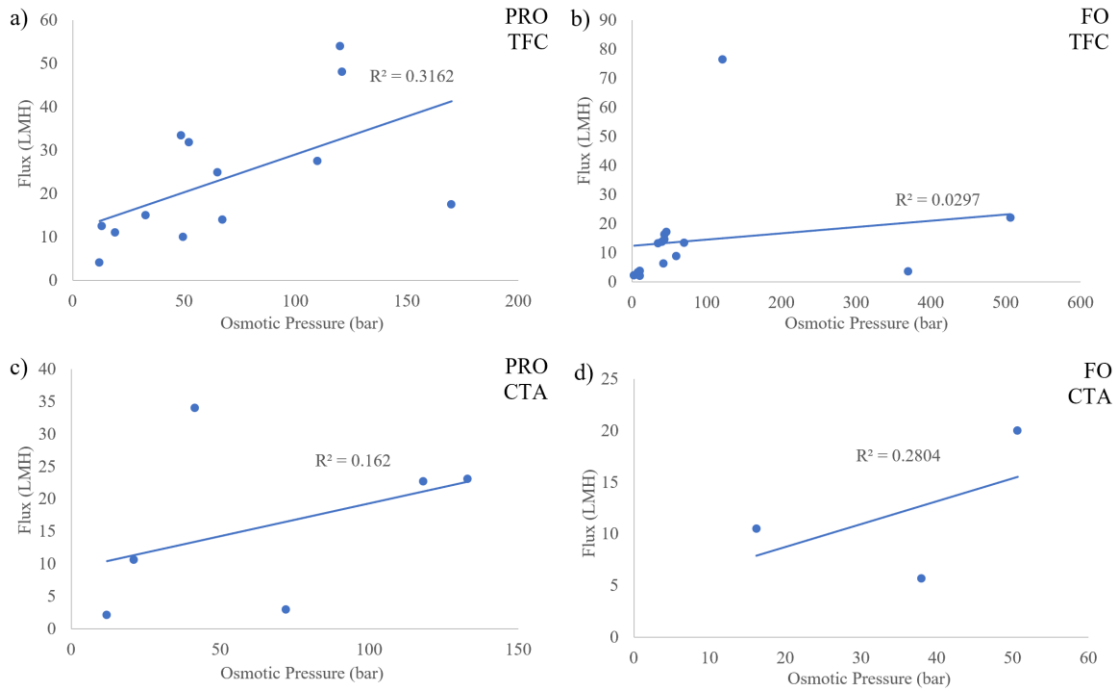

Fig. 2.6 Osmotic pressure versus flux differentiated by membrane type and modes.

Figure 2.7 compared flux and reverse flux taking into account membrane and membrane orientation mode. No correlation was found between these variables and showed that one cannot predict the other.

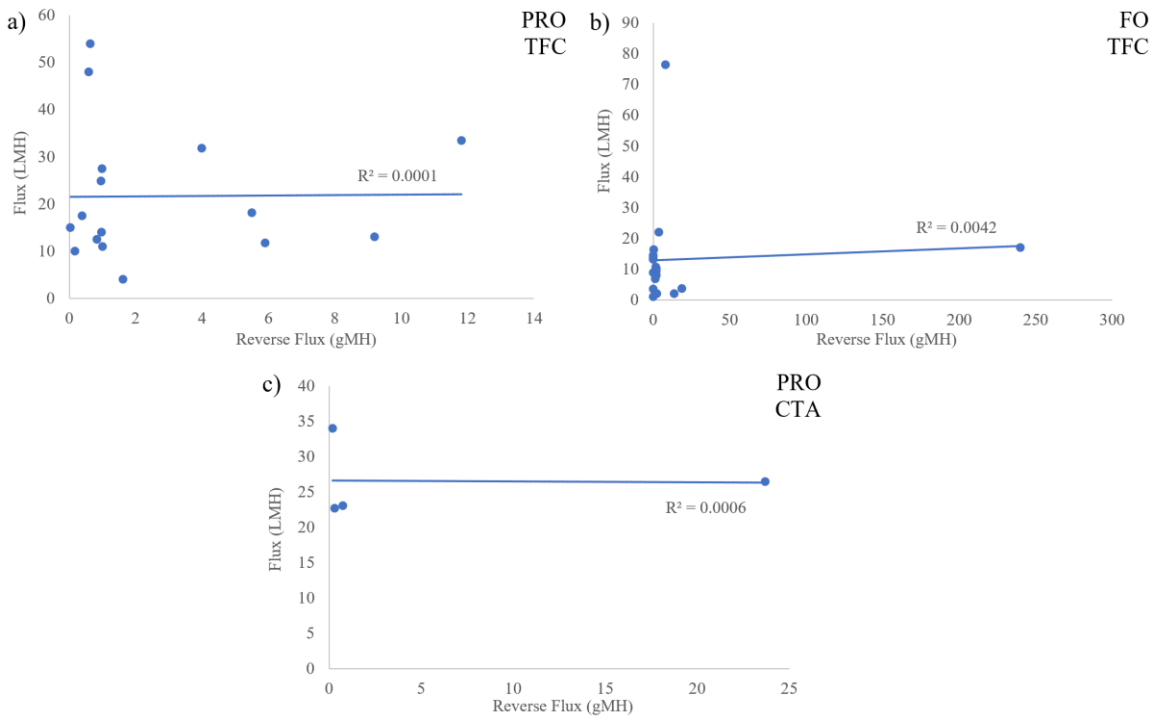

Fig. 2.7 Reverse flux versus flux differentiated by membrane type and modes.

The weak correlations observed in Figure 2.4-2.7 may indicate that the chemical properties of the draw agent play a major role in determining the magnitude of flux that it generates. For example, osmotic pressure alone may not be a sufficient indicator for the magnitude of flux that a draw agent produces. Furthermore, these analyses indicate that linearly examining the relationship between draw agent properties and experimental methods is not sufficient in predicting FO performance. Ranking these draw agents would require accounting for and cross-examining multiple parameters. To achieve this goal, multi-criteria decision-making analysis was performed herein.

2.3.2 MCDM Results

2.3.2.1 AHP Results

Identified criteria from the literature review were used to construct the pairwise comparison (Table A.5). The completed pairwise comparison matrix using Saaty's scale in Table 2.6 showed the relative importance of each parameter in comparison with one another. For example, the row variable flux compared to the column variable reverse flux had a relative importance of 5 indicating that the flux criteria was five times more, or more strongly, important than reverse solute flux.

Table 2.6 Pairwise Comparison Matrix

Criteria	Flux	Reverse Flux	Replenishment Cost	Regeneration Cost	Regeneration Efficacy
Flux	1	5	3	3	3
Reverse Flux	0.2	1	2	2	2
Replenishment Cost	0.33	0.5	1	1	1
Regeneration Cost	0.33	0.5	1	1	2
Regeneration Efficacy	0.33	0.5	1	0.5	1

The main criterion of importance taken into consideration when ranking the draw agents is water flux since that was the FO performance's goal. Water flux is then followed by reverse flux which for an ideal draw agent would be minimal. Regeneration cost would then have a higher relative importance compared to replenishment cost since regeneration would be a reoccurring rather than a single cost. Cost considerations are then followed by regeneration efficacy. This relative importance ranking is further reflected by the final weights in Table 2.7. The weights had a consistency ratio which was below 0.1 that met the desired level of consistency. These were used as the final weightings in the TOPSIS method to determine the ranking of the draw agents.

Table 2.7 Final criteria Weights and Consistency Ratio

Criteria	Weight %
Flux	45%
Reverse Flux	19%
Replenishment Cost	12%
Regeneration Cost	14%
Regeneration Efficacy	10%
CR	**0.05**

2.3.2.2 TOPSIS Results

The numerical values of water flux, reverse solute flux, and replenishment cost values were used for the TOPSIS analysis. Reverse flux was not reported in some of the studies, so an assumption of 5 gMH was made for the missing data as previously discussed in Section 2.3.2. Regeneration cost, or the cost to separate and regenerate the draw agent was not reported in most of the studies. So, regeneration cost and efficacy was ranked on a scale of 1-5 based on general cost information reported in literature, with rank 5 being the highest and 1 being the lowest cost or efficacy (Table 2.8).

Table 2.8 Converted Regeneration Methods to Numerical Ranking

Regeneration Cost Ranking		Regeneration Efficacy Ranking	
Rank	Separation Technology	Rank	Separation Technology
5	Reverse Osmosis (RO)	5	Reverse Osmosis (RO)
4	Membrane Distillation (MD)	4	Nanofiltration (NF)
3	Ultrafiltration (UF)	3	Ultrafiltration (UF)
3	Nanofiltration (NF)	3	Membrane Distillation (MD)
3	Heating	3	Phase Separation
3	Phase Separation	3	Chemical Precipitation
2	Magnetic Recovery	2	Magnetic Recovery
2	Chemical Precipitation	2	Heating
1	Evaporation	1	Evaporation

Appendix B, Tables 7, 8, and 9 details the normalized matrix, the weighted normalized matrix, the Euclidean distances from the ideal best and worst, the performance index, and the final ranking. The ranking pattern for the top 10 draw agents from this analysis (Table 2.9) indicates that most draw agents that ranked highly were organic and inorganic compounds. Of the inorganic compounds, only two were traditional draw agents, NaCl and NH_4-CO_2, which was ranked fourth and fifth respectively.

Table 2.9 Final TOPSIS Ranking

Ranking	Draw Agent	PI
1	1,4-piperazinediethanesulfonic acid disodium salt (P-2SO_3-2Na)	0.95
2	tetraethylenepentamine heptakis-(methylphosphonic) sodium salt (TPHMP-Na)	0.81
3	polyethylenimine (methylenephosphonic) sodium salt (PEI-600P-Na)	0.76
4	Sodium Chloride (NaCl)	0.69
5	Ammonia Carbon Dioxide (NH_4-CO_2)	0.68
6	Hydrolyzed poly(isobutylene-alt-maleicacid) (PIAM-Na)	0.67
7	trimethylamine–carbon dioxide (TMA–CO_2)	0.66
8	diethylenetriamine pentakis(methylphosphonic) sodium salt (DTPMP-Na)	0.63
9	sodium carboxymethyl dextrans (CM-dextran-1000)	0.62
10	triethylenetetramine hexapropionic acid sodium (TTHP-Na)	0.61

The distribution of performance indexes showed a skewness towards the right (Fig. 2.8). This further indicates that P-2SO_3-2NA was by far the highest ranked draw agent. The

rest of the top 10 ranking draw agents were also above the median and average of 0.55 and 0.57 respectively. So, these top ranked draw agents were found best with performance indexes higher than 0.61.

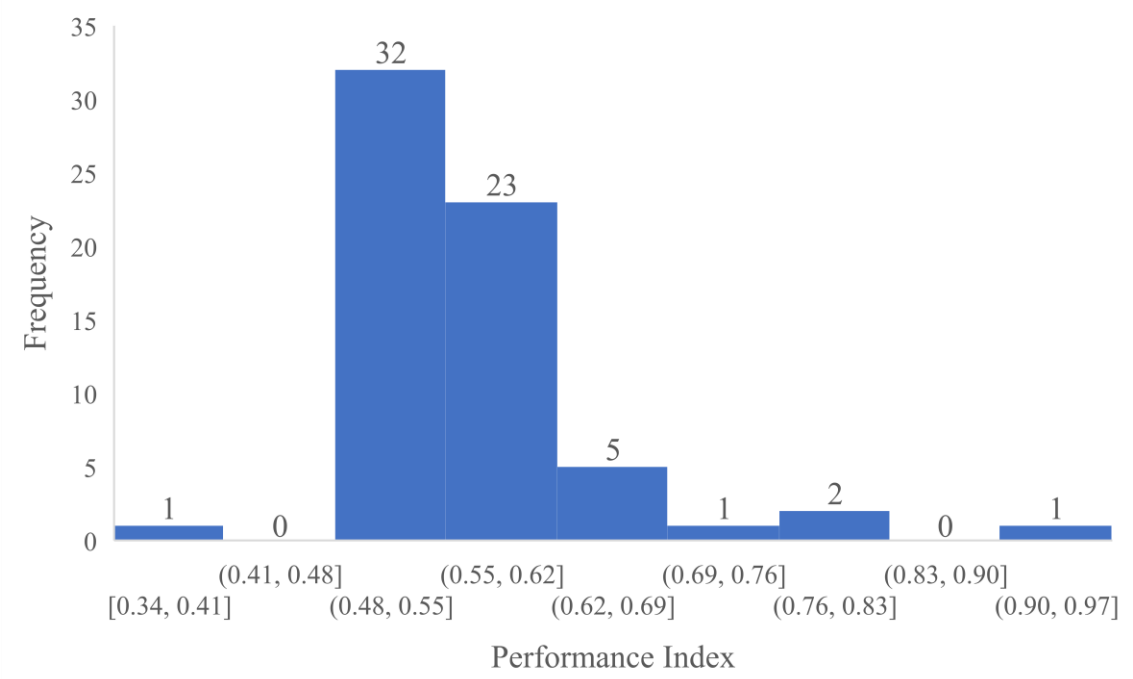

Fig. 2.8 Distribution of the performance indexes for the all the draw agent ranked.

2.3.3 Sensitivity Analysis Results

A sensitivity analysis was performed on the assumptions made from disregarding viscosity as an evaluation criteria, assuming missing reverse flux data, and judgement on weightings to assess the robustness of the ranking recommendation.

2.3.3.1 Viscosity Assumptions

Viscosity was initially included in the AHP and TOPSIS analysis with a criteria weighting of 6% and on the scale of relative importance it was ranked last since it was

not expected to affect overall FO performance or costs (Figure 2.9). This was compared with the original weighting used in the analysis that did not include viscosity.

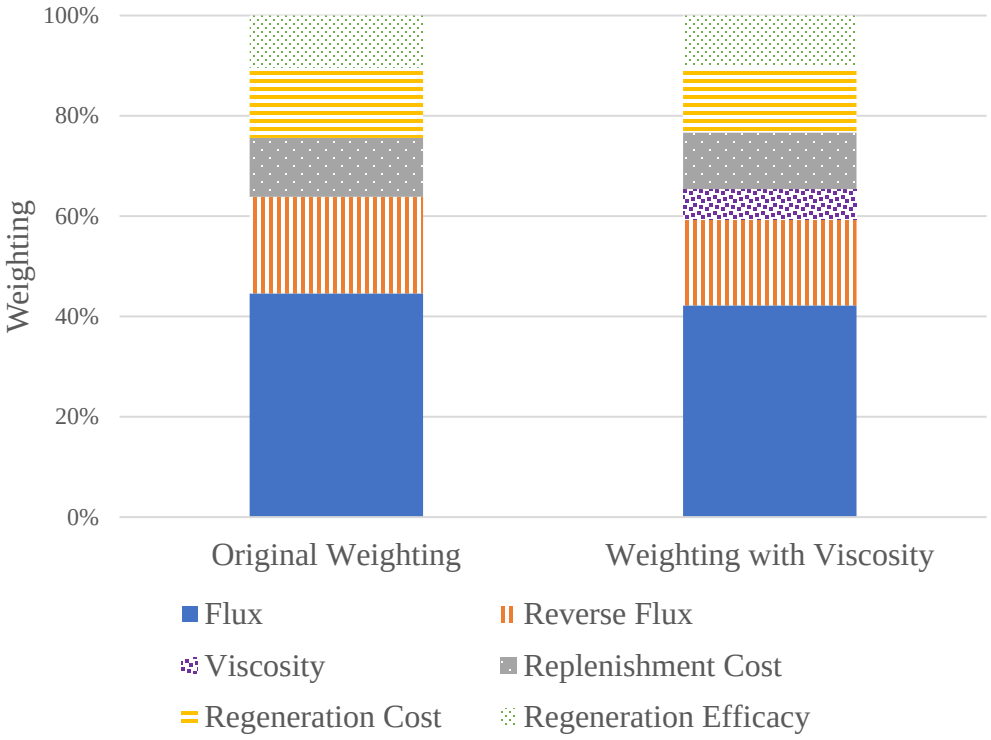

Fig. 2.9 Weightings of criteria with and without viscosity.

The top 10 ranking draw agents remained the same with the addition of viscosity as one of the criteria. So, removing viscosity did not have an effect on the ranks of draw agents.

2.3.3.2 Reverse Flux Assumptions

The original AHP and TOPSIS analyses assumed a reverse flux value of 5 gMH for non-reported data. A sensitivity analysis of this assumption required changing the reverse flux values to the minimum, average, and maximum reverse flux values of the draw agents reviewed, or 0.04 gMH, 9.34 gMH, and 240 gMH, respectively. The top 10 rankings remained the same for all three values in comparison to the original TOPSIS analysis

performed. So, the assumption of 5gMH was appropriate for the ranking recommendations.

2.3.3.3 Weightings Assumptions

The AHP weightings based on the judgement made by the author about relative importance of the evaluation criteria was tested by changing the weightings individually of each criteria within a certain range. Excess weighting was evenly distributed to the other criteria (Figure 2.10). For instance, when the water flux criteria weighting was changed from the original weighting of 44.6% to 30%, the difference of 14.6% was evenly distributed to the other criterion. This added about 3.8% of weighting to each of the other criteria. Water flux weighting fluctuated within a range of 30-70% and reverse solute flux, replenishment cost, regeneration cost, and regeneration efficacy fluctuated within a range of 10-50%.

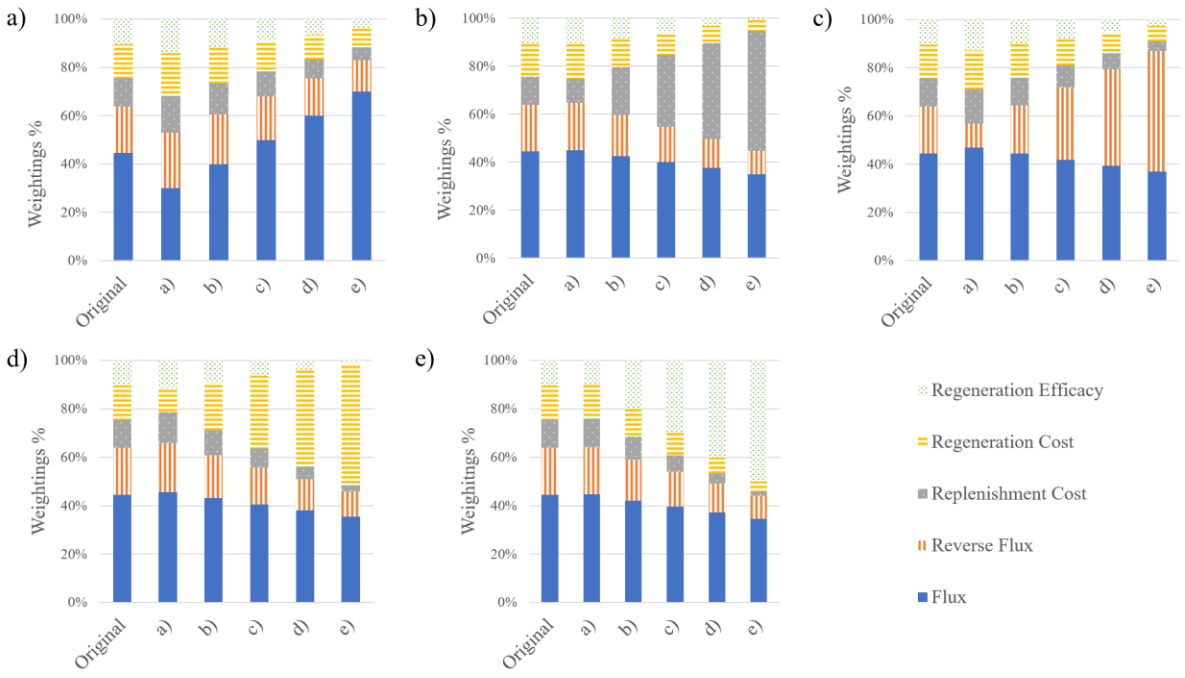

Fig. 2.10 Weightings sensitivity analysis with weightings changed within range for a) flux, b) replenishment cost, c) reverse flux, d) regeneration cost, and e) regeneration efficacy.

The original top 10 ranked draw agents were compared to rankings when the weightings were altered from the original values used in the TOPSIS analysis (Figure 2.10). For water flux weighting changes, the ranking had minimal differences compared to the original (Figure 2.11a). The top 5 draw agents ranked the same for all weighting increments, but PAspNA regenerated by nanofiltration and membrane distillation rose from their original ranking of 37 and 41 to 8 and 9, respectively. Figure 2.11 b)-e) detailed the other ranking bump charts for the weighting fluctuations. Reverse flux weighting fluctuations showed the same pattern as water flux weighting fluctuations where PAspNA regenerated by NF and MD moved up to rank 8 and 9. Replenishment cost fluctuations did not change the top 9 rankings, and only when the weighting

fluctuated to 30% and greater, EDTP acid moved from rank 11 to 9. A weighting of 40% and 50% for the criteria of regeneration cost caused PAspNA regenerated through NF to take the 10th spot from TTHP-Na. The rest of the ranking remained the same. Regeneration efficacy weighting fluctuation of 40 to 50% brought PAspNA regenerated by MD, PAspNA regenerated by UF, and TTHP-Na to spots 8, 9, and 10, respectively while the rest of the ranking remained unchanged. The overall robustness of the ranking system proved to be solid since the top five ranking draw agents never changed.

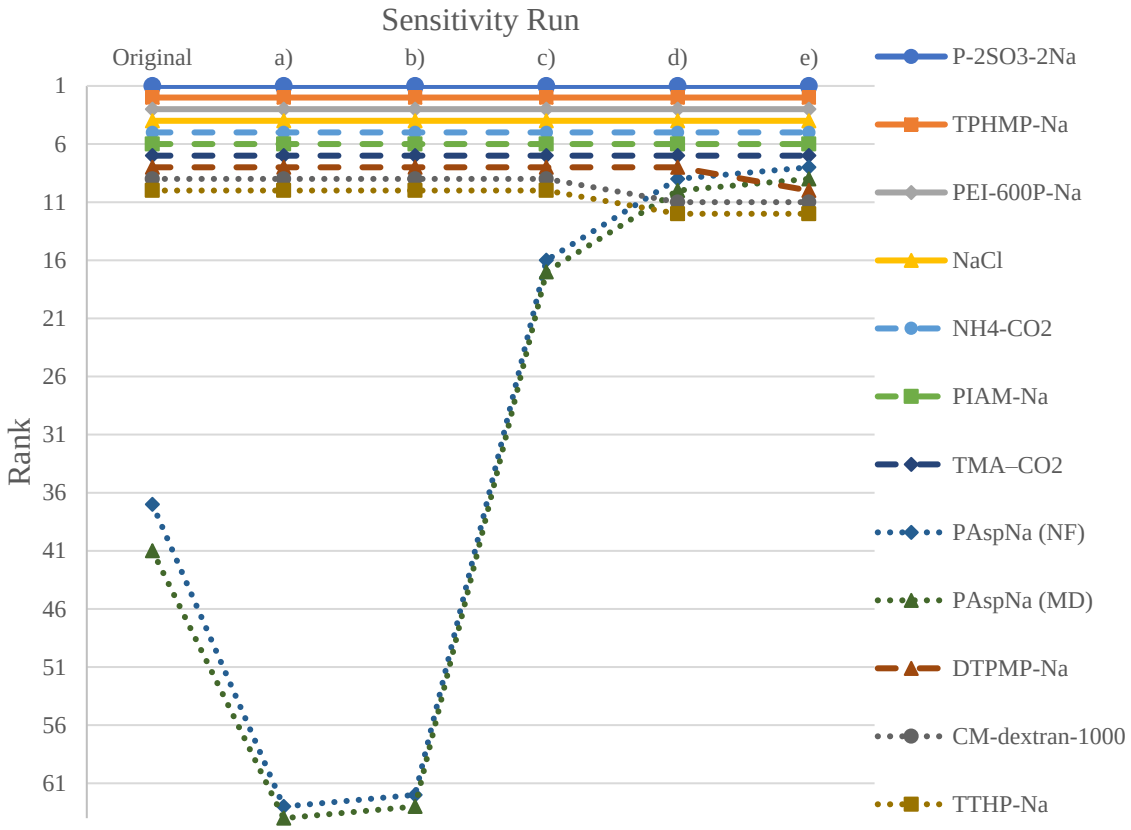

Fig. 2.11 Bump chart of rankings with the change of weightings for flux.

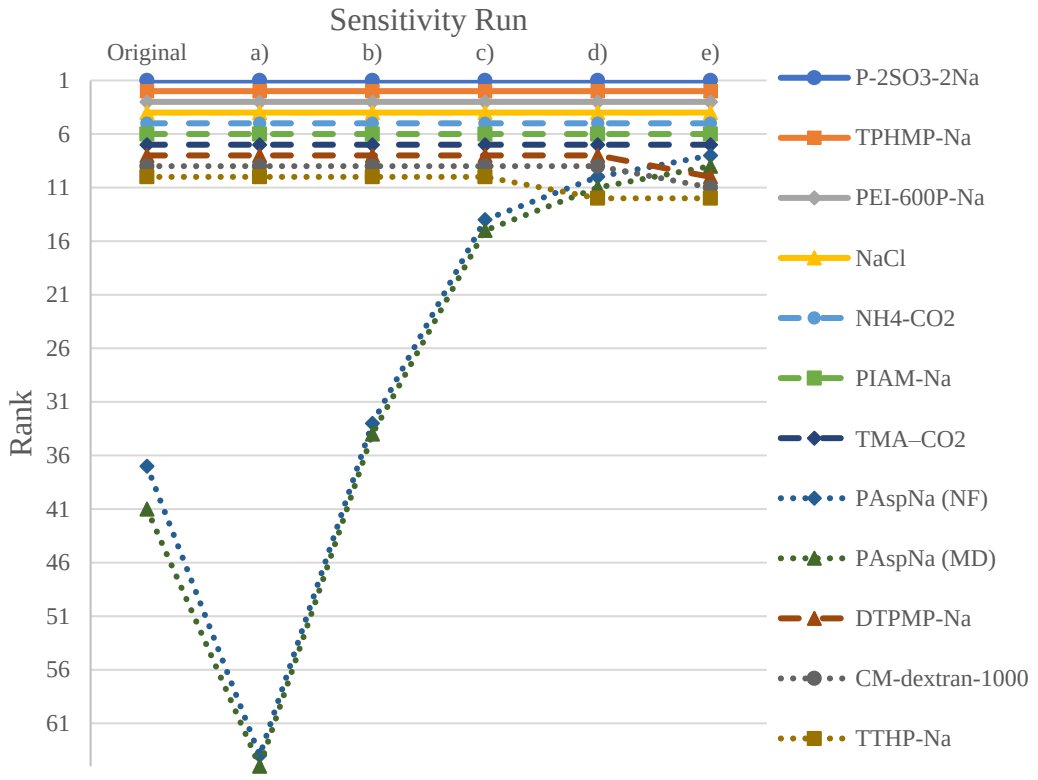

Fig. 2.12 Bump chart of rankings with the change of weightings for reverse flux.

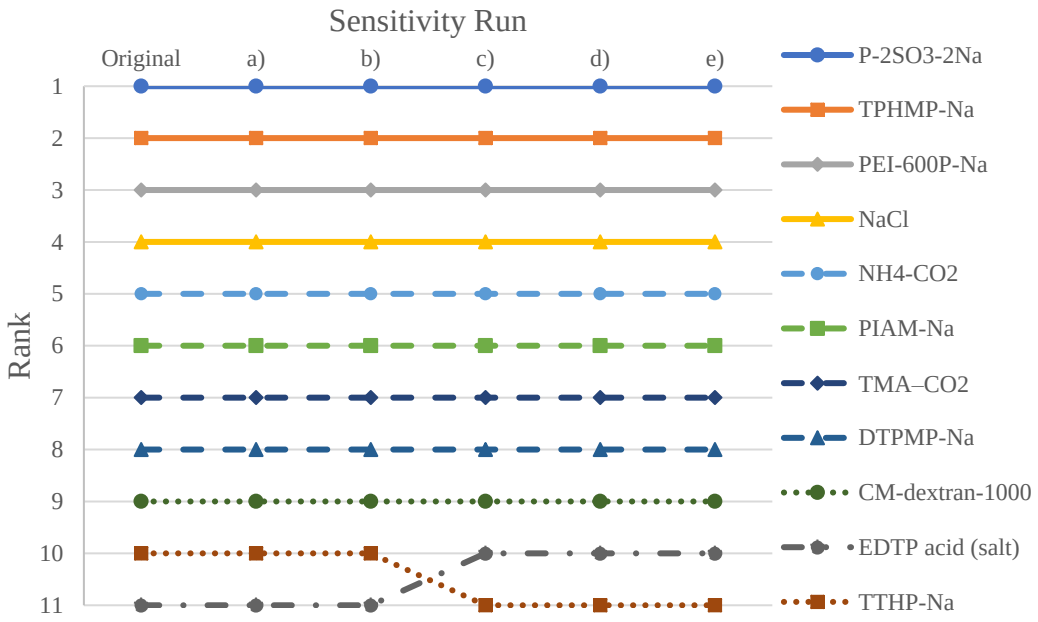

Fig. 2.13 Bump chart of rankings with the change of weightings for replenishment cost.

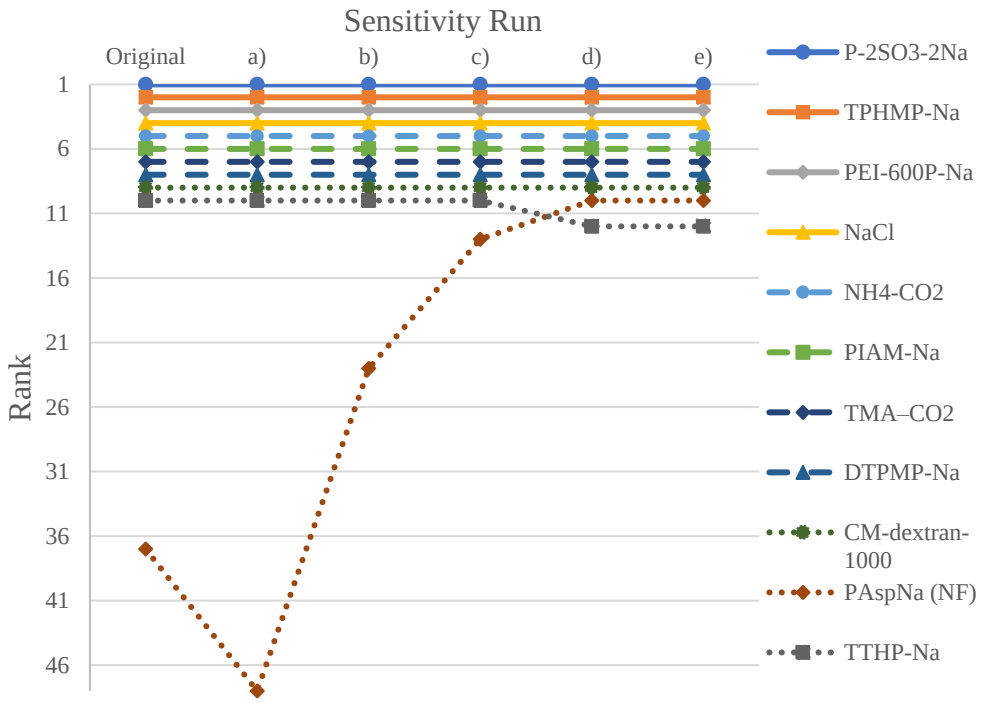

Fig. 2.14 Bump chart of rankings with the change of weightings for regeneration cost.

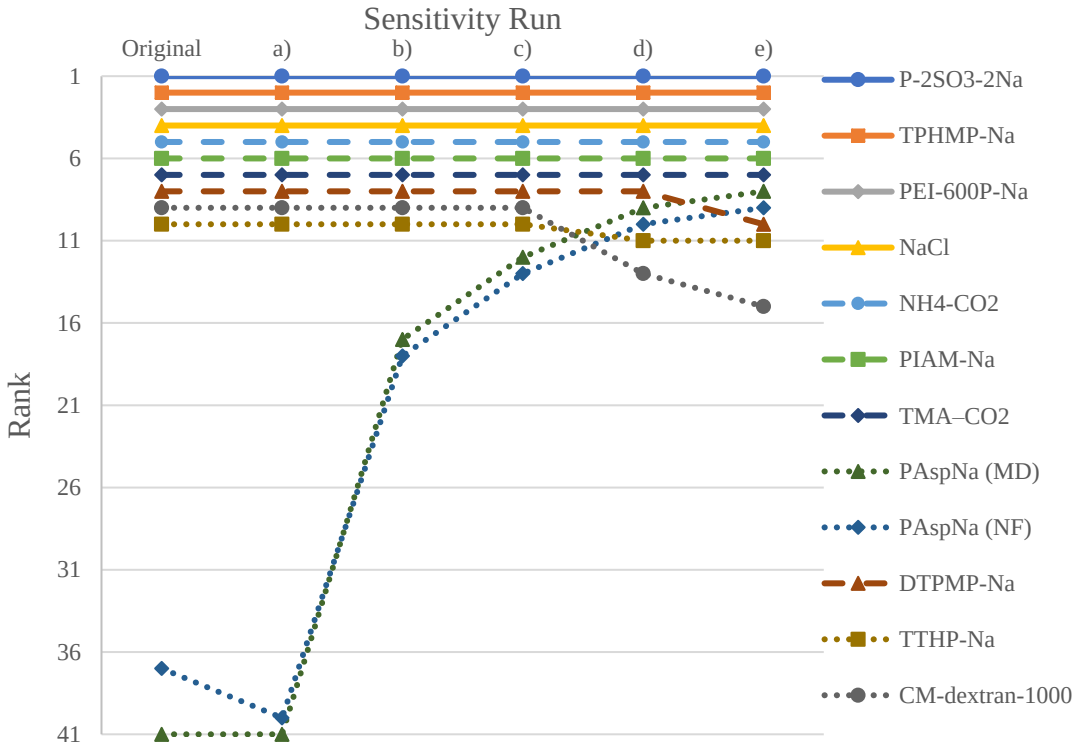

Fig. 2.15 Bump chart of rankings with the change of weightings for regeneration efficacy.

2.4 DISCUSSION

The results from the literature review and systematic ranking method were discussed in this section. Analysis of the literature review showed gaps in research that impacted the criteria chose for the MCDM. This section details further work that needs to be done that would improve upon this ranking system and assist research and commercialization of draw agents in the future.

2.4.1 Literature Review Discussion

The top five draw agents showed robustness in the sensitivity analysis. However, further criteria that were considered in this review could have been assessed in the AHP and TOPSIS and had possible impacts on the final ranking. Gaps in research led to a more streamlined review and therefore less thorough analysis and ranking. These gaps highlight areas for future research especially for the top 5 draw agents. Gaps in the reported data in the literature reviewed resulted in criteria not being analyzed in the MCDM. For instance, less than a third of the studies analyzed reported or addressed the potential toxicity of draw agents (Table A.4). TMA-CO_2 ranked 7th among the other draw agents, but it has a high toxicity and it was advised that human exposure should be limited while handling it [69]. A cytotoxicity assay performed on CM-dextran-1000 indicated that the draw agent was nontoxic and considered a safe draw agent, but CM-dextran-1000 was ranked 2 spots lower than TMA-CO_2 [45]. Furthermore, the top five draw agents did not report any toxicity testing or a qualitative toxicity evaluation. So, if toxicity was considered as a criterion in the ranking of the draw agents, the final rankings might be different.

Sustainability was another criterion that was not reported by many studies. Sustainability is an important criterion because steady availability and less harmful impacts on the environment would lead to more widely available usage and economical consumption of the draw agents. These studies need to be further researched to make a more thorough ranking assessment to improve upon draw agent selection.

2.4.2 MCDM Discussion

The MCDM resulted in the top five ranking draw agents to be P-2SO_3-2Na, TPHMP-Na, PEI-600P-Na, NaCl, and NH_4-CO_2. The weighting scale prioritized flux, followed by reverse flux, replenishment cost, regeneration cost, and regeneration efficacy. P-2SO_3-2Na had the highest water flux of 76.4 LMH, which is greater than the 2nd highest ranked draw agent by almost double. The water flux of the other four draw agents were significantly greater than the average with the fifth ranked draw agent's, NH_4-CO_2, flux be more than double the average of about 15 LMH. With this weighting, the top ranking of the draw agents achieves the goal of prioritizing FO performance. However, ranking is still incomplete due to unreported data and criteria that were not considered. Further testing of the top 10 draw agents will be needed to fill these information gaps to better guide draw agent selection for research and commercialization.

The studies compared in the MCDM were all tested with DI as the feed solution to make a fair comparison among the criteria. However, many of these draw agents would be applied in industry to purify or desalinate water that has different compositions and ionic strength. Therefore, further testing is needed to evaluate the performance of the highly

ranked draw agents for different applications. For instance, TPHMP-Na and PEI-600P-Na were also tested with emulsified soybean oil and water to assess their capabilities in the separation of oil and water [49]. Other draw agents may perform better than others depending on the type of feed solution. So, ranking of draw agents with other feed solutions could give more insight on the suitability of these draw agents in large scale real applications.

All the studies reviewed were tested in laboratory conditions and performed in a pilot-scale. Testing and analysis in the field would be necessary to assess the feasibility of the draw agent. TMA-CO_2's high toxicity makes the draw agent unusable in applications that would have an impact on human health and the environment, but usage in industrial applications like wastewater treatment from power plants could be feasible [69]. However, more research on large-scale performance of these draw agents would be necessary to provide a more practical guide to the selection of draw agents.

Other criteria that may be helpful to aid selection for industrial use would be cost-benefit and life-cycle analyses of the draw agents. These missing criteria may change the ranking of draw agents based on the economic feasibility of them to use in a large-scale industrial process. Analyses of water recovery compared to processing costs could be made to better inform decisions on regeneration costs. The magnitude of the industrial operation could also contribute to the cost-benefit analyses of the draw agent. Economic analyses would further inform the ranking and improve the selection of the draw agents.

This review and MCDM analysis outlined draw agents recently developed and compared them through a systematic ranking system. Through this process, the highly ranked draw agents could be prioritized to bridge the information gaps revealed in this review and ranking. This study will further guide future research and development for these promising draw agents to be utilized in the field or commercialized.

2.5 CONCLUSIONS

The main goal of this study was to provide not only a literature review on FO draw agents investigated in the past five years, but also systematically rank the draw agents to aid future research and commercialization of these draw agents. This was achieved through a thorough literature review process which determined important characteristics of the draw agents that would inform upon criteria used in the MCDM. The MCDM utilized two methods, AHP and TOPSIS, to weight the criteria and systematically rank the draw agents. The robustness of this ranking system was tested using a sensitivity analysis on the judgements made by the author related to the relative importance of the evaluation criteria and any other assumptions made. The top five draw agents, P-2SO_3-2Na, TPHMP-Na, PEI-600P-Na, NaCl, and NH_4-CO_2, ranked highly due to their ideal draw agent characteristics of high water flux, low reverse solute flux, low replenishment and regeneration cost, and high regeneration efficacy. Gaps in reported data from the studies proved to be a challenge in ranking the draw agents by limiting to the number of evaluation criteria to five. Future work should expand upon these studies to include more characteristics to further inform upon decisions such as toxicity, sustainability, life cycle analyses, and cost-benefit analyses. Overall, this review and ranking process achieved

the goal of setting apart high performing FO draw agents from the myriad of options to aid future research and development.

WORKS CITED

[1] “Drinking-water.” https://www.who.int/news-room/fact-sheets/detail/drinking-water (accessed Dec. 31, 2019).

[2] R. L. McGinnis and M. Elimelech, “Global Challenges in Energy and Water Supply: The Promise of Engineered Osmosis,” *Environ. Sci. Technol.*, vol. 42, no. 23, pp. 8625–8629, Dec. 2008, doi: 10.1021/es800812m.

[3] N. K. Rastogi, “1 - Forward osmosis: Principles, applications, and recent developments,” in *Current Trends and Future Developments on (Bio-) Membranes*, A. Basile, A. Cassano, and N. K. Rastogi, Eds. Elsevier, 2020, pp. 3–35.

[4] S. Zhao, L. Zou, C. Y. Tang, and D. Mulcahy, “Recent developments in forward osmosis: Opportunities and challenges,” *Journal of Membrane Science*, vol. 396, pp. 1–21, Apr. 2012, doi: 10.1016/j.memsci.2011.12.023.

[5] S. Li and Z. Li, “11 - Reverse osmosis and forward osmosis in integrated systems,” in *Current Trends and Future Developments on (Bio-) Membranes*, A. Basile, A. Cassano, and N. K. Rastogi, Eds. Elsevier, 2020, pp. 261–280.

[6] A. Tiraferri and R. Sethi, “Enhanced transport of zerovalent iron nanoparticles in saturated porous media by guar gum,” *Journal of Nanoparticle Research*, vol. 11, pp. 635–645, Apr. 2009, doi: 10.1007/s11051-008-9405-0.

[7] T. Alejo, M. Arruebo, V. Carcelen, V. M. Monsalvo, and V. Sebastian, “Advances in draw solutes for forward osmosis: Hybrid organic-inorganic nanoparticles and conventional solutes,” *Chemical Engineering Journal*, vol. 309, pp. 738–752, Feb. 2017, doi: 10.1016/j.cej.2016.10.079.

[8] Q. Long *et al.*, “Recent Advance on Draw Solutes Development in Forward Osmosis,” *Processes*, vol. 6, no. 9, p. 165, Sep. 2018, doi: 10.3390/pr6090165.

[9] Y. Cai and X. ‘Matthew’ Hu, “A critical review on draw solutes development for forward osmosis,” *Desalination*, vol. 391, pp. 16–29, Aug. 2016, doi: 10.1016/j.desal.2016.03.021.

[10] H. K. Shon, L. Chekli, S. Phuntsho, J. Kim, and J. Cho, “CHAPTER 5 Draw Solutes in Forward Osmosis Processes,” 2015.

[11] T. Y. Cath, A. E. Childress, and M. Elimelech, “Forward osmosis: Principles, applications, and recent developments,” *Journal of Membrane Science*, vol. 281, no. 1, pp. 70–87, Sep. 2006, doi: 10.1016/j.memsci.2006.05.048.

[12] K. Y. Wang, T.-S. Chung, and G. Amy, “Developing thin-film-composite forward osmosis membranes on the PES/SPSf substrate through interfacial polymerization,” *AIChE Journal*, vol. 58, no. 3, pp. 770–781, 2012, doi: 10.1002/aic.12635.

[13] M. Eyvaz, S. Arslan, D. İmer, E. Yüksel, and İ. Koyuncu, “Forward Osmosis Membranes – A Review: Part II,” *Osmotically Driven Membrane Processes - Approach, Development and Current Status*, Mar. 2018, doi: 10.5772/intechopen.74659.

[14] P. Dey and E. L. Izake, “Magnetic nanoparticles boosting the osmotic efficiency of a polymeric FO draw agent: Effect of polymer conformation,” *Desalination*, vol. 373, pp. 79–85, Oct. 2015, doi: 10.1016/j.desal.2015.07.010.

[15] S. Y. Park, H.-W. Ahn, J. W. Chung, and S.-Y. Kwak, “Magnetic core-hydrophilic shell nanosphere as stability-enhanced draw solute for forward osmosis (FO) application,” *Desalination*, vol. 397, pp. 22–29, Nov. 2016, doi: 10.1016/j.desal.2016.06.017.

[16] "MSDS Sheets_Peptone_516_00.pdf." Accessed: Apr. 30, 2020. [Online]. Available: https://www.mccsd.net/cms/lib/NY02208580/Centricity/Shared/Material%20Safety%20Data%20Sheets%20_MSDS_/MSDS%20Sheets_Peptone_516_00.pdf.

[17] M. E. Mahmoud, A. E. H. Abdou, M. E. Sobhy, and N. A. Fekry, "Solid–solid crosslinking of carboxymethyl cellulose nanolayer on titanium oxide nanoparticles as a novel biocomposite for efficient removal of toxic heavy metals from water," *International Journal of Biological Macromolecules*, vol. 105, pp. 1269–1278, Dec. 2017, doi: 10.1016/j.ijbiomac.2017.07.156.

[18] D. M. Cassidy-Hanley, "Chapter 8 - Tetrahymena in the Laboratory: Strain Resources, Methods for Culture, Maintenance, and Storage," in *Methods in Cell Biology*, vol. 109, K. Collins, Ed. Academic Press, 2012, pp. 237–276.

[19] "Freezing Point Depression," *Chemistry LibreTexts*, Oct. 02, 2013. https://chem.libretexts.org/Bookshelves/Physical_and_Theoretical_Chemistry_Textbook_Maps/Supplemental_Modules_(Physical_and_Theoretical_Chemistry)/Physical_Properties_of_Matter/Solutions_and_Mixtures/Colligative_Properties/Freezing_Point_Depression (accessed May 30, 2020).

[20] K. Kiyosawa, "Theoretical and experimental studies on freezing point depression and vapor pressure deficit as methods to measure osmotic pressure of aqueous polyethylene glycol and bovine serum albumin solutions," *Biophysical Chemistry*, vol. 104, no. 1, pp. 171–188, May 2003, doi: 10.1016/S0301-4622(02)00365-4.

[21] John C. Crittenden, R. Rhodes Trussell, David W. Hand, Kerry J. Howe, and George Tchobanoglous, *MWH's Water Treatment: Principles and Design, Third Edition: Principles and Design, Third Edition*, 3rd ed. Wiley, 2012.

[22] B. Faure, G. Salazar-Alvarez, and L. Bergström, "Hamaker Constants of Iron Oxide Nanoparticles," *Langmuir*, vol. 27, no. 14, pp. 8659–8664, Jul. 2011, doi: 10.1021/la201387d.

[23] W. Xi, H. T. Phan, and A. J. Haes, "How to Accurately Predict Solution-phase Gold Nanostar Stability," *Anal Bioanal Chem*, vol. 410, no. 24, pp. 6113–6123, Sep. 2018, doi: 10.1007/s00216-018-1115-6.

[24] Steven Abbott and Nigel Holmes, *Nanocoatings: Principles and Practice*. U.K.: DEStech Publications, Inc., 2013.

[25] "Fe3O4 Iron Oxide Nanoparticles / Nanopowder Water Dispersion (Fe3O4, 99.5+%, 15-20nm, 20wt% in water, excellent stability, black color)." https://www.us-nano.com/inc/sdetail/16809 (accessed May 27, 2020).

[26] A. Barhoum, M. L. García-Betancourt, H. Rahier, and G. Van Assche, "Chapter 9 - Physicochemical characterization of nanomaterials: polymorph, composition, wettability, and thermal stability," in *Emerging Applications of Nanoparticles and Architecture Nanostructures*, A. Barhoum and A. S. H. Makhlouf, Eds. Elsevier, 2018, pp. 255–278.

[27] F. Bouyer, A. Robben, W. L. Yu, and M. Borkovec, "Aggregation of Colloidal Particles in the Presence of Oppositely Charged Polyelectrolytes: Effect of Surface Charge Heterogeneities," *Langmuir*, vol. 17, no. 17, pp. 5225–5231, Aug. 2001, doi: 10.1021/la010548z.

[28] A. M. E. Badawy, T. P. Luxton, R. G. Silva, K. G. Scheckel, M. T. Suidan, and T. M. Tolaymat, “Impact of Environmental Conditions (pH, Ionic Strength, and Electrolyte Type) on the Surface Charge and Aggregation of Silver Nanoparticles Suspensions,” *Environ. Sci. Technol.*, vol. 44, no. 4, pp. 1260–1266, Feb. 2010, doi: 10.1021/es902240k.

[29] A. J. Worthen, V. Tran, K. A. Cornell, T. M. Truskett, and K. P. Johnston, “Steric stabilization of nanoparticles with grafted low molecular weight ligands in highly concentrated brines including divalent ions,” *Soft Matter*, vol. 12, no. 7, pp. 2025–2039, Feb. 2016, doi: 10.1039/C5SM02787J.

[30] M. Erdemoğlu and M. Sarıkaya, “Effects of heavy metals and oxalate on the zeta potential of magnetite,” *Journal of Colloid and Interface Science*, vol. 300, no. 2, pp. 795–804, Aug. 2006, doi: 10.1016/j.jcis.2006.04.004.

[31] H. T. Nguyen, N. C. Nguyen, S.-S. Chen, H. H. Ngo, W. Guo, and C.-W. Li, “A new class of draw solutions for minimizing reverse salt flux to improve forward osmosis desalination,” *Science of The Total Environment*, vol. 538, pp. 129–136, Dec. 2015, doi: 10.1016/j.scitotenv.2015.07.156.

[32] H. Luo *et al.*, “A review on the recovery methods of draw solutes in forward osmosis,” *Journal of Water Process Engineering*, vol. 4, pp. 212–223, Dec. 2014, doi: 10.1016/j.jwpe.2014.10.006.

[33] J. Su, S. Zhang, M. M. Ling, and T.-S. Chung, “Forward osmosis: an emerging technology for sustainable supply of clean water,” *Clean Techn Environ Policy*, vol. 14, no. 4, pp. 507–511, Aug. 2012, doi: 10.1007/s10098-012-0486-1.

[34] Q. Ge, M. Ling, and T.-S. Chung, “Draw solutions for forward osmosis processes: Developments, challenges, and prospects for the future,” *Journal of Membrane Science*, vol. 442, pp. 225–237, Sep. 2013, doi: 10.1016/j.memsci.2013.03.046.

[35] F. Dweiri, S. A. Khan, and A. Almulla, “A multi-criteria decision support system to rank sustainable desalination plant location criteria,” *Desalination*, vol. 444, pp. 26–34, Oct. 2018, doi: 10.1016/j.desal.2018.07.007.

[36] “AHP_Lesson_1.pdf.” Accessed: May 15, 2020. [Online]. Available: http://rad.ihu.edu.gr/fileadmin/labsfiles/decision_support_systems/lessons/ahp/AHP_Lesson_1.pdf.

[37] T. L. Saaty, “A scaling method for priorities in hierarchical structures,” *Journal of Mathematical Psychology*, vol. 15, no. 3, pp. 234–281, Jun. 1977, doi: 10.1016/0022-2496(77)90033-5.

[38] S. Opricovic and G.-H. Tzeng, “Compromise solution by MCDM methods: A comparative analysis of VIKOR and TOPSIS,” *European Journal of Operational Research*, vol. 156, no. 2, pp. 445–455, Jul. 2004, doi: 10.1016/S0377-2217(03)00020-1.

[39] Y. Cai and X. ‘Matthew’ Hu, “A critical review on draw solutes development for forward osmosis,” *Desalination*, vol. 391, pp. 16–29, Aug. 2016, doi: 10.1016/j.desal.2016.03.021.

[40] S. Zhao, “Osmotic Pressure versus Swelling Pressure: Comment on ‘Bifunctional Polymer Hydrogel Layers As Forward Osmosis Draw Agents for Continuous Production of Fresh Water Using Solar Energy,’” *Environ. Sci. Technol.*, vol. 48, no. 7, pp. 4212–4213, Apr. 2014, doi: 10.1021/es5006994.

[41] V. Ammarapala, T. Chinda, P. Pongsayaporn, W. Ratanachot, K. Punthutaecha, and K. Janmonta, “Cross-border shipment route selection utilizing analytic hierarchy process (AHP) method,” *Songklanakarin Journal of Science and Technology*, vol. 40, Mar. 2018, doi: 10.14456/sjst-psu.2018.3.

[42] Y.-J. Wang and H.-S. Lee, “Generalizing TOPSIS for fuzzy multiple-criteria group decision-making,” *Computers & Mathematics with Applications*, vol. 53, no. 11, pp. 1762–1772, Jun. 2007, doi: 10.1016/j.camwa.2006.08.037.

[43] G. R. Jahanshahloo, F. H. Lotfi, and M. Izadikhah, “Extension of the TOPSIS method for decision-making problems with fuzzy data,” *Applied Mathematics and Computation*, vol. 181, no. 2, pp. 1544–1551, Oct. 2006, doi: 10.1016/j.amc.2006.02.057.

[44] Y. Cai and X. ‘Matthew’ Hu, “A critical review on draw solutes development for forward osmosis,” *Desalination*, vol. 391, pp. 16–29, Aug. 2016, doi: 10.1016/j.desal.2016.03.021.

[45] C. Ding *et al.*, “Application of polysaccharide derivatives as novel draw solutes in forward osmosis for desalination and protein concentration,” *Chemical Engineering Research and Design*, vol. 146, pp. 211–220, Jun. 2019, doi: 10.1016/j.cherd.2019.04.005.

[46] S. Laohaprapanon *et al.*, “Evaluation of a natural polymer-based cationic polyelectrolyte as a draw solute in forward osmosis,” *Desalination*, vol. 421, pp. 72–78, Nov. 2017, doi: 10.1016/j.desal.2017.04.027.

[47] S. S. Ray *et al.*, “Exploration of polyelectrolyte incorporated with Triton-X 114 surfactant based osmotic agent for forward osmosis desalination,” *Journal of*

Environmental Management, vol. 209, pp. 346–353, Mar. 2018, doi: 10.1016/j.jenvman.2017.12.086.

[48] S. S. Ray *et al.*, "Forward osmosis desalination by utilizing chlorhexidine gluconate based mouthwash as a reusable draw solute," *Chemical Engineering Journal*, vol. 304, pp. 962–969, Nov. 2016, doi: 10.1016/j.cej.2016.07.023.

[49] Q. Long, L. Shen, R. Chen, J. Huang, S. Xiong, and Y. Wang, "Synthesis and Application of Organic Phosphonate Salts as Draw Solutes in Forward Osmosis for Oil–Water Separation," *Environ. Sci. Technol.*, vol. 50, no. 21, pp. 12022–12029, Nov. 2016, doi: 10.1021/acs.est.6b02953.

[50] Y. Wang *et al.*, "An easily recoverable thermo-sensitive polyelectrolyte as draw agent for forward osmosis process," *Chinese Journal of Chemical Engineering*, vol. 24, no. 1, pp. 86–93, Jan. 2016, doi: 10.1016/j.cjche.2015.11.015.

[51] R. Kumar, S. Al-Haddad, M. Al-Rughaib, and M. Salman, "Evaluation of hydrolyzed poly(isobutylene-alt-maleic anhydride) as a polyelectrolyte draw solution for forward osmosis desalination," *Desalination*, vol. 394, pp. 148–154, Sep. 2016, doi: 10.1016/j.desal.2016.05.012.

[52] H. G. Zeweldi *et al.*, "The potential of monocationic imidazolium-, phosphonium-, and ammonium-based hydrophilic ionic liquids as draw solutes for forward osmosis," *Desalination*, vol. 444, pp. 94–106, Oct. 2018, doi: 10.1016/j.desal.2018.07.017.

[53] A. Mahto *et al.*, "Sustainable Water Reclamation from Different Feed Streams by Forward Osmosis Process Using Deep Eutectic Solvents as Reusable Draw

Solution," *Ind. Eng. Chem. Res.*, vol. 56, no. 49, pp. 14623–14632, Dec. 2017, doi: 10.1021/acs.iecr.7b03046.

[54] M. Amjad, J. Gardy, A. Hassanpour, and D. Wen, "Novel draw solution for forward osmosis based solar desalination," *Applied Energy*, vol. 230, pp. 220–231, Nov. 2018, doi: 10.1016/j.apenergy.2018.08.021.

[55] A. Inada, T. Takahashi, K. Kumagai, and H. Matsuyama, "Morpholine Derivatives as Thermoresponsive Draw Solutes for Forward Osmosis Desalination," *Ind. Eng. Chem. Res.*, vol. 58, no. 27, pp. 12253–12260, Jul. 2019, doi: 10.1021/acs.iecr.9b01712.

[56] Y. Wu, W. Zhang, and Q. Ge, "Piperazine-Based Functional Materials as Draw Solutes for Desalination via Forward Osmosis," *ACS Sustainable Chem. Eng.*, vol. 6, no. 11, pp. 14170–14177, Nov. 2018, doi: 10.1021/acssuschemeng.8b02796.

[57] J. Kim, J. Kim, J. Lim, and S. Hong, "Evaluation of ethanol as draw solute for forward osmosis (FO) process of highly saline (waste)water," *Desalination*, vol. 456, pp. 23–31, Apr. 2019, doi: 10.1016/j.desal.2019.01.012.

[58] S. Kalafatakis, S. Braekevelt, V. Carlsen, L. Lange, I. V. Skiadas, and H. N. Gavala, "On a novel strategy for water recovery and recirculation in biorefineries through application of forward osmosis membranes," *Chemical Engineering Journal*, vol. 311, pp. 209–216, Mar. 2017, doi: 10.1016/j.cej.2016.11.092.

[59] J. Kim, H. Kang, Y.-S. Choi, Y. Ah. Yu, and J.-C. Lee, "Thermo-responsive oligomeric poly(tetrabutylphosphonium styrenesulfonate)s as draw solutes for forward osmosis (FO) applications," *Desalination*, vol. 381, pp. 84–94, Mar. 2016, doi: 10.1016/j.desal.2015.11.013.

[60] M. J. A. Hamad and E. M. N. Chirwa, “Forward osmosis for water recovery using polyelectrolyte PolyDADMAC and DADMAC draw solutions as a low pressure energy saving process,” *Desalination*, vol. 453, pp. 89–101, Mar. 2019, doi: 10.1016/j.desal.2018.11.016.

[61] S. Dutta and K. Nath, “Feasibility of forward osmosis using ultra low pressure RO membrane and Glauber salt as draw solute for wastewater treatment,” *Journal of Environmental Chemical Engineering*, vol. 6, no. 4, pp. 5635–5644, Aug. 2018, doi: 10.1016/j.jece.2018.08.037.

[62] S. Y. Park, H.-W. Ahn, J. W. Chung, and S.-Y. Kwak, “Magnetic core-hydrophilic shell nanosphere as stability-enhanced draw solute for forward osmosis (FO) application,” *Desalination*, vol. 397, pp. 22–29, Nov. 2016, doi: 10.1016/j.desal.2016.06.017.

[63] B. Wang, X. Wen, B. Shen, and P. Zhang, “A systematic evaluation on the performance and mechanism of surfactants as additive of draw solution in forward osmosis,” *Desalination*, vol. 445, pp. 170–180, Nov. 2018, doi: 10.1016/j.desal.2018.08.007.

[64] C. J. Orme and A. D. Wilson, “1-Cyclohexylpiperidine as a thermolytic draw solute for osmotically driven membrane processes,” *Desalination*, vol. 371, pp. 126–133, Sep. 2015, doi: 10.1016/j.desal.2015.05.024.

[65] E. Tian *et al.*, “A study of poly (sodium 4-styrenesulfonate) as draw solute in forward osmosis,” *Desalination*, vol. 360, pp. 130–137, Mar. 2015, doi: 10.1016/j.desal.2015.01.001.

[66] G. Gwak, B. Jung, S. Han, and S. Hong, “Evaluation of poly (aspartic acid sodium salt) as a draw solute for forward osmosis,” *Water Research*, vol. 80, pp. 294–305, Sep. 2015, doi: 10.1016/j.watres.2015.04.041.

[67] P. Zhao *et al.*, “Explore the forward osmosis performance using hydrolyzed polyacrylamide as draw solute for dye wastewater reclamation in the long-term process,” *Chemical Engineering Journal*, vol. 273, pp. 316–324, Aug. 2015, doi: 10.1016/j.cej.2015.03.093.

[68] P. Dey and E. L. Izake, “Mixed Polymer-Coated Magnetic Nanoparticles as Forward Osmosis Draw Agents of Tuned Hydrophilicity,” *Chem. Eur. J.*, vol. 22, no. 32, pp. 11253–11260, Aug. 2016, doi: 10.1002/chem.201600144.

[69] C. Boo, Y. F. Khalil, and M. Elimelech, “Performance evaluation of trimethylamine–carbon dioxide thermolytic draw solution for engineered osmosis,” *Journal of Membrane Science*, vol. 473, pp. 302–309, Jan. 2015, doi: 10.1016/j.memsci.2014.09.026.

[70] Q. Long, G. Qi, and Y. Wang, “Synthesis and application of ethylenediamine tetrapropionic salt as a novel draw solute for forward osmosis application,” *AIChE Journal*, vol. 61, no. 4, pp. 1309–1321, 2015, doi: 10.1002/aic.14720.

[71] Y. Zhong *et al.*, “Using UCST Ionic Liquid as a Draw Solute in Forward Osmosis to Treat High-Salinity Water,” *Environ. Sci. Technol.*, vol. 50, no. 2, pp. 1039–1045, Jan. 2016, doi: 10.1021/acs.est.5b03747.

[72] M. Cho, S. H. Lee, D. Lee, D. P. Chen, I.-C. Kim, and M. S. Diallo, “Osmotically driven membrane processes: Exploring the potential of branched polyethyleneimine as draw solute using porous FO membranes with NF separation layers,” *Journal of*

Membrane Science, vol. 511, pp. 278–288, Aug. 2016, doi: 10.1016/j.memsci.2016.02.041.

[73] H. T. Nguyen, S.-S. Chen, N. C. Nguyen, H. H. Ngo, W. Guo, and C.-W. Li, "Exploring an innovative surfactant and phosphate-based draw solution for forward osmosis desalination," *Journal of Membrane Science*, vol. 489, pp. 212–219, Sep. 2015, doi: 10.1016/j.memsci.2015.03.085.

[74] N. C. Nguyen *et al.*, "Exploring high charge of phosphate as new draw solute in a forward osmosis–membrane distillation hybrid system for concentrating high-nutrient sludge," *Science of The Total Environment*, vol. 557–558, pp. 44–50, Jul. 2016, doi: 10.1016/j.scitotenv.2016.03.025.

[75] Q. Long and Y. Wang, "Novel carboxyethyl amine sodium salts as draw solutes with superior forward osmosis performance," *AIChE Journal*, vol. 62, no. 4, pp. 1226–1235, 2016, doi: 10.1002/aic.15126.

[76] H. T. Nguyen, N. C. Nguyen, S.-S. Chen, H. H. Ngo, W. Guo, and C.-W. Li, "A new class of draw solutions for minimizing reverse salt flux to improve forward osmosis desalination," *Science of The Total Environment*, vol. 538, pp. 129–136, Dec. 2015, doi: 10.1016/j.scitotenv.2015.07.156.

[77] J. Huang, Q. Long, S. Xiong, L. Shen, and Y. Wang, "Application of poly (4-styrenesulfonic acid-co-maleic acid) sodium salt as novel draw solute in forward osmosis for dye-containing wastewater treatment," *Desalination*, vol. 421, pp. 40–46, Nov. 2017, doi: 10.1016/j.desal.2017.01.039.

[78] “Selection of inorganic-based draw solutions for forward osmosis applications,” *Journal of Membrane Science*, vol. 364, no. 1–2, pp. 233–241, Nov. 2010, doi: 10.1016/j.memsci.2010.08.010.

[79] Q. Long *et al.*, “Recent Advance on Draw Solutes Development in Forward Osmosis,” *Processes*, vol. 6, no. 9, p. 165, Sep. 2018, doi: 10.3390/pr6090165.

[80] X. Liu, J. Wu, L. Hou, and J. Wang, “Removal of Co, Sr and Cs ions from simulated radioactive wastewater by forward osmosis,” *Chemosphere*, vol. 232, pp. 87–95, Oct. 2019, doi: 10.1016/j.chemosphere.2019.05.210.

[81] G. Blandin *et al.*, “Volatile fatty acids concentration in real wastewater by forward osmosis,” *Journal of Membrane Science*, vol. 575, pp. 60–70, Apr. 2019, doi: 10.1016/j.memsci.2019.01.006.

[82] A. H. Hawari, N. Kamal, and A. Altaee, “Combined influence of temperature and flow rate of feeds on the performance of forward osmosis,” *Desalination*, vol. 398, pp. 98–105, Nov. 2016, doi: 10.1016/j.desal.2016.07.023.

[83] D. H. Jung *et al.*, “Simulation of forward osmosis membrane process: Effect of membrane orientation and flow direction of feed and draw solutions,” *Desalination*, vol. 277, no. 1, pp. 83–91, Aug. 2011, doi: 10.1016/j.desal.2011.04.001.

[84] C. Suh and S. Lee, “Modeling reverse draw solute flux in forward osmosis with external concentration polarization in both sides of the draw and feed solution,” *Journal of Membrane Science*, vol. 427, pp. 365–374, Jan. 2013, doi: 10.1016/j.memsci.2012.08.033.

[85] M. P. Ayach, “Comparison of CTA and TFC FO-membranes for water recovery,” p. 26.

[86] B. D. Coday, B. G. M. Yaffe, P. Xu, and T. Y. Cath, “Rejection of Trace Organic Compounds by Forward Osmosis Membranes: A Literature Review,” *Environ. Sci. Technol.*, vol. 48, no. 7, pp. 3612–3624, Apr. 2014, doi: 10.1021/es4038676.

[87] M. Yasukawa, Y. Tanaka, T. Takahashi, M. Shibuya, S. Mishima, and H. Matsuyama, “Effect of Molecular Weight of Draw Solute on Water Permeation in Forward Osmosis Process,” *Ind. Eng. Chem. Res.*, vol. 54, no. 33, pp. 8239–8246, Aug. 2015, doi: 10.1021/acs.iecr.5b01960.

APPENDIX

A. SUPPORTING INFORMATION – TABLES

Table A.1 Peptone Weight, TDS, and Conductivity Measurements over Time

DI (Draw at 60 g/L)					
Time (min)	Weight (g)	TDS (mg/L)	Conductivity (µS)	Flux ($L/m^2 \cdot hr$)	Reverse Flux ($g/m^2 \cdot hr$)
0	496.46	2.11	2.82		
15	495.36	4.31	6.35	2.14	2.04
30	494.07	4.98	6.71	2.50	0.19
45	492.5	4.63	6.34	3.05	0.00
60	491.17	4.73	6.65	2.58	0.16
75	490.02	4.96	6.98	2.23	0.18
90	488.62	5.03	7.00	2.72	0.00
105	487.13	5.16	7.15	2.89	0.07
120	485.32	5.46	7.75	3.51	0.32
DI (Draw at 120 g/L)					
Time	Weight (g)	TDS (mg/L)	Conductivity (µS)	Flux ($L/m^2 \cdot hr$)	Reverse Flux ($g/m^2 \cdot hr$)
0	481.57	4.66	6.45		
15	481.08	4.66	6.18	0.95	0.00
30	479.94	4.45	6.22	2.21	0.01
45	478.55	4.61	6.42	2.70	0.10
60	477.16	4.72	7.01	2.70	0.32
75	475.68	5.12	7.12	2.87	0.04
90	474.45	5.44	7.46	2.38	0.18
105	472.92	5.75	8.11	2.97	0.35
120	471.64	5.96	8.56	2.48	0.24
DI (Draw at 200 g/L)					
Time	Weight (g)	TDS (mg/L)	Conductivity (µS)	Flux ($L/m^2 \cdot hr$)	Reverse Flux ($g/m^2 \cdot hr$)
0	483.15	3.78	5.45		
15	477.98	3.95	5.66	10.0	0.06
30	475.69	4.39	5.78	4.45	0.04
45	473.89	4.79	6.47	3.49	0.38
60	471.66	5.3	7.42	4.33	0.52
75	469.92	6.07	8.55	3.38	0.63
90	467.76	6.8	9.69	4.19	0.62
105	465.89	7.74	10.66	3.63	0.53

120	463.61	8.55	11.83	4.43	0.63

Table A.2 CMC Weight, TDS, and Conductivity Measurements over Time

DI (Draw at 10 g/L)					
Time	Weight (g)	TDS (mg/L)	Conductivity (µS)	Flux ($L/m^2 \cdot hr$)	Reverse Flux ($g/m^2 \cdot hr$)
0	391.38	2.32	3.18		
15	389.18	2.56	3.39	4.27	0.11
30	386.05	2.58	3.52	6.08	0.05
45	385.71	2.76	3.81	0.66	0.17
60	384.74	2.78	3.9	1.88	0.05
75	384	2.8	3.92	1.44	0.01
90	383.49	2.82	4.03	0.99	0.06
105	382.26	2.88	4.16	2.39	0.07
120	381.33	3.08	4.19	1.81	0.01
DI (Draw at 50 g/L)					
Time (min)	Weight (g)	TDS (mg/L)	Conductivity (µS)	Flux ($L/m^2 \cdot hr$)	Reverse Flux ($g/m^2 \cdot hr$)
0	491.26	3.31	3.91		
15	489.42	2.89	3.74	3.57	0.00
30	488.02	3.09	4.07	2.72	0.18
45	486.09	2.95	3.96	3.75	0.00
60	484.59	3.29	4.36	2.91	0.22
75	483.54	3.16	4.29	2.04	0.00
90	482.47	3.17	4.16	2.08	0.00
105	481.49	2.89	3.99	1.90	0.00
120	480.45	3.02	4.15	2.02	0.08
DI (Draw at 60g/L)					
Time	Weight (g)	TDS (mg/L)	Conductivity (µS)	Flux ($L/m^2 \cdot hr$)	Reverse Flux ($g/m^2 \cdot hr$)
0	492.45	4.49	5.87		
15	491.46	4.55	6.07	1.92	0.10
30	490.63	4.86	6.12	1.61	0.02
45	489.37	5.02	6.18	2.45	0.02
60	485.55	4.57	6.49	7.42	0.13
75	484.65	4.26	5.73	1.75	0.00
90	482.72	5	6.12	3.75	0.20
105	481.93	5.04	6.45	1.53	0.18
120	481.05	4.48	6.32	1.71	0.00

Table A.3 Fe_3O_4 NPs Weight, TDS, and Conductivity Measurements over Time

DI (Draw at 0.1 g/L)					
Time (min)	Weight (g)	TDS (mg/L)	Conductivity (µS)	Flux ($L/m^2 \cdot hr$)	Reverse Flux ($g/m^2 \cdot hr$)
0	483.74	2.33	3.07		
15	484.04	2.42	3.22	0.00	0.09
30	483.86	2.56	3.31	0.35	0.05
45	483.68	2.6	3.44	0.35	0.07
60	483.26	2.55	3.53	0.82	0.05
75	482.9	2.46	3.32	0.70	0.00
90	482.52	2.5	3.44	0.74	0.07
105	482.03	2.47	3.42	0.95	0.00
120	481.38	2.39	3.29	1.26	0.00
DI (Draw at 0.5 g/L)					
Time	Weight (g)	TDS (mg/L)	Conductivity (µS)	Flux ($L/m^2 \cdot hr$)	Reverse Flux ($g/m^2 \cdot hr$)
0	514.16	3.61	5.39		
15	513.52	3.86	4.87	1.24	0.00
30	512.99	4	5.18	1.03	0.18
45	512.73	4.03	5.52	0.50	0.20
60	512.48	4.12	5.61	0.49	0.05
75	511.82	4.21	5.63	1.28	0.00
90	511.72	4.44	6.37	0.19	0.43
105	511.51	4.25	5.93	0.41	0.00
120	511.31	4.63	6.27	0.39	0.20
DI (Draw at 1 g/L)					
Time	Weight (g)	TDS (mg/L)	Conductivity (µS)	Flux ($L/m^2 \cdot hr$)	Reverse Flux ($g/m^2 \cdot hr$)
0	491.37	2.39	3.04		
15	491.07	2.51	3.18	0.58	0.08
30	490.45	2.23	2.97	1.20	0.00
45	490	2.52	3.26	0.87	0.17
60	489.62	2.38	3.17	0.74	0.00
75	489.23	2.32	3.24	0.76	0.04
90	488.89	2.39	3.17	0.66	0.00
105	488.55	2.46	3.39	0.66	0.13
120	488.28	2.56	3.48	0.52	0.05

Table A.3 Fe_3O_4 NPs Weight, TDS, and Conductivity Measurements over Time (cont.)

DI (Draw at 3 g/L)					
Time	Weight (g)	TDS (mg/L)	Conductivity (µS)	Flux ($L/m^2 \cdot hr$)	Reverse Flux ($g/m^2 \cdot hr$)
0	511.54	2.36	3.56		
15	504.14	2.23	3.47	14.37	0.00
30	504.12	2.21	3.52	0.04	0.03
45	503.91	2.23	3.54	0.41	0.01
60	503.71	2.25	3.65	0.39	0.06
75	503.44	2.23	3.68	0.52	0.02
90	503.19	2.32	3.75	0.49	0.04
105	503.01	2.22	3.78	0.35	0.02
120	502.7	2.27	3.79	0.60	0.00
DI (Draw at 5 g/L)					
Time	Weight (g)	TDS (mg/L)	Conductivity (µS)	Flux ($L/m^2 \cdot hr$)	Reverse Flux ($g/m^2 \cdot hr$)
0	484.31	1.98	3.85		
15	483.86	1.96	3.88	0.87	0.01
30	483.71	2..03	4.04	0.29	0.09
45	483.57	1.9	3.97	0.27	0.00
60	483.23	1.94	3.99	0.66	0.01
75	482.7	1.89	3.98	1.03	0.00
90	482.45	1.94	4.09	0.49	0.06
105	482.23	1.96	4.21	0.43	0.07
120	481.94	2.01	4.23	0.56	0.01

Table A.4 Literature Review Draw Agent Characteristics

Source	Feed Solution	FS Concentration	Draw Agent	DS Concentration	Membrane Mode	Flowrate	Water Flux	Reverse Solute Flux	Osmotic Pressure	Membrane	Viscosity	Separation Method	Separation Difficulty	Cost	Toxicity	Pilot/Industry Scale	Category of Draw Agent	Purpose
[57]	treated sewage effluent (TSE) collected from MBR and salinity within brackish water range	treated sewage effluent collected from a wastewater treatment plant in Doha, Qatar	NaCl	0.5M (equal to seawater concentration at 35 g/L)	FO	2L/min	11.8 LMH	44.9 gMH	39 atm	TFC	NA	RO	NA	NA	NA	Pilot Scale	Inorganic Salts	Industry - Irrigation
			engineered fertilizing solutions (EFS)	0.5M NaCl and 0.01M diammonium phosphate ((NH4)2HPO4)	FO	2L/min	13.2 LMH	70.3 gMH	50 atm			RO						
[44]	DI Water	NA	NaCl and Oleic Acid	0.6 M NaCL and less than 25 mmol/L surfactants based on their CMC (Table 2)	FO	42.5 cm/s	1.1 LMH	0.3 gMH	NA	TFC		NA	NA	NA	NA	Pilot Scale	Organic Compounds	Research
			NaCl and Sodium dodecyl benzene sulfonate (SDBS)				10.2 LMH	2.1 gMH			0.88 cP							
			NaCl and Potassium Oleate (PO)				10.7 LMH	2.0 gMH			0.91 cP							
			NaCl and Sodium Dodecyl Sulfate (SDS)				9.3 LMH	2.2 gMH			0.93 cP							
			NaCl and Polyoxyethylene lauryl ether (Brij35)				6.9 LMH	1.6 gMH			0.87 cP							
			NaCl and Polyethylene glycol tert-octylphenyl ether (Triton X-100)				8 LMH	2.2 gMH			0.88 cP							
[19]	DI Water	NA	thermo-sensitive polyelectrolyte of poly(N-isopropylacrylamide-co-acrylic acid) (PNA)	0.20 g·ml−1	PRO	NA	2.09 LMH	Speculated as low - literature values 1.2 LMH but this polyelectrolyte is negatively charged and larger	~12*10^-5 Pa	CTA	8.3 Pa*s	Heating and Centrifuging	For water recovery, the supernatant liquid should be dewatered by hot ultrafiltration or nanofiltration later to recover the draw agents completely.	NA	NA	Pilot Scale	Polymers	Research
				0.38 g·ml−2			2.95 LMH		72*10^-5 Pa		59.8 Pa*s	Heating and Standing						
[35]	DI Water & NaCL	0M, 0.6M NaCL, 1.2M NaCL	CO2-rich Monoethanolamine (MEA) solution	5.0 M	FO	17.0 cm/s	39.6 LMH, 14.8	29.4 gMH	NA	TFC	NA	Membrane Distillation (MD)	99.99% rejection of MEA	NA	NA	Pilot Scale	Organic Compound	Industry - CO2 capture

							LMH, 7.43 LMH											for fossil-fuel power stations
	flue gas desulfurization (FGD) wastewater from from a coal-fired power plant in Samcheonpo, Korea	Table 2					feed wastewater was successfully concentrated by more than 75%	NA										
[14]	DI Water	NA	CM-dextran-1000	40 wt%	PRO	0.15 L/min	24.9 LMH	0.97gMH	65 bar	Home-made PVDF-TFC	NA	NA	NA	NA	cytotoxic-ities were assessed through CCK-8 assay, nontoxic nature of synthesized CM-dextrans and their potential application as safe draw solutes in FO process.	commercial lab-scale FO facility	Organic Compund	Research - Desalination
	NaCL	0.6M NaCl					6.07 LMH											
[58]	DI Water	NA	concentrated brine/virgin sea bittern	24.17 °Bé, 26.15 °Bé and 29.00 °Bé	recirculation (RC) & continuous single pass (CSP) mode	Feed = 45 L/h & Draw = 1.5 L/h		4560–6066 mGH	24 °Bé = 549.5 bar, 26 °Bé = 621.4 bar, 29 °Bé = 716.0 bar	Aquaporin Inside™ hollow fibre FO membrane module	NA	NA	NA	NA	NA	Pilot Scale	Inorganic Salts	Industry - salt production
	NaCl	36,000 m/L and 24 °Bé		24.17 °Bé, 26.15 °Bé and 29.00 °Bé			6.17, 6.48 and 6.73 LMH											
	natural seawater	2.84 °Bé		29 °Bé			8.3 LMH											
[59]	palm oil mill effluent (POME) digestate (humic acid solution)	0-100 g/L	Na lignosulfonate	150 g/L	NA	Flowrate = 100 ml/min & Cross velocity = 5.2 cm/s	2.4 LMH	<1 mGH (extrapolated from graph)	1.89 bar	Asymmetric flat-sheet membranes	NA	NA	NA	NA	NA	NA	Polymers	Industry - palm oil production
			Ca lignosulfonate	150 g/L			1.3 LMH	~5 mGH	1.46 bar									
[15]	DI Water	NA	Cationic Starch	30 wt%	PRO	NA	4.10 LMH	1.62 gMH	11.91 atm	TFC	~70 mPa*s (from graph)	dead-end ultrafiltration	ultrafiltration was effective to reconcentrate the diluted draw solution with a rejection rate > 99% at a concentration	low cost	complete biodegradability	Pilot Scale	Polymers	Research
	NaCL	2 g/L					2.20 LMH	11.83 gMH										

												< 6 wt% cationic starch					
[26]	DI Water	NA	Ethanol	10 wt%	PRO	cross-flow velocity of 12.8 cm/s	~17 LMH (graph)	~240 gMH (graph)	46.7 bar	TFC.	NA	vacuum distillation	successfully reconcentrated, exergy analysis estimated the energy required for separation into product water and reusable draw solution as 8.8 kWh/m3	ethanol as a draw solute in FO for high salinity wastewater treatment is economically feasible	NA	Pilot Scale	Volatile Organic Compund	Research - saline wastewater treatment
	NaCL	0.5-1.5 M			FO												
[20]	DI Water	NA	Hydrolyzed poly(isobutylene-alt-maleicacid) (PIAM-Na)	0.375 g/mL	PRO	8.5 cm/s	34 LMH	0.196 gMH	`1500 mmol/kg (graph)	CTA	~16 relative viscosity (graph @ 60C)	MD	easy method for the draw solute recovery and produced ultrapure water with N99.99% rejection of PIAM-Na ions	low cost	Nontoxic - MTT assay method	Pilot Scale	Polymers	Research - Deslination
	synthetic seawater	3.5 wt% NaCl					NA	NA									
[16]	DI Water	NA	Poly(propylene glycol) (PPG-725)	40% wt	PRO	6 cm/s	10 LMH	NA	2000 mOsmol/kg	TFC	8 cP	MD	solute rejection of 97% was achieved for 40% PPG-725/Triton X-114	replenishment cost of PPG-725/TX-114 will be extremely less compared to other draw agents	LD50 value of PPG-725 is much higher than other draw agents, which means PPG-725 can be considered to be safer than that of other osmotic agents	Pilot Scale	Polymers	Research - Deslination
	DI Water	NA	Poly(propylene glycol) and non-ionic surfactant (Triton X-114) (PPG-725/TX-114)	40%/0.8 mM			10 LMH	0.18 gMH									
	Synthetic brackish water	TDS = 5000 g/L					~8 LMH (graph)										
	Synthetic Seawater	TDS = 350000 g/L					~6 LMH (graph)										
[30]	DI Water	NA	Glauber salt (sodium sulfate decahydrate, Na2SO4·10H2O)	1-1.5M	FO	flowrate = 1L/min & cross-flow velocity = 0.015m/s	4.60-7.03 LMH	0.42 gMH	95.2 atm (2M)	A membrane taken out from domestic RO spiral module incorporated in to the test cell as a FO membrane	0.0013 kg/ms	low pressure nanofiltration (NF) process	Good quality permeate containing negligible salt (< 150 mg L−1 TDS) was generated at<5 atm. Pressure	Glauber salt is inexpensive and widely available.	minimal toxicity	Pilot Scale	Inorganic Salts	Research - Textile Wastewater & Brackish Water
	Synthetic Wastewater	(Table 2)					3.30-4.30 LMH										
	Industrial Wastewater	(Table 2)					4.40-5.37 LMH										
	Synthethic Seawater	0.6 M NaCl					1.87-2.58 LMH										
	Synthetic Brackish Water	0.25 M NaCl					4.22-4.74 LMH										

[17]	DI	NA	Chlorhexidine gluconate based mouthwash (CMW)	25-100%	PRO	6 cm/s	8-14 LMH	0.98 gMH	700-2709 mOSm/kg	TFC	1.2-2.2 cP	thermally driven MD	The salt rejection percentage approximately 94%, 45.45% of the feed was recovered as permeate	less replenishnment cost for CMW compared to NaCl	very less toxic due to its high lethal dose (LD50) value	Pilot Scale	Cationic Surfactant	Research - Desalination
	Brackish Water	5000ppm NaCl		1			9 LMH		2709 mOSm/kg		2.2 cP							
	Seawater	32000ppm NaCl		1			6 LMH											
[60]	DI	NA	Ferric Sulfate	280000ppm	FO	flowrate = 1L/min & cross-flow velocity = 1.4 cm/s		1.88 gMH	52.6 atm	CTA	5.08 cP	Precipitation	Pure water samples with salt contents of 60 and 80 ppm were obtained by desalinating brackish and seawater	NA	NA	Pilot Scale	Inorganic Salts	Research - Desalination
	Brackish Water	5000ppm NaCl					3.75 LMH											
	Seawater	40000ppm NaCl					1.61 LMH											
[29]	Distilled Water	NA	Polydiallyldimethylammonium Chloride (PolyDADMAC)	0.035, 0.085, 0.120 and 0.155 g/mL	FO	flow rate = 60 L/h	10.50 LMH (initial)	High	3-16 atm	CTA	21-72E-4 Pa*s	NF	High ion rejection of DADMAC (96%) and poor ion rejection of PolyDADMAC (85%) werem observed	NA	NA	Pilot Scale	Cationic Polyelectrolyte - Polymers?	Research
			DADMAC	0.035, 0.085, 0.120 and 0.155 g/mL			20 LMH (initial)		8-50 atm	Aquaporin flat sheet membrane,	9-12E-4Pa*s							
[61]	NaCl	0.6 M NaCl	mixtures of two different glycol ethers, tripropylene glycol methyl ether and tripropylene glycol n-butyl ether	20 wt%	FO, PRO, FO assisted, and PRO assisted	200 ml/min	1.3 LMH (FO), 3.0 LMH (PRO), 1.6 LMH (FO assisted), 4.2 LMH (PRO assisted) (@ 50wt% & 295K)	4.9 gMH (FO), 2.9 gMH (PRO), 3.8 gMH (FO assisted), 3.0 gMH (PRO assisted)	30 atm	Cellulose acetate FO membrane	0.5-3.5 mm2/s (T vary)	RO	NA	NA	NA	Pilot Scale	Volatile Organic Compound	Research - Desalination
				50 wt%					75 atm		1-6 mm2/s (T vary)							
				80 wt%					140 atm		2-13 mm2/s (T vary)							
[31]	Methylene Blue	DI	magnetic core-hydrophilic shell nanospheres with attached ligands		NA	NA	2.13 LMH (SiPEG-MN 50g/L)	NA		CTA	NA	magnetic recovery processes	the covalently bound surface hydrophilic agents ensured a high level of particle stability during the repetitive magnetic recovery processes.	NA	NA	Pilot Scale	Magnetic Nanoparticles	Research
		500ppm	SiPEG-MN	10g/L - 50g/L			1.58 LMH											
		1000ppm					1.41 LMH		1.4-7.6 atm									
		5000ppm	SiCOOH-MN				0.87 LMH		1.1-6.3 atm									

[37]	DI Water	NA	Poly sodium acrylate (PSA)-coated Magnetic Nanoparticles (PSA-MNPs)	0.13 wt.%	NA	NA	5.32 LMH	NA	11.37 atm	carbon nanotube FO membrane	similar to that of water	applying an external magnetic field	could be recovered under a low magnetic field	low production cost owing to the low draw solute concentration	bio-compatible and environment-friendly as it can be recycled without releasing chemicals as by-products in water or air	Pilot Scale	Magnetic Nanoparticles	Research
[23]	DI Water	NA	potassium functionalised carbon nanofibers suspended in triethylene glycol (TEG-K/CNF)	TEG (10, 15, 20 vol%)	FO	crossflow velocity = 8.50 cm/s	13.3 LMH (0.2 wt% K/CNF in 20 vol% TEG aqueous solution)	0.25 gMH	28-70.3 bar	FO flat sheet membrane	NA	Evaporation	vapours condensed and the quality of product water is found to be comparable with potable water standard	NA	NA	Pilot Scale	Nanofiber	Research - Desalination
	Brackish Water	3.0 wt%		K/CNF (0.05, 0.1, 0.15, 0.2 wt%)			8.6 LMH	NA										
[27]	Milli-Q water	NA	Pretreated and enzymatically Hydrolysed Wheat Straw (PHWS)	1	FO	50 ml/min	6.21 LMH	NA	1.8-42.6 bar	Flat sheet membranes	density of crude glycerol was measured to be 1.249 g/ml	water can be directly recovered and transferred back into the fermentation loop without further purification	NA	Indicative major FO operational and capital costs were very low compared to the potential economic benefits of the process due to water re-use.	NA	Pilot Scale	Organic Compunds	Research/Industry - Biorefinery reduce GHG
	PHWS	0.05					5.37 LMH											
		0.2					1.33 LMH											
	DAKA Crude Glycerol	0.05	DAKA Crude Glycerol	1		51 ml/min	8.39 LMH		2.54-468.5 bar									
		0.02					8.99 LMH											
		0.01					10.5 LMH											
[62]	Synthetic Wastewater	NA	DS - EDTA-Na2	0.05, 0.1, 0.15, 0.2, and 0.25 mol/L	NA	20 ml/min	1.57 LMH (0.2 mol/L EDTA)	0.36 gMH	NA	CTA	NA	Precipitation	90% of EDTA DS could be recovered and then successfully reused in the subsequent OsMFC operation	NA	NA	Pilot Scale	Organic Compounds	Research - Osmoticmicrobial fuel cell (OsMFC) electricity generation
[49]	simulated radioactive wastewater	20 mg CoCl2/L, 20mg SrCl2/L and 20 mg CsCl/L	NaCl	0.5- 2.0 M	PRO	2-11 cm/s	16.99-38.03 LMH	3.28-9.78 gMH	NA	CTA	NA	NA	NA	NA	NA	Pilot Scale	Inorganic Salt	Research/Industry - radioactive wastewater from nuclear facilities
[21]			monocationic hydrophilic ionic liquids (ILs) -		PRO	flowrate = 0.25 L/min &			(0.5 M)	CTA	NA	direct contact membrane	The consistent Jw values demonstrate	NA	MTT and cytotoxicity Assay -	Pilot Scale		Research - Desalination

			Tetraethylammonium bromide			crossflow velocity = 5.4 cm/s						distillation (DCMD)	the suitability of DCMD to regenerate		[N2222]Br showed minor detrimental effects on cell viability, [N2222]Br can be safely used as DS for seawater desalination			
	DI	NA	[N2222]Br	0.5 -M			10.65 LMH	0.0397 molMH	21 bar								Thermally responsive hydrogels	
				1M			14.20 LMH	0.066 molMH										
				2M			21.27 LMH	0.086 molMH										
				4M			26.46 LMH	0.1128 molMH										
	Seawater	0.6 M NaCl		4.0 M			12.10 LMh	0.12 molMH	NA									
[28]	DI	NA	oligomeric poly(tetrabutylphosphonium styrenesulfonate)s (PSSP#)	10-40 wt%	FO	NA	(10 and 20 wt%)	(10 and 20 wt%)	(10 and 40 wt%)	TFC	(10 and 40 wt%)	Thermal precipitation	easy separation of the PSSPs	PSSP requires much less operating cost for the operation compared to the SSP or other ionic salts	bactericidal property of the PSSP series was tested against model negative bacteria. More than 99.9% of the calculated bactericidal properties were observed for SSP, PSSP5, PSSP6, and PSSP11	Pilot Scale	Inorganic Salt	Research - Desalination
			SSP				8.02 - 16.28 LMH	0.29 - 0.53 gMH	8.79 - 43.11 atm		0-14 cP							
			PSSP5				7.58 - 14.50 LMH	0.11 - 0.14 gMH	8.04-42.96 atm		3-25 cP							
			PSSP6				7.43 - 13.66 LMH	0.05 - 0.08 gMH	8.01-40.06 atm		3-30 cP							
			PSSP11				6.32 - 13.14 LMH	0.01 - 0.05 gMH	7.16-34.44 atm		12-75 cP							
	NaCl	2000 ppm	PSSP5	20 wt%			6.12 LMH	NA	NA		NA							
[24]			morpholine derivatives		FO	constant flowrate				polyketone (PK) TFC		LCST-type phase separation	dilute phase of the BuMP solution after phase separation at 70 °C showed a considerably low concentration (3.3 wt %) and low osmotic pressure (3.16 bar	reduced energy consumption in postprocessing low-pressure RO to obtain fresh water.	biodegradable, and thus, if used on a large scale, it will have a low environmental burden	Pilot Scale	Thermally responsive organic compounds	Research - Desalination
	Milli-Q Water	NA	BuMP	55.0 wt%			2.09 LMH	14.0 gMH	3.2 bar (dilute phase)		7.06 mPa*s							
			CPMP	9.0 wt%			1.98 LMH	2.53 gMH	11.0 bar (dilute phase)		1.64 mPA*s							
			PPG400	28.8 wt%			3.64 LMH	19.0 gMH	11.0 bar (dilute phase)		6.64 mPa*s							
	NaCl	0.6 M	BuMP	94.6 wt%			0.56 LMH	8.30 gMH	NA		3.02 mPa*s							

[63]	DI	NA	CO2-responsive polymers with high nitrogen to carbon ratios		NA	NA	NA	NA	@ 25 wt./vol% in DI in CO2	NA	NA	NA	NA	NA	NA	Pilot Scale	CO2 - responsive polymer	Research
			linear poly(N-methylethylenimine) (l-PMEI),	5-10 mg/L					25.0 bar									
			branched poly-(N-methylethylenimine) (b-PMEI)						15.0 bar									
			poly(N,N-dimethylallylamine) (PDMAAm)						19.5 bar		3.5-1000 cst (in CO2)							
[25]	DI	NA	1,4-piperazinediethanesulfonic acid disodium salt (P-2SO3-2Na)	1.0 M	FO	0.014 L/min	76.4 LMH	0.5 gMH	10 - 120 atm (0.1-1M)	Home-made TFC membranes coated on a poly(ether sulfone) (PES) support layer of either flat sheet (TFC-PES(FS)) or hollow fiber (TFC-PES(HF))	1.25 - 3.6 Relative Viscosity (0.1-1M)	MD	complete recovery of the draw solute. Reproducible results were achieved when the recovered P-2SO3-2Na was reused to the FO process	lower the draw solute replenishment cost	NA	Pilot Scale	piperazine-based ionized functional materials (PIFMs)	Research - Desalination
	NaCl	0.1-3.5 wt%					11.3−35.0 LMH	NA										
[22]	DI	NA	deep eutectic solvents (DESs)	1:2 mol ratio	FO	1.8 L/min		0.098 gMH	4750 - 1300 mmol/kg (1:3-1:11 DES:water ratio (v/v))	Indigenous thin-film composite polyamide (TFC-PA) membrane	CC-EG: 33 cP & CC-Gly: 222cP	solid−liquid phase separation on freezing DES: freezing at ∼−7 °C	Although this study confirms the possibility of extracting DES from aqueous systems, much work needs to be done in this direction to minimize the loss of DS and production of high quality water from difficult FS.	HBA is inexpensive. With appropriate process design and better membranes, DESs can be an economically viable draw solution.	made from HBA - nontoxic. CC-EG and CC-Gly solutions exhibit low toxicity	Pilot Scale	Ionic Liquids - Deep Eutectic Solvents	Industry - brackish water, seawater, dye contaminated wastewater, and tannery wastewater
			choline chloride-ethylene glycol (CC-EG)				3.6 LMH											
			choline chloride-glycerol (CC-Gly)															
	NaCl	2000 ppm	CC-EG				5.2 LMH											
			CC-Gly				7.54 LMH											
	MgSO4		CC-Gly				4.5 LMH											
	Tannery waste effluent	concentrated powder extracts of real tannery effluents namely polyphenol, phenol-HCHO, red brown dye, and ∼2000 ppm	CC-EG				~3.2-1.8 LMH											

		of NaCl in 1000 mL of water (TDS- 60,600 ppm),															
	Sea Water	collected form Gujarat coast (Table 1)															
	Brackish Water	locally sourced brackish water (Table 1)	CC-EG			~7 LMH											
			CC-Gly			~7 LMH											
	Simulated dye wastewater	20 ppm RB5	CC-EG			~5 LMH											
[18]	DI	NA	Organic phosphonate salts (OPs)	0.5M	PRO	0.3 L/min				homemade thin-film composite membrane (PSF-TFC) HTI-TFC membranes	Relative Viscosity	NF	rejection above 92%, pressure-driven NF process is actually an energy-intensive process for the recovery of the concentrated draw solution	NA	NA	Pilot Scale	Thermally responsive organic compounds	Research - wastewater reclamation and seawater desalination
			diethylenetriamine pentakis(methylphosphonic) sodium salt (DTPMP-Na)			27.5 LMH (HTI-TFC membrane)	0.5-1 gMH (HTI-TFC membrane)	110 bar (0.85 M)			13 (0.8 mol/kg)							
			tetraethylenepentamine heptakis-(methylphosphonic) sodium salt (TPHMP-Na)			54 LMH (PSF-TFC membrane), 30.6 LMH (HTI-TFC membrane)	0.83 gMH (PSF-TSC membrane), 0.64 gMH (HTI-TFC membrane)	120 bar (0.55 M)			22 (0.6 mol/kg)							
			polyethylenimine (methylenephosphonic) sodium salt (PEI-600P-Na)			48 LMH (PSF-TFC membrane), 27 LMH (HTI-TFC membrane)	0.4 gMH (PSF-TSC membrane), 0.6 gMH (HTI-TFC membrane)	121 bar (0.55 M)			45 (0.55 mol/kg)							
			PEI-1800P-Na			17.5 LMH (HTI-TFC membrane)	0-0.4 gMH (HTI-TFC membrane)	170 bar (0.25 M)			83 (0.2 mol/kg)							
	Emulsified Oil and Water: soybean oil, DI water, and Tween 80	(the weight ratio of soybean oil and Tween 80 is 9:1) to get an emulsion of 100,000 ppm TOC	TPHMP-N			water flux decreases slowly from 26.5 to 18 LMH over 8h (PSF-TFC membrane)	NA	NA			NA							

[50]	Wastewater	real domestic WW pre-treated in an hydrolytic anaerobic reactor working in a domestic WW treatment plant operated by FCC Aqualia in Spain	RO SW desalination plants brine	70 g/L	FO	0.3 L/min	19 LMH	NA	NA	TFC	NA	NA	NA	NA	NA	Pilot Scale	Inorganic Salts	Research - Wastewater treatment
[64]	DNA - extracted from salmon testes in the sodium salt form	500 ppm in 0.01 M Tris-HCl buffer	choline chloride–ethylene glycol (ChoCl–EG 1 : 2)	1 : 2 molar ratio	FO	1.8 L/min	3.1 LMH per bar (1 bar applied)	NA	CC-EG: 365 atm & CC: Gly: 317 atm	TFC	CC-EG: 33 cP & CC-GLy: 222cP	CC-EG chilled to -5C to separate	The recovered CC–EG was reused for three different cycles in the protein enrichment process maintaining identical flux that was recorded with pure CC–EG 1 : 2.	Energy benefits from freezing of the diluted draw solution to recover product reusable draw solution compared to pressure driven processes and other FO systems are very significant.	NA	Pilot Scale	Ionic Liquids - deep eutectic solvents (DESs)	Research - concentration of proteins and DNA in biotechnology, molecular biology, food sciences and clinical research
[33]	DI Water	NA	1-cyclohexylpiperidine (CHP)	7.6 mol/kg	FO	300 mL/min	22 kg/m2h	NA	500 atm	FO polyamide thin film composite membrane	NA	solution was “degassed” removing carbon dioxide and converting the aqueous ammonium bicarbonate solute to a water immiscible CHP which can be decanted from water.	The initial degassing studies suggest that 70 °C should be sufficient to degas CHP at ambient pressure with the use of lower temperatures possible given reduced pressures. These results are very promising and address all of the major challenges in developing an integrated SPS-FO process as identified in our initial SPS-FO study [11]. A forthcoming techno-	cost of CHP and draw solute regeneration process for CHP are expected to be more economic than nearly any other next generation draw solute reported to date	NA	Pilot Scale	switchable polarity solvent (SPS)	Research - Desalination
	NaCl	0.5 mol/kg		5 mol/kg		linear velocity = 6 cm/s	8.5 kg/m2h	0.004 kg/m2h										
		1 mol/kg		5 mol/kg			5.1 kg/m2h	0.0094 kg/m2h										

												economic process model of SPS-FO is also favorable					
[34]	DI Water	NA	poly (sodium4-styrenesulfonate) (PSS) polyelectrolytes		PRO	184 mL/min	Conc: 0.24 g/mL	Conc: 0.24 g/mL	NA	TFC	NA	low pressure-driven ultrafiltration (UF) system	under 2 bar with low energy consumption	NA	NA	Pilot Scale	polyelectrolytes	Research - Desalination
			PSS (70,000)	0.04, 0.12. 0.24, 0.48 g/mL			18.2 LMH	5.5 gMH			4, 6, 12, 1014 cP							
			PSS (200,000)				13 LMH	9.2 gMH			5, 10, 30, 15000 cP							
			PSS (1,000,000)				11.8 LMH	5.9 gMH			28, 120, 537.9 cP							
[35]	DI Water	NA	Poly (aspartic acid sodium salt) (PAspNa)	0.3 g/mL	PRO	8.5 cm/s	31.8 LMH	4 gMH	5.08 - 51.5 atm	TFC	1.2 - 4.5 cP	pressure-driven NF	demonstrate the effectiveness of size exclusion by large molecular size of PAspNa with low energy consumption	commercially available with reasonable unit price, $8.8/kg	non-toxic, PAspNa does not harm human skin cells	Pilot Scale	polyelectrolytes	Research - Wastewater Treatment
	Synthetic Wastewater	Table 1					8.22 LMH					thermal-driven MD	reduce the viscosity of the PAspNa solution					
[36]	synthetic dyeing wastewater	Reactive Brilliant Red K-2BP (RBR K-2BP, purity> 99%)	hydrolyzed polyacrylamide (HPAM)	20 g/L	FO	10 cm/s	3.2 LMH	NA	366 mOsm/kg H2O	TFC	180.4 mPa s	physical cleaning	results do not necessarily indicate that the combined fouling in FO process is irreversible, as it is still possible to fully recover the membrane flux by appropriate chemical cleaning	NA	neutral and non-toxic	Pilot Scale	Polymer	Research - dye wastewater reclamation
[37]	DI Water	NA	poly(sodium acrylate) polymer poly(N-isopropylacrylamide) (PSA–PNIPAM)-coated MNPs	0.062% (w/v)	PRO	NA	11.66 LMH	NA	24.92 atm	carbon nanotube FO membrane	NA	temperature-assisted magnetic separation	The easy and quick separation of the diluted draw solution within 1–5 min under the	Cost-effective recycling	environmentally friendly	Pilot Scale	MNP	Research - Desalination

													combined effect of magnetic field and heating above 328C					
[38]	DI water	NA	trimethylamine–carbon dioxide (TMA–CO2)	1M	PRO	17.1 cm/s	33.4 LMH	0.2 mol/m2h	48.8 bar	TFC	1.04 cP	Thermal separation	the reduced energy requirement for recovery of the TMA–CO2 draw solution allows leveraging low-grade heat sources typically available in many industrial settings.	NA	Considering TMA extremely low odor threshold, pungent fishy odor, and toxicity, rigorous and thorough care must be taken to limit human exposure to TMA when handling TMA–CO2 draw solution	Pilot Scale	Amines	Research
[39]	DI Water	NA	ethylenediamine tetrapropionic (EDTP) acid (salt)	0.8M	PRO	0.3 L/min	22.69 LMH	0.32 gMH	118.14 bar	CTA	4.4 (DI)	nanofiltration (NF)	a solute rejection about 71% is achieved	NA	NA	Pilot Scale	carboxyl-containing org solutesanic draw	Research
[40]	DI Water	NA	protonated betaine bis(trifluoromethylsulfonyl)imide ([Hbet][Tf2N])	3.2M	NA	NA	2.27 LMH	NA	NA	polyamide type of membrane	NA	thermal-driven phase separation	relatively high saturation concentration in the α phase at room temperature. Hence, the α phase will need further purification by either RO or NF to reach the drinkable water level	NA	NA	Pilot Scale	thermoresponsive ionic liquid (IL)	Research
	NaCl	0.17					0.85 LMH	0.98 gMH										
		0.6					0.5 LMH	2.31 gMH										
		1					0.44 LMH	4.65 gMH										
		2					0.25 LMH	3.86 gMH										
		3					0.14 LMH	2.17 gMH										
[41]	DI Water	NA	Branched PEI (Mw =25,000 Da)	20 wt%	PRO	1 mL/h	11 LMH	1.01 gMH	19 bar	TFC	25.98 mPa s	NF	drop of permeate flux when recovering with NF	NA	NA	Pilot Scale	polyelectrolyte	Research
[42]	DI Water	NA	Triton X100 coupled to Na3PO4	0.55 M Na3PO4+ 0.5 mM Triton X100	FO	500 mL/min	5.68 LMH	0.13 gMH	3.8 Mpa	CTA	1.63 cP	Two stage UF-NF system	complicated and energy-intensive recovery, 98%	NA	NA	Pilot Scale	nonionic surfactant & inorganic	Research
	Brackish water	4090 ppm NaCl					4.89 LMH	NA	NA		NA							

												recovery of solutes					
[43]	DI Water	NA	High charge Na3PO4	0.2M	PRO	0.5 L/min	12.5 LMH	0.84 gMH	580 mOsm/kg H2O	TFC	1.2 cP	MD (50C)	most effective in achieving a high water flux (10.28 L/m2 h) and high salt rejection (approximately 100%) in a diluted Na3PO4 draw solution	NA	NA	Pilot Scale	inorganic	concentrating high-nutrient sludge
[44]	DI Water	NA	triethylenetetramine hexapropionic acid sodium (TTHP-Na)	0.5g/mL	PRO	300 mL/min	23.07 LMH	0.75 gMH	133 bar	CTA	11 (DI)	NF	high rejection rate achieved in NF process is obtained using 3-bar external pressure, energy efficiency in NF process drops significantly with the increase in the feed solution concentration	NA	NA	Pilot Scale	inorganic	Research - dye wastewater
	Dye Wastewater	1000 ppm Congo red		0.3 g/mL			12.5 LMH	NA										
[45]	DI Water	NA	ethylenediaminetetraacetic acid (EDTA-2Na) coupled with nonylphenol ethoxylates (NP7)	1M EDTA-2Na + 15 mM NP7	FO	NA	8.8 LMH	0.067 gMH	59.46 bar	TFC	1.2 cP	NF	95% recovery of draw solute	NA	NA	Pilot Scale	organic	Research - Desalination
	seawater	35 g/L NaCl					3.81 LMH	NA										
[46]	DI Water	NA	polyelectrolyte salt-poly (4-styrenesulfonic acid-co-maleic acid) sodium - P(SSA-co-MA)-Na-1	0.25 g/mL	PRO	300 mL/min	15 LMH	0.04 gMH	32.8 bar	TFC	6 (DI)	NF	diluted drawsolution can also be easily regenerated via NF with a comparable water flux and a high rejection rate	NA	NA	Pilot Scale	inorganic	Research - dye wastewater
	Dye Wastewater																	

Table A.5 AHP Pairwise Comparison Matrix

Item Description	Flux	Reverse Flux	Replenishment Cost	Regeneration Cost	Regeneration Efficacy
Flux	1.00	5.00	3.00	3.00	3.00
Reverse Flux	0.20	1.00	2.00	2.00	2.00
Replenishment Cost	0.33	0.50	1.00	1.00	1.00
Regeneration Cost	0.33	0.50	1.00	1.00	2.00
Regeneration Efficacy	0.33	0.50	1.00	0.50	1.00
Sum	2.20	7.50	8.00	7.50	9.00

Table A.6 AHP Standardized Matrix

Item Description	Flux	Reverse Flux	Replenishment Cost	Regeneration Cost	Regeneration Efficacy	Weight
Flux	0.45	0.67	0.38	0.40	0.33	0.45
Reverse Flux	0.09	0.13	0.25	0.27	0.22	0.19
Replenishment Cost	0.15	0.07	0.13	0.13	0.11	0.12
Regeneration Cost	0.15	0.07	0.13	0.13	0.22	0.14
Regeneration Efficacy	0.15	0.07	0.13	0.07	0.11	0.10

Table A.7 TOPSIS Pairwise Comparison Matrix

Beneficial/Non-Beneficial Criteria	Benf.	Non Benf.	Non Benf.	Non Benf.	Benf.
Weightage	0.44	0.19	0.12	0.14	0.10
Criteria	**Flux (LMH)**	**Reverse Flux (gMH)**	**Capital Cost ($/kg)**	**Regeneration Cost**	**Regeneration Efficacy**
CM-dextran-1000	24.9	0.97	1990.00	2	2
Cationic Starch	4.1	1.62	721.22	3	4
Poly(propylene glycol) and non-ionic surfactant (Triton X-114) (PPG-725/TX-114)	10	0.18	3752.43	4	4
Chlorhexidine gluconate based mouthwash (CMW)	14	0.98	148.38	4	4
diethylenetriamine pentakis(methylphosphonic) sodium salt (DTPMP-Na)	27.5	1	1401.02	3	5
tetraethylenepentamine heptakis-(methylphosphonic) sodium salt (TPHMP-Na)	54	0.64	1200.02	3	5
polyethylenimine (methylenephosphonic) sodium salt (PEI-600P-Na)	48	0.6	1826.71	3	5
PEI-1800P-Na	17.5	0.4	1616.71	3	5
thermo-sensitive polyelectrolyte of poly(N-isopropylacrylamide-co-acrylic acid) (PNA)	2.09	1.2	2813.04	3	2
Hydrolyzed poly(isobutylene-alt-maleicacid) (PIAM-Na)	34	0.196	202.80	4	4
monocationic hydrophilic ionic liquids (ILs) Tetraethylammonium bromide ([N2222]Br)	10.65	23.71	216.60	4	4
choline chloride-ethylene glycol (CC-EG)	3.6	0.10	18361.66	3	4
potassium functionalised carbon nanofibers suspended in triethylene glycol (TEG-K/CNF)	13.3	0.25	5800.00	1	2
BuMP	2.09	14	52250.00	3	4
CPMP	1.98	2.53	4440.00	3	4
PPG400	3.64	19	107.92	3	4
1,4-piperazinediethanesulfonic acid disodium salt (P-2SO3-2Na)	76.4	8.3	4401.54	4	4
Ethanol	17	240	66.32	4	4
Pretreated and enzymatically Hydrolysed Wheat Straw (PHWS)	6.21	5	11.00	1	5
SSP	16.28	0.53	1380.00	3	4
PSSP5	14.5	0.14	2909.00	3	4
PSSP6	13.66	0.08	2909.00	3	4
PSSP11	13.14	0.05	2909.00	3	4
Polydiallyldimethylammonium Chloride (PolyDADMAC)	10.5	5	1021.28	3	5
DADMAC	20	5	99.20	3	5

Glauber salt (sodium sulfate decahydrate, Na2SO4·10H2O)	7.03	0.42	152.20	3	5
SiPEG-MN	2.13	5	31354.40	2	3
NaCl and Oleic Acid (OA)	1.1	0.3	598.37	2	2
NaCl and Sodium dodecyl benzene sulfonate (SDBS)	10.2	2.1	386.08	2	2
NaCl and Potassium Oleate (PO)	10.7	2	935.45	2	2
NaCl and Sodium Dodecyl Sulfate (SDS)	9.3	2.2	1022.50	2	2
NaCl and Polyoxyethylene lauryl ether (Brij35)	6.9	1.6	610.60	2	2
NaCl and Polyethylene glycol tert-octylphenyl ether (Triton X-100)	8	2.2	149.48	2	2
1-cyclohexylpiperidine (CHP)	22	4	3526.48	3	4
PSS (70,000)	18.2	5.5	2768.00	3	4
PSS (200,000)	13	9.2	111.80	3	4
PSS (1,000,000)	11.8	5.9	3453.33	3	4
Poly (aspartic acid sodium salt) (PAspNa) (NF)	31.8	4	965500.00	3	4
Poly (aspartic acid sodium salt) (PAspNa) (MD)				4	5
hydrolyzed polyacrylamide (HPAM)	3.2	5	13900.00	2	2
poly(sodium acrylate) polymer poly(N-isopropylacrylamide) (PSA–PNIPAM)-coated MNPs	11.66	5	30184.65	2	4
trimethylamine–carbon dioxide (TMA–CO2)	33.4	11.82	76.67	3	4
ethylenediamine tetrapropionic (EDTP) acid (salt)	22.69	0.32	3403.96	3	5
protonated betaine bis(trifluoromethylsulfonyl)imide ([Hbet][Tf2N])	2.27	0.98	5329.55	3	4
Branched PEI (Mw =25,000 Da)	11	1.01	543.04	3	5
Triton X100 coupled to Na3PO4	5.68	0.13	1229.63	3	4
High charge Na3PO4	12.5	0.84	46.26	4	4
triethylenetetramine hexapropionic acid sodium (TTHP-Na)	23.07	0.75	13649.33	3	5
ethylenediaminetetraacetic acid (EDTA-2Na) coupled with nonylphenol ethoxylates (NP7)	8.8	0.067	378.10	3	5
polyelectrolyte salt-poly (4-styrenesulfonic acid-co-maleic acid) sodium - P(SSA-co-MA)-Na-1	15	0.04	184.40	3	5
Ammonia Carbon Dioxide (NH4-CO2)	36	10.82	495.30	3	4
Sodium Chloride (NaCl)	40	22.2	99.40	5	5
Magnesium Sulfate (MgSO4)	5.544	1.2	284.17	5	5
Potassium Bicarbonate (KHCO3)	10.08	2	256.00	5	5
Sodium Bicarbonate (NaHCO3)	8.892	1.7	104.33	5	5

Sodium Sulfate (Na2SO4)	9.216	3.1	141.00	5	5
Ammonium Sulfate ((NH4)2(SO)4)	9.864	3.6	158.83	5	5
Potassium Sulfate (K2SO4)	9.072	3.7	496.00	5	5
Magnesium Chloride (MgCl2)	9.72	5.6	128.84	5	5
Calcium Nitrate (Ca(NO3)2)	10.692	6.6	289.33	5	5
Ammonium Chloride (NH4Cl)	12.996	10.2	226.00	5	5
Calcium Chloride (CaCl2)	11.592	9.5	264.93	5	5
Potassium Chloride (KCl)	13.464	15.3	199.00	5	5
Ammonium Bicarbonate (NH4HCO3)	10.26	20.6	216.00	5	5
Potassium Bromide (KBr)	12.924	29.2	356.83	5	5

Table A.8 TOPSIS Weighted Normalized Matrix

	Flux (LMH)	Reverse Flux (gMH)	Capital Cost ($/kg)	Regeneration Cost	Regeneration Efficacy
CM-dextran-1000	0.1542	0.0039	0.0021	0.0708	0.0586
Cationic Starch	0.0254	0.0065	0.0007	0.1061	0.1172
Poly(propylene glycol) and non-ionic surfactant (Triton X-114) (PPG-725/TX-114)	0.0619	0.0007	0.0039	0.1415	0.1172
Chlorhexidine gluconate based mouthwash (CMW)	0.0867	0.0039	0.0002	0.1415	0.1172
diethylenetriamine pentakis(methylphosphonic) sodium salt (DTPMP-Na)	0.1703	0.0040	0.0014	0.1061	0.1465
tetraethylenepentamine heptakis-(methylphosphonic) sodium salt (TPHMP-Na)	0.3344	0.0026	0.0012	0.1061	0.1465
polyethylenimine (methylenephosphonic) sodium salt (PEI-600P-Na)	0.2972	0.0024	0.0019	0.1061	0.1465
PEI-1800P-Na	0.1084	0.0016	0.0017	0.1061	0.1465
thermo-sensitive polyelectrolyte of poly(N-isopropylacrylamide-co-acrylic acid) (PNA)	0.0129	0.0048	0.0029	0.1061	0.0586
Hydrolyzed poly(isobutylene-alt-maleicacid) (PIAM-Na)	0.2105	0.0008	0.0002	0.1415	0.1172
monocationic hydrophilic ionic liquids (ILs) Tetraethylammonium bromide ([N2222]Br)	0.0659	0.0954	0.0002	0.1415	0.1172
choline chloride-ethylene glycol (CC-EG)	0.0223	0.0004	0.0190	0.1061	0.1172
potassium functionalised carbon nanofibers suspended in triethylene glycol (TEG-K/CNF)	0.0824	0.0010	0.0060	0.0354	0.0586
BuMP	0.0129	0.0563	0.0540	0.1061	0.1172
CPMP	0.0123	0.0102	0.0046	0.1061	0.1172
PPG400	0.0225	0.0765	0.0001	0.1061	0.1172
1,4-piperazinediethanesulfonic acid disodium salt (P-2SO3-2Na)	0.4731	0.0334	0.0045	0.1415	0.1172
Ethanol	0.1053	0.9659	0.0001	0.1415	0.1172
Pretreated and enzymatically Hydrolysed Wheat Straw (PHWS)	0.0385	0.0201	0.0000	0.0354	0.1465
SSP	0.1008	0.0021	0.0014	0.1061	0.1172
PSSP5	0.0898	0.0006	0.0030	0.1061	0.1172
PSSP6	0.0846	0.0003	0.0030	0.1061	0.1172
PSSP11	0.0814	0.0002	0.0030	0.1061	0.1172
Polydiallyldimethylammonium Chloride (PolyDADMAC)	0.0650	0.0201	0.0011	0.1061	0.1465
DADMAC	0.1238	0.0201	0.0001	0.1061	0.1465
Glauber salt (sodium sulfate decahydrate, Na2SO4·10H2O)	0.0435	0.0017	0.0002	0.1061	0.1465
SiPEG-MN	0.0132	0.0201	0.0324	0.0708	0.0879

NaCl and Oleic Acid (OA)	0.0068	0.0012	0.0006	0.0708	0.0586
NaCl and Sodium dodecyl benzene sulfonate (SDBS)	0.0632	0.0085	0.0004	0.0708	0.0586
NaCl and Potassium Oleate (PO)	0.0663	0.0080	0.0010	0.0708	0.0586
NaCl and Sodium Dodecyl Sulfate (SDS)	0.0576	0.0089	0.0011	0.0708	0.0586
NaCl and Polyoxyethylene lauryl ether (Brij35)	0.0427	0.0064	0.0006	0.0708	0.0586
NaCl and Polyethylene glycol tert-octylphenyl ether (Triton X-100)	0.0495	0.0089	0.0002	0.0708	0.0586
1-cyclohexylpiperidine (CHP)	0.1362	0.0161	0.0036	0.1061	0.1172
PSS (70,000)	0.1127	0.0221	0.0029	0.1061	0.1172
PSS (200,000)	0.0805	0.0370	0.0001	0.1061	0.1172
PSS (1,000,000)	0.0731	0.0237	0.0036	0.1061	0.1172
Poly (aspartic acid sodium salt) (PAspNa) (NF)	0.1969	0.0161	0.9970	0.1061	0.1172
Poly (aspartic acid sodium salt) (PAspNa) (MD)				0.1415	0.1465
hydrolyzed polyacrylamide (HPAM)	0.0198	0.0201	0.0144	0.0708	0.0586
poly(sodium acrylate) polymer poly(N-isopropylacrylamide) (PSA–PNIPAM)-coated MNPs	0.0722	0.0201	0.0312	0.0708	0.1172
trimethylamine–carbon dioxide (TMA–CO2)	0.2068	0.0476	0.0001	0.1061	0.1172
ethylenediamine tetrapropionic (EDTP) acid (salt)	0.1405	0.0013	0.0035	0.1061	0.1465
protonated betaine bis(trifluoromethylsulfonyl)imide ([Hbet][Tf2N])	0.0141	0.0039	0.0055	0.1061	0.1172
Branched PEI (Mw =25,000 Da)	0.0681	0.0041	0.0006	0.1061	0.1465
Triton X100 coupled to Na3PO4	0.0352	0.0005	0.0013	0.1061	0.1172
High charge Na3PO4	0.0774	0.0034	0.0000	0.1415	0.1172
triethylenetetramine hexapropionic acid sodium (TTHP-Na)	0.1429	0.0030	0.0141	0.1061	0.1465
ethylenediaminetetraacetic acid (EDTA-2Na) coupled with nonylphenol ethoxylates (NP7)	0.0545	0.0003	0.0004	0.1061	0.1465
polyelectrolyte salt-poly (4-styrenesulfonic acid-co-maleic acid) sodium - P(SSA-co-MA)-Na-1	0.0929	0.0002	0.0002	0.1061	0.1465
Ammonia Carbon Dioxide (NH4-CO2)	0.2229	0.0435	0.0005	0.1061	0.1172
Sodium Chloride (NaCl)	0.2477	0.0893	0.0001	0.1769	0.1465
Magnesium Sulfate (MgSO4)	0.0343	0.0048	0.0003	0.1769	0.1465
Potassium Bicarbonate (KHCO3)	0.0624	0.0080	0.0003	0.1769	0.1465
Sodium Bicarbonate (NaHCO3)	0.0551	0.0068	0.0001	0.1769	0.1465
Sodium Sulfate (Na2SO4)	0.0571	0.0125	0.0001	0.1769	0.1465
Ammonium Sulfate ((NH4)2(SO)4)	0.0611	0.0145	0.0002	0.1769	0.1465

Potassium Sulfate (K2SO4)	0.0562	0.0149	0.0005	0.1769	0.1465
Magnesium Chloride (MgCl2)	0.0602	0.0225	0.0001	0.1769	0.1465
Calcium Nitrate (Ca(NO3)2)	0.0662	0.0266	0.0003	0.1769	0.1465
Ammonium Chloride (NH4Cl)	0.0805	0.0411	0.0002	0.1769	0.1465
Calcium Chloride (CaCl2)	0.0718	0.0382	0.0003	0.1769	0.1465
Potassium Chloride (KCl)	0.0834	0.0616	0.0002	0.1769	0.1465
Ammonium Bicarbonate (NH4HCO3)	0.0635	0.0829	0.0002	0.1769	0.1465
Potassium Bromide (KBr)	0.0800	0.1175	0.0004	0.1769	0.1465

Table A.9 TOPSIS Final MCDM Ranking Matrix

	Flux (LMH)	Reverse Flux (gMH)	Capital Cost ($/kg)	Regeneration Cost	Regeneration Efficacy	Si+	Si-	Pi	Rank
CM-dextran-1000	0.0688	0.0008	0.0002	0.0099	0.0061	0.1426	0.2292	0.62	**9**
Cationic Starch	0.0113	0.0013	0.0001	0.0148	0.0122	0.1999	0.2192	0.52	**55**
Poly(propylene glycol) and non-ionic surfactant (Triton X-114) (PPG-725/TX-114)	0.0276	0.0001	0.0005	0.0198	0.0122	0.1840	0.2210	0.55	**32**
Chlorhexidine gluconate based mouthwash (CMW)	0.0387	0.0008	0.0000	0.0198	0.0122	0.1730	0.2223	0.56	**19**
diethylenetriamine pentakis(methylphosphonic) sodium salt (DTPMP-Na)	0.0759	0.0008	0.0002	0.0148	0.0153	0.1354	0.2313	0.63	**8**
tetraethylenepentamine heptakis-(methylphosphonic) sodium salt (TPHMP-Na)	0.1491	0.0005	0.0001	0.0148	0.0153	0.0626	0.2639	0.81	**2**
polyethylenimine (methylenephosphonic) sodium salt (PEI-600P-Na)	0.1325	0.0005	0.0002	0.0148	0.0153	0.0790	0.2551	0.76	**3**
PEI-1800P-Na	0.0483	0.0003	0.0002	0.0148	0.0153	0.1629	0.2245	0.58	**14**
thermo-sensitive polyelectrolyte of poly(N-isopropylacrylamide-co-acrylic acid) (PNA)	0.0058	0.0009	0.0003	0.0148	0.0061	0.2056	0.2192	0.52	**59**
Hydrolyzed poly(isobutylene-alt-maleicacid) (PIAM-Na)	0.0939	0.0002	0.0000	0.0198	0.0122	0.1180	0.2379	0.67	**6**
monocationic hydrophilic ionic liquids (ILs) Tetraethylammonium bromide ([N2222]Br)	0.0294	0.0184	0.0000	0.0198	0.0122	0.1831	0.2064	0.53	**51**
choline chloride-ethylene glycol (CC-EG)	0.0099	0.0001	0.0022	0.0148	0.0122	0.2013	0.2191	0.52	**56**
potassium functionalised carbon nanofibers suspended in triethylene glycol (TEG-K/CNF)	0.0367	0.0002	0.0007	0.0049	0.0061	0.1745	0.2228	0.56	**21**
BuMP	0.0058	0.0109	0.0063	0.0148	0.0122	0.2058	0.2077	0.50	**64**
CPMP	0.0055	0.0020	0.0005	0.0148	0.0122	0.2058	0.2183	0.51	**60**
PPG400	0.0101	0.0147	0.0000	0.0148	0.0122	0.2017	0.2080	0.51	**63**
1,4-piperazinediethanesulfonic acid disodium salt (P-2SO3-2Na)	0.2110	0.0064	0.0005	0.0198	0.0122	0.0164	0.2986	0.95	**1**
Ethanol	0.0469	0.1861	0.0000	0.0198	0.0122	0.2485	0.1254	0.34	**65**
Pretreated and enzymatically Hydrolysed Wheat Straw (PHWS)	0.0171	0.0039	0.0000	0.0049	0.0153	0.1938	0.2182	0.53	**53**
SSP	0.0450	0.0004	0.0002	0.0148	0.0122	0.1663	0.2237	0.57	**16**
PSSP5	0.0400	0.0001	0.0004	0.0148	0.0122	0.1712	0.2230	0.57	**18**
PSSP6	0.0377	0.0001	0.0004	0.0148	0.0122	0.1735	0.2227	0.56	**20**
PSSP11	0.0363	0.0000	0.0004	0.0148	0.0122	0.1750	0.2225	0.56	**22**
Polydiallyldimethylammonium Chloride (PolyDADMAC)	0.0290	0.0039	0.0001	0.0148	0.0153	0.1823	0.2185	0.55	**33**
DADMAC	0.0552	0.0039	0.0000	0.0148	0.0153	0.1561	0.2232	0.59	**13**
Glauber salt (sodium sulfate decahydrate, Na2SO4·10H2O)	0.0194	0.0003	0.0000	0.0148	0.0153	0.1918	0.2206	0.53	**47**
SiPEG-MN	0.0059	0.0039	0.0038	0.0099	0.0092	0.2053	0.2151	0.51	**62**

NaCl and Oleic Acid (OA)	0.0030	0.0002	0.0001	0.0099	0.0061	0.2082	0.2202	0.51	**61**
NaCl and Sodium dodecyl benzene sulfonate (SDBS)	0.0282	0.0016	0.0000	0.0099	0.0061	0.1831	0.2204	0.55	**31**
NaCl and Potassium Oleate (PO)	0.0295	0.0016	0.0001	0.0099	0.0061	0.1817	0.2206	0.55	**29**
NaCl and Sodium Dodecyl Sulfate (SDS)	0.0257	0.0017	0.0001	0.0099	0.0061	0.1856	0.2201	0.54	**38**
NaCl and Polyoxyethylene lauryl ether (Brij35)	0.0191	0.0012	0.0001	0.0099	0.0061	0.1922	0.2199	0.53	**49**
NaCl and Polyethylene glycol tert-octylphenyl ether (Triton X-100)	0.0221	0.0017	0.0000	0.0099	0.0061	0.1892	0.2198	0.54	**46**
1-cyclohexylpiperidine (CHP)	0.0607	0.0031	0.0004	0.0148	0.0122	0.1506	0.2249	0.60	**12**
PSS (70,000)	0.0503	0.0043	0.0003	0.0148	0.0122	0.1611	0.2215	0.58	**15**
PSS (200,000)	0.0359	0.0071	0.0000	0.0148	0.0122	0.1755	0.2167	0.55	**24**
PSS (1,000,000)	0.0326	0.0046	0.0004	0.0148	0.0122	0.1787	0.2181	0.55	**27**
Poly (aspartic acid sodium salt) (PAspNa) (NF)	0.0878	0.0031	0.1172	0.0148	0.0122	0.1703	0.2020	0.54	**37**
Poly (aspartic acid sodium salt) (PAspNa) (MD)				0.0198	0.0153	0.1707	0.2019	0.54	**41**
hydrolyzed polyacrylamide (HPAM)	0.0088	0.0039	0.0017	0.0099	0.0061	0.2024	0.2163	0.52	**58**
poly(sodium acrylate) polymer poly(N-isopropylacrylamide) (PSA–PNIPAM)-coated MNPs	0.0322	0.0039	0.0037	0.0099	0.0122	0.1789	0.2172	0.55	**30**
trimethylamine–carbon dioxide (TMA–CO2)	0.0922	0.0092	0.0000	0.0148	0.0122	0.1195	0.2305	0.66	**7**
ethylenediamine tetrapropionic (EDTP) acid (salt)	0.0627	0.0002	0.0004	0.0148	0.0153	0.1486	0.2278	0.61	**11**
protonated betaine bis(trifluoromethylsulfonyl)imide ([Hbet][Tf2N])	0.0063	0.0008	0.0006	0.0148	0.0122	0.2049	0.2192	0.52	**57**
Branched PEI (Mw =25,000 Da)	0.0304	0.0008	0.0001	0.0148	0.0153	0.1809	0.2213	0.55	**26**
Triton X100 coupled to Na3PO4	0.0157	0.0001	0.0001	0.0148	0.0122	0.1955	0.2204	0.53	**52**
High charge Na3PO4	0.0345	0.0007	0.0000	0.0198	0.0122	0.1771	0.2217	0.56	**23**
triethylenetetramine hexapropionic acid sodium (TTHP-Na)	0.0637	0.0006	0.0017	0.0148	0.0153	0.1476	0.2272	0.61	**10**
ethylenediaminetetraacetic acid (EDTA-2Na) coupled with nonylphenol ethoxylates (NP7)	0.0243	0.0001	0.0000	0.0148	0.0153	0.1869	0.2213	0.54	**40**
polyelectrolyte salt-poly (4-styrenesulfonic acid-co-maleic acid) sodium - P(SSA-co-MA)-Na-1	0.0414	0.0000	0.0000	0.0148	0.0153	0.1698	0.2236	0.57	**17**
Ammonia Carbon Dioxide (NH4-CO2)	0.0994	0.0084	0.0001	0.0148	0.0122	0.1123	0.2339	0.68	**5**
Sodium Chloride (NaCl)	0.1104	0.0172	0.0000	0.0247	0.0153	0.1039	0.2321	0.69	**4**
Magnesium Sulfate (MgSO4)	0.0153	0.0009	0.0000	0.0247	0.0153	0.1966	0.2196	0.53	**54**
Potassium Bicarbonate (KHCO3)	0.0278	0.0016	0.0000	0.0247	0.0153	0.1842	0.2202	0.54	**35**
Sodium Bicarbonate (NaHCO3)	0.0246	0.0013	0.0000	0.0247	0.0153	0.1875	0.2200	0.54	**44**
Sodium Sulfate (Na2SO4)	0.0254	0.0024	0.0000	0.0247	0.0153	0.1866	0.2192	0.54	**43**

Ammonium Sulfate ((NH4)2(SO)4)	0.0272	0.0028	0.0000	0.0247	0.0153	0.1848	0.2191	0.54	**39**
Potassium Sulfate (K2SO4)	0.0250	0.0029	0.0001	0.0247	0.0153	0.1870	0.2187	0.54	**45**
Magnesium Chloride (MgCl2)	0.0268	0.0043	0.0000	0.0247	0.0153	0.1852	0.2177	0.54	**42**
Calcium Nitrate (Ca(NO3)2)	0.0295	0.0051	0.0000	0.0247	0.0153	0.1826	0.2174	0.54	**36**
Ammonium Chloride (NH4Cl)	0.0359	0.0079	0.0000	0.0247	0.0153	0.1764	0.2159	0.55	**25**
Calcium Chloride (CaCl2)	0.0320	0.0074	0.0000	0.0247	0.0153	0.1802	0.2158	0.54	**34**
Potassium Chloride (KCl)	0.0372	0.0119	0.0000	0.0247	0.0153	0.1753	0.2129	0.55	**28**
Ammonium Bicarbonate (NH4HCO3)	0.0283	0.0160	0.0000	0.0247	0.0153	0.1844	0.2083	0.53	**50**
Potassium Bromide (KBr)	0.0357	0.0226	0.0000	0.0247	0.0153	0.1778	0.2039	0.53	**48**

B. SUPPORTING INFORMATION – FIGURES

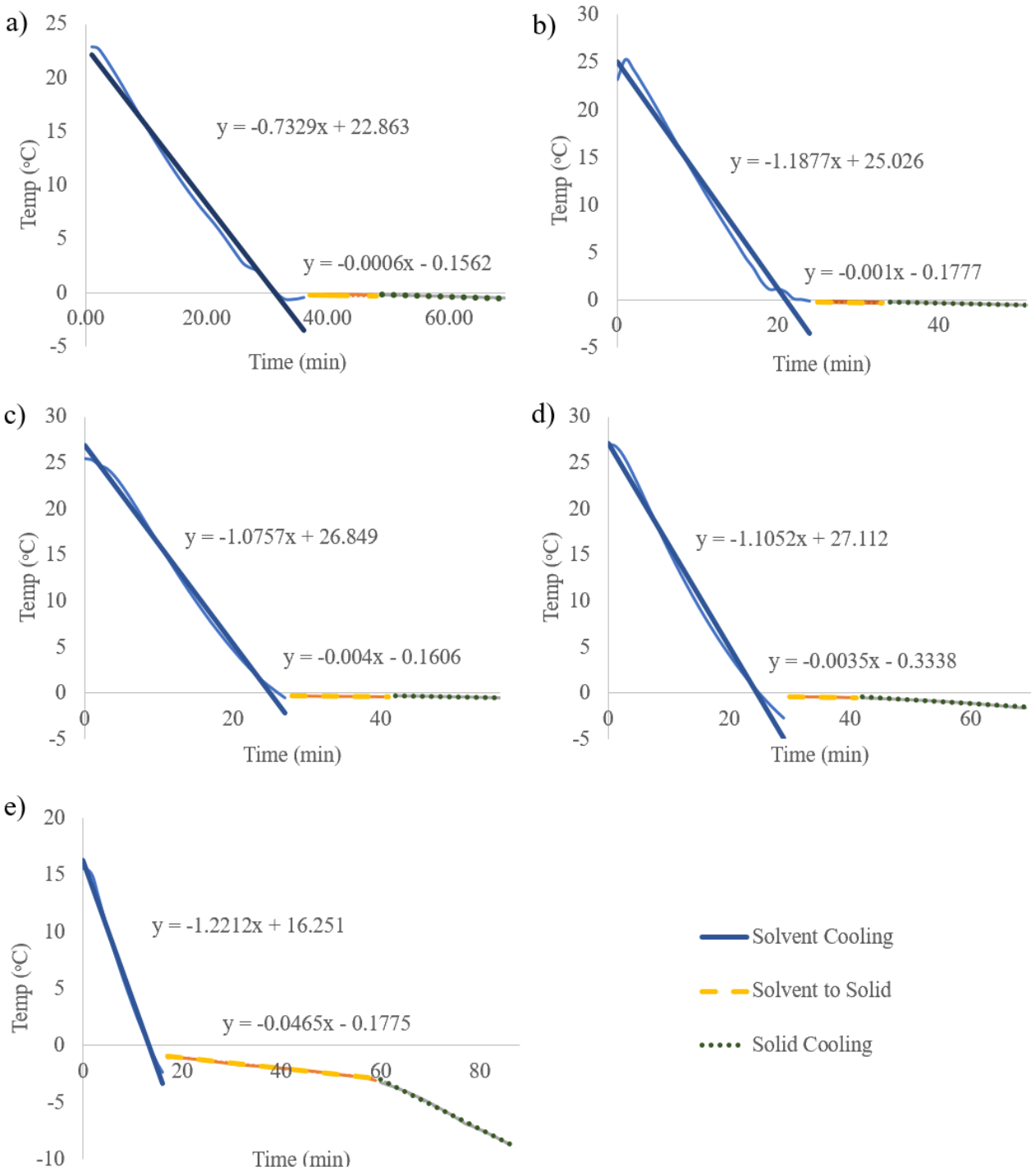

Fig. B.1 Freezing-point depression curves of peptone solution at a) 1 g/L, b) 10 g/L, c) 30 g/L, d) 100 g/L, e) 200 g/L

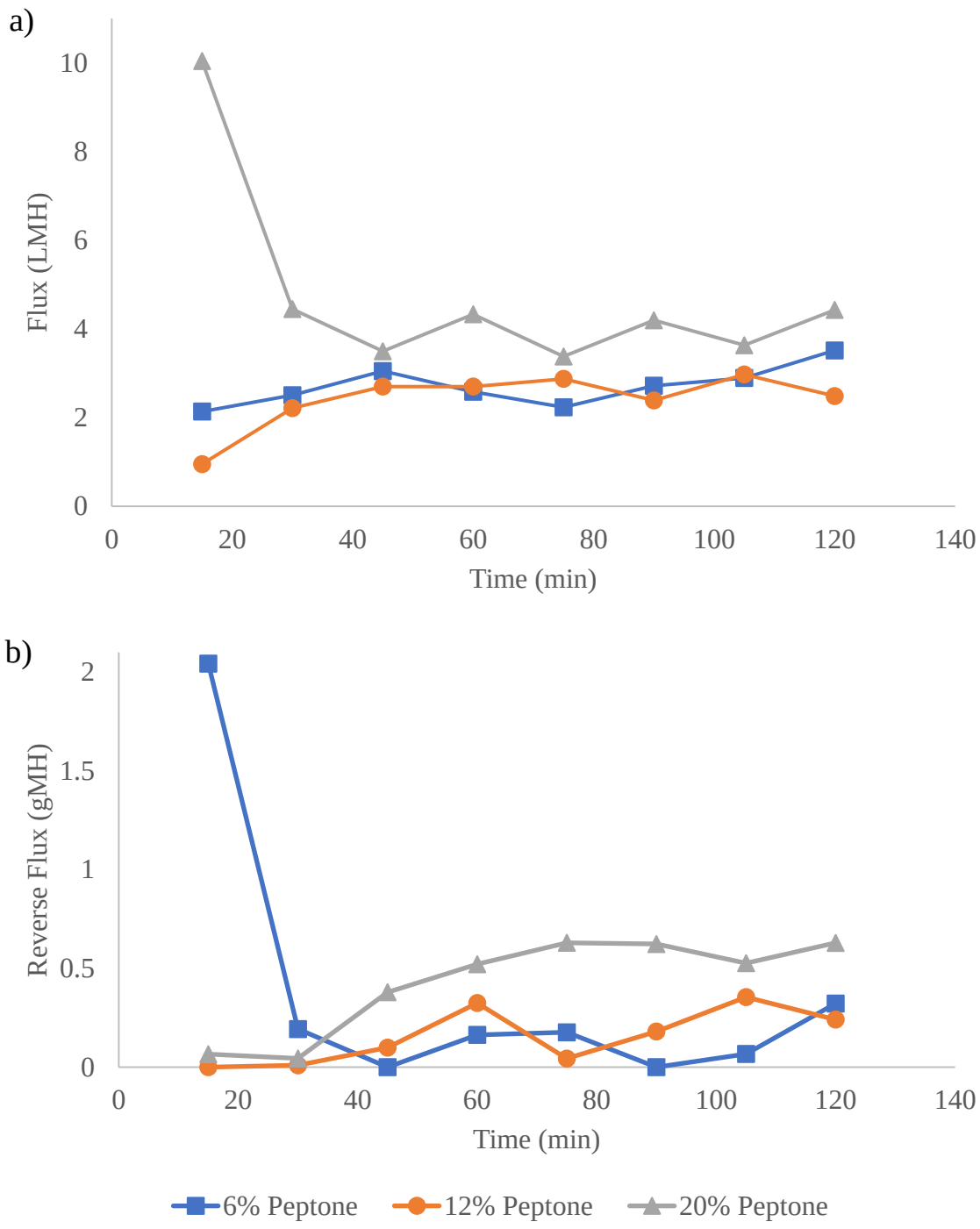

Fig. B.2 Peptone concentration effect on (a) water flux and (b) reverse solute flux over time.

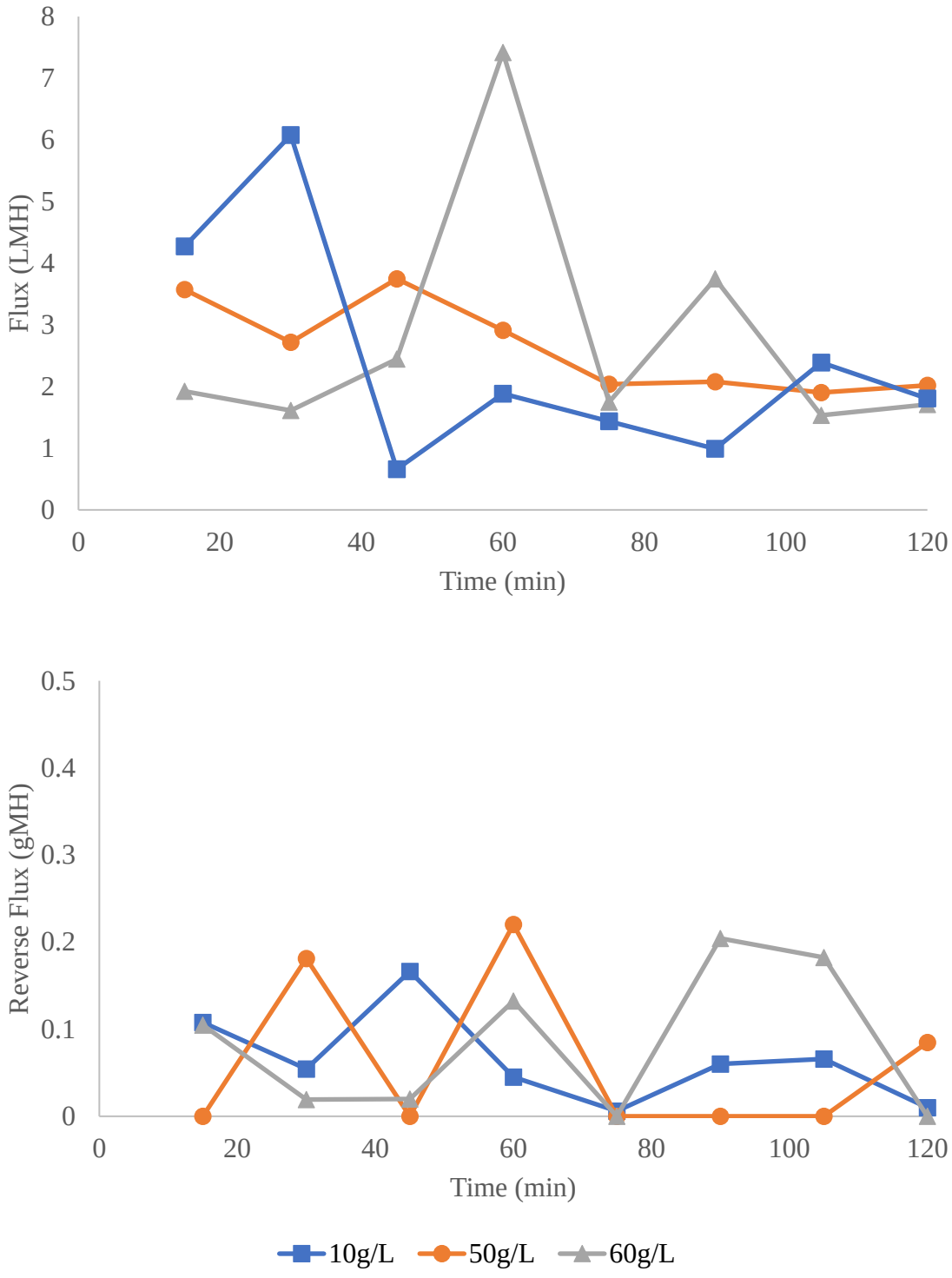

Fig. B.3 CMC concentration effect on (a) water flux and (b) reverse solute flux over time.

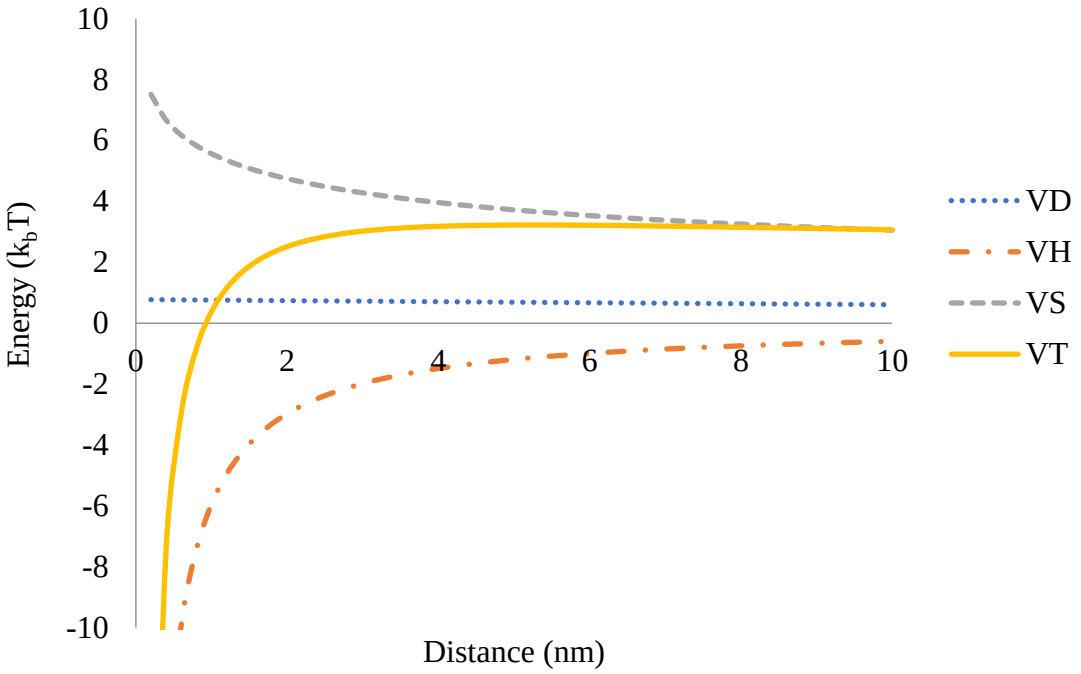

Fig. B.4 Energy profile of Fe_3O_4 NPs in 0.1 mM ionic strength solution considering electrostatic, vdW, and steric energies.